KAUNAS UNIVERSITY OF TECHNOLOGY

DARIUS EIDUKYNAS

RESEARCH AND DEVELOPMENT OF PIEZOELECTRIC IMPACT ENERGY HARVESTER FOR BURST-TYPE SIGNAL GENERATION

Doctoral Dissertation
Technological Sciences, Mechanical Engineering (09T)

2017, Kaunas

This dissertation was prepared at Kaunas University of Technology, Institute of Mechatronics, during the period of 2012 – 2017.

Scientific Supervisor:

Assoc. prof. Dr. Vytautas JŪRĖNAS, (Kaunas University of Technology, Technological Sciences, Mechanical Engineering – 09T).

This doctoral dissertation has been published in:
http://ktu.edu

Editor:

Dovilė Dumbrauskaitė (publishing house “Technologija”)

ISBN 978-609-02-1307-0

The bibliographical information of this issue is available at Martynas Mazvydas National Library of Lithuania National Bibliographic Database (NBD)

KAUNO TECHNOLOGIJOS UNIVERSITETAS

DARIUS EIDUKYNAS

PJEZOELEKTRINIO SMŪGINIO ENERGIJOS SURINKIMO PRIETAISO, GENERUOJANČIO SLOPSTANČIŲJŲ VIRPESIŲ SIGNALĄ KŪRIMAS IR TYRIMAS

Daktaro disertacija
Technologijos mokslai, mechanikos inžinerija (09T)

2017, Kaunas

Disertacija rengta 2012-2017 metais Kauno technologijos universitete, Mechatronikos institute.

Mokslinis vadovas:

Doc. dr. Vytautas JŪRĖNAS (Kauno technologijos universitetas, technologijos mokslai, mechanikos inžinerija – 09T).

Interneto svetainės, kurioje skelbiama disertacija, adresas:
http://ktu.edu

Redagavo:

Dovilė Dumbrauskaitė (leidykla “Technologija”)

ISBN 978-609-02-1307-0

Leidinio bibliografinė informacija pateikiama Lietuvos nacionalinės Martyno Mažvydo bibliotekos Nacionalinės bibliografijos duomenų banke (NBDB)

CONTENT

NOMENCLATURE

BaTiO3 – Barium titanate piezo ceramic;
BIPC – Ball-impact piezoelectric converter;
CMOS – Complementary Metal-Oxide Semiconductor technology for constructing integrated circuits;
FEM – Finite element method;
KNN – $(K,Na)NbO_3$;
LST – Lithuanian standards board
MEMS – Micro-Electro-Mechanical Systems;
PVDF – Polyvinylidene fluoride;
PZT – Lead zirconate titanate piezo ceramic;
UAD – ultrasonic-assisted drilling;
USM – ultrasonic motor;
USMW – Ultrasonic metal welding;
VIPEH – Vibro-Impacting Piezoelectric Energy Harvester

INTRODUCTION

Research relevance

Energy harvesting, which, in general, is the conversion of ambient energy into usable electrical energy, nowadays is one of the most popular topics between scientists and industry users due to the fact that extended life of electronic devices is imperative. Energy harvesting devices can reduce the size of traditional power supply thus reducing the size and mass of the whole system. Moreover, energy harvesting devices can be used in such environments where replacing traditional batteries is difficult or impossible, e.g. in implanted medical devices or space technologies.

Conventional energy harvesters are based on 5 basic principles of energy conversion: photoelectric, piezoelectric, electromagnetic, electrostatic and thermoelectric. Piezoelectric energy harvesters are the most used nowadays due to their relatively simple design, direct conversion and the highest energy density comparing to others.

Energy harvesters used for harvesting from mechanical ambient energy are based on resonant behaviour, which means that they generate maximum energy power when they are excited by a harmonic excitation signal, the frequency of which is close to the resonant frequency of the harvester. Thus if the frequency of ambient vibrations does not correspond with the resonant frequency of the harvester, the amount of generated energy significantly reduces; because of this, most of them could not be used in practice, since the frequency of ambient vibrations of excitation is accidental. Due to this fact, energy harvesters which are excited by impact have been over the last decade. Some of such harvesters are based on cantilever structure while others use impact directly to the piezoelectric material. Both types of energy harvesters generate the maximum power when they oscillate at their resonant frequencies, which is why all energy harvesters have resonators (a cantilever or a piezoelectric structure on which direct impact occurs) which are intended to generate resonant frequency of the harvester from the excitation impact.

The main disadvantage of the developed impact energy harvesters is that they generate signal in a low frequency range – up to 4 kHz. Another disadvantage, especially of those who use impact directly to the piezoelectric material, is low protection from impact of piezoelectric material. This means that after a few energy generation cycles the piezoelectric material could crack or totally shatter. Moreover, all of the energy generated with the practically developed impact energy harvesters transmits to traditional “power banks”, such as batteries, capacitors, etc.

In this research, a novel piezoelectric impact energy harvester for burst-type signal generation is researched and developed. Such a harvester generates relatively high, ultrasonic-range frequency burst-type electric signal and is intended for direct drive of some kind of ultrasonic motor (USM). It can also operate as an alternative method when traditional methods, such as electric signal generators are unavailable or damaged. This decreases the risk of ultrasonic motor exploitation failure when traditional systems are damaged or are unavailable in areas such as nature, space, etc. Since the presented piezoelectric impact energy harvester for burst-type signal

generation can drive both rotational and linear USM, it allows to increase reliability of precision positioning drive exploitation. Moreover, the developed impact energy harvester has resonator-type waveguide, which protects the piezoelectric material from impacts.

Aim and objectives of the research

The aim of this research is to design and develop a piezoelectric impact energy harvester for burst-type signal generation and adapt it for the drive of the ultrasonic motor.

The following objectives are set in order to reach the aim:

1. to review the literature regarding the research fields of vibrational and impact energy harvesting, mechanical impact generation methods, horn-type waveguides used as resonators, and techniques of ultrasonic motor control as well as to determine the main advantages and disadvantages of energy harvesters.
2. to design and theoretically investigate the novel piezoelectric impact energy harvester for burst-type signal generation by modelling a mechanical impact and horn-type waveguide with harmonic and impulse excitation when it is applied on a surface with smaller cross-sectional area.
3. to experimentally investigate the piezoelectric impact energy harvester for burst-type signal generation, including experimental research of mechanical impact, horn-type waveguides, and ultrasonic motor control.
4. to create and investigate a methodology for designing an impact energy harvester for certain ultrasonic motor drive.

Research methods

The research was carried out by using theoretical and experimental methods of investigation.

Theoretical research is based on several methods – analytical and finite element methods, which were performed using ANSYS 17.1 and SolidWorks 2016 software packages.

The theoretical results were verified with experimental investigation which was carried out at Kaunas University of Technology, Institute of Mechatronics and Technological Systems Diagnostics Institute. During experimental research for measuring the surface vibrations, 1D and 3D scanning laser Doppler vibrometers (Polytec Inc.), holographic interferometry system PRISM 100 (Hytec Inc.), impedance meter Wayne Kerr 6500B and high frequency accelerometers (Bruel and Kjaer) were used. PicoScope hardware and software were used to measure and process the researched signals. The noise of piezoelectric shock-type impact energy harvester was evaluated using the sound Investigator 2260 (Bruel and Kjaer).

Scientific novelty

The following scientific novelties are presented in the research:

1. Designed a novel piezoelectric impact energy harvester, intended for high frequency burst-type signal generation using horn-type waveguide as resonator of particular frequency, which increases the amplitude of generated burst-type signal and protects the brittle piezoceramic material from breakage due to by impact.
2. Designed and developed a piezoelectric impact energy harvester for burst-type signal generation which is intended for direct control of ultrasonic motor. Therefore, such a device allows to drive and control an ultrasonic motor in environments where traditional power supplies, such as power supply or batteries are unavailable or when they are damaged.
3. Horn-type waveguide was investigated in different ways – with harmonic and impulse excitation on the surface with a smaller cross-sectional area thus allowing to uniformly transmit the impact energy to piezoelectric transducer with a surface of greater cross-sectional area.
4. The methodology of piezoelectric impact energy harvester for burst-type signal generation design of certain ultrasonic motor drive was created. Experimental studies show that such a methodology works correctly and could be applied in practice.

Research approbation

The results of the research were published in 6 scientific papers: 3 papers with impact factor, listed in the database of the Institute for Scientific Information (ISI), 1 paper is listed in other international databases, and 2 articles are published in peer-reviewed conference proceedings.

The results of this research were also presented in four international conferences: "Vibroengineering-2014", Poland, "Mechanika 2015", Kaunas, "Mechatronic Systems and Materials 2015", Kaunas and "Mechanika 2016", Kaunas.

Registered by a scientific invention patent application of the Republic of Lithuania.

Practical value

The piezoelectric impact energy harvester designed during this research is intended for ultrasonic frequency burst type-signal generation, which could be directly used in ultrasonic motor drive. The aforementioned piezoelectric impact energy harvester for burst-type signal generation can operate as an alternative for ultrasonic motor drive when traditional methods, such as signal generators are unavailable or damaged. This decreases the risk of ultrasonic motor exploitation failure when traditional control systems are damaged or are unavailable in areas such as nature, space, etc. Since the presented piezoelectric impact energy harvester for burst-type signal generation can drive both rotational and linear ultrasonic motors, it allows to increase the reliability of precision positioning drive exploitation.

The structure of the dissertation

The thesis consists of an introduction, four sections, general conclusions, references and the author's publications list.

The first section of the thesis reviews the literature of vibrational and impact energy harvesters, mechanical impact methods, horn-type waveguides, and the techniques for ultrasonic motor control.

The second section presents the theoretical investigations. It describes the design of the piezoelectric impact energy harvester for burst-type signal generation and explains mechanical impact modelling. Moreover, the section also presents the horn-type waveguide with harmonic and impact excitation on its surface with a smaller cross-sectional area.

In the third section, the results of theoretical investigations are verified with experimental studies of piezoelectric impact energy harvester for burst-type signal generation, including experimental research of mechanical impact, horn-type waveguides, and ultrasonic motor control.

The fourth section presents the methodology for designing the piezoelectric impact energy harvester for burst-type signal generation for a certain ultrasonic motor drive. This methodology is also verified by experimental investigation. At the end of the section, the noise generated by the piezoelectric impact energy harvester is evaluated according to the LST standard.

Conclusions present the results of the theoretical and experimental investigations.

The total volume of the thesis is 110 pages, including 89 figures, 12 tables, and 7 pages of appendixes.

1. LITERATURE REVIEW

Nowadays all electrical systems or devices are decreasing in size and power supply, however, less energy is available on board, leading to a short run-time for the device or battery life. Considering that extended life of the electronic devices is very important, the area of energy harvesting is one of the most popular topics between scientists and industry users. In general, energy harvesting is the conversion of ambient energy into usable electrical energy. Energy harvesting can be obtained from different energy sources, such as mechanical vibrations, electromagnetic sources, light, acoustic, air flow, heat, and temperature variations. When compared with the energy stored in common storage elements, such as batteries, capacitors, etc., the environment represents a relatively infinite source of available energy.

Energy harvesting devices can reduce the size of traditional power supply thus reducing the size and mass of the entire system. Moreover, energy harvesting devices could be used in places where replacing traditional batteries is difficult or impossible – e.g. in implanted medical devices or space technologies.

One of the disadvantages of an energy harvesting device is its small (5–20 %) efficiency.

This section presents a review of publication as well as other types of scientific data in recent advantages in energy harvesting systems, impact generation, and horn-type waveguides. The section begins with the basic information about energy harvesting principles. These are followed by piezoelectric energy harvesters, piezoelectric materials, and coupling modes. The next sub-sections provide information about the use of mechanical impacts and common information regarding horn-type waveguides.

1.1. The principles of energy harvesting

As it has been mentioned above, the operating principles of energy harvesting devices could be based on photoelectric, thermoelectric, electromagnetic, electrostatic, and piezoelectric phenomena.

Photoelectric energy harvesters use photovoltaic cells (e.g. solar panels) which have the ability to convert light energy into electrical energy [1]. Each cell consists of a reverse biased pn+ junction, in which the light crosses with the heavily conservative and narrow n+ region. Photons containing the light energy are absorbed within the depletion region, generating electron-hole pairs. The built-in electric field of the junction immediately separates each pair, accumulating the electrons and holes in the n+ and p regions, respectively, and establishing an open circuit voltage. With a load connected, the accumulated electrons travel through the load and recombine with holes at the p-side, generating a photocurrent that is directly proportional to the light intensity and independent of the cell voltage [2].

Thermoelectric energy harvesters are based on the Seebeck effect and are capable of directly converting the temperature differences to electrical voltage [3]. Temperature changes between the opposite segments of a conducting material result in heat flow and, consequently, charge flow, since mobile, high-energy carriers diffuse from high to low concentration regions. Thermopiles consisting of n- and p-type

materials electrically joined at the high-temperature junction are therefore constructed, which allows heat flow to carry the dominant charge carriers of each material to the low temperature end, establishing in the process a voltage difference across the base electrodes. The generated voltage and power is relative to the temperature differential and the Seebeck coefficient of thermoelectric materials [2].

Electromagnetic energy harvesters are based on the electromagnetic induction effect governed by Faraday's law; they use a magnetic field to convert mechanical energy to electrical energy [4]. A coil attached to the oscillating mass is passed through a magnetic field, which is established by a stationary magnet, to produce electric energy. The coil travels through a varying amount of magnetic flux, inducing a voltage according to Faraday's law [2].

Electrostatic energy harvesters typically use a variable capacitor structure, the capacitance of which changes when the overlapping area varies in response to an external vibration source. As a result, the induced charge moves back and forth through an external load resistance, and electric power is generated when the proof mass-spring structure resonates in response to the vibration source [5].

The most popular device for converting ambient vibrations to electric energy is the piezoelectric energy harvester [6-8]. This device uses a method which alters the mechanical energy into electrical energy by straining a piezoelectric material. The strain or deformation of a piezoelectric material causes charge separation across the device, producing an electric field and, consequently, a voltage drop proportional to the stress applied [2]. A linear spring-mass-damper system has been the most common type of such energy harvesting device [8].

Ambient energy harvesting systems and their basic features are presented in Table 1.

Table 1. Energy harvesting systems and their basic features

Energy harvesting type	Photoelectric	Thermoelectric	Electromagnetic	Electrostatic	Piezoelectric
Energy generating tool	Photovoltaic cells	Thermopiles	Ambient mechanical effect (generator)	Charged variable capacitor	Ambient mechanical effect (piezoelectric material)
Energy generating technique	Light interfaces with heavily doped narrow n+ region	Temperature differentials between opposite segments	Magnetic field (converters)	Vibration, separation of capacitor plates	Deformation, vibration, strain of piezoelectric material

Energy harvesting type	Photoelectric	Thermoelectric	Electromagnetic	Electrostatic	Piezoelectric
Energy Source	Light: indoor room light or outdoor sunlight	Thermal: waste heat energy from furnaces, heaters, friction sources.	Electromagnetic: inductors, coils, transformers.	Mechanical: vibrations from machines, manufacturing devices.	Mechanical: human motion, vibrations from machines, mechanical stress, strain from motors, manufacturing machines, waste rotations.
Energy type, used for harvesting	Light energy	Thermal energy	Mechanical energy	Mechanical energy	Mechanical energy
Advantages	• Natural source; • Excellent power density in direct sunlight;	• Relatively high efficiency when temperatures differences are reached;	• Unnecessary an external voltage source; • Unnecessary mechanical contacts between segments;	• Compactible with CMOS technology;	• Relatively easy manufacture; • Unnecessary an external voltage source; • High power density;
Disadvantages	• Limited operating conditions (light time); • Necessary relatively large surface area;	• Limited operating conditions (operating environment);	• Not compatible with CMOS technology; • Difficult manufacture; • Difficult miniaturization; • Low output voltage.	• Necessary an external voltage source; • Difficult manufacture; • High output voltage.	• Necessary overload protection; • Low output voltage

As Table 1 shows, the most common modes of transduction which are implemented in the field of mechanical-vibration energy harvesting are electrostatic, electromagnetic, and piezoelectric energy harvesting systems.

Vibration energy from ambient vibrations could be harvested when other types of energy harvesting, e.g. photoelectric or thermoelectric are unavailable. Examples of ambient vibration sources, as an available source for vibration harvesting could be the human body (limb motion, breathing, blood pressure, etc.), the industrial environment (cutting, milling, compressors, fans, etc.), structures (bridges, roads, high buildings, etc.), or vehicles (automobiles tires, brakes, aircrafts, trains, etc.).

The scheme of general vibration energy conversion to electric energy is presented in Fig. 1.1 [9].

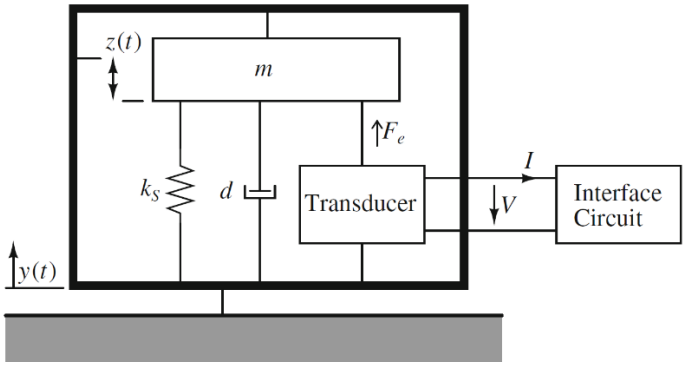

Fig. 1.1 The scheme of general vibration energy conversion to electric energy [10]

The scheme consists of a seismic mass *m*, and a spring *k*. When the harvester is vibrated, the mass moves out of phase with the generator housing, so that there is a net movement between the mass and the housing. This relative displacement is sinusoidal in amplitude, and can drive a suitable transducer to generate electrical energy. The transducer is depicted as a dashpot *d* because the conversion of mechanical energy into electrical energy damps the mass [9]. The motion of the harvester presented in Fig 1.1 is defined with:

$$m\ddot{z}(t) + d\dot{z}(t) + kz(t) = -m\ddot{y}(t) \tag{1.1}$$

where *z(t)* – the displacement of the mass with respect to the housing, *y(t)* – excitation, *m* – seismic mass, *d* – damping constant, *k* – spring constant.

When the generator operates at resonance and the ambient vibration excitation is sinusoidal($y(t) = Y_0 * \cos(\omega t)$), the generated power is inversely proportional to the transducer damping factor [9]:

$$P = \frac{m{Y_0}^2\omega_n^3}{4\zeta} \tag{1.2}$$

where ζ – the harvester damping factor, ω_n – the resonant angular frequency, Y_0 – the amplitude of vibration.

The average generated power against the frequency for various damping factors is presented in Fig. 1.2 [9].

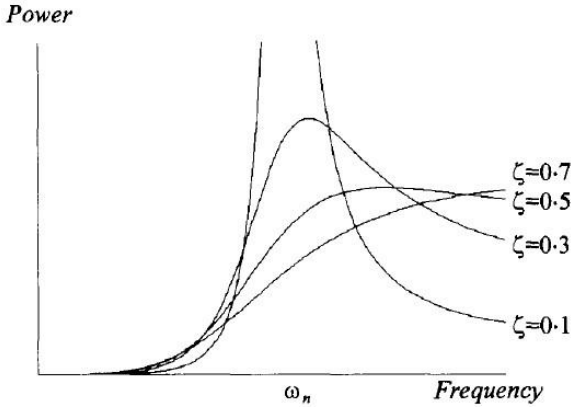

Fig. 1.2 Harvester-generated power against the frequency for various damping factors [9]

Fig. 1.2 shows that the generated power increases when the damping factor decreases, and the maximum power is generated at the resonance frequency – when the damping factor of the construction is close to zero. As it is seen in Fig. 1.2., in principle, a damping factor of zero would generate infinite power but in practice this is impossible. When the damping factor is greater than zero, the generated power is finite and depends on the construction of the harvester [9].

The electrostatic and electromagnetic transductions require a "two-part" design: the two plates of the variable capacitor in the electrostatic configuration, the coil and the magnet in the electromagnetic one [11]. This design feature is not necessary for piezoelectric energy conversion. With regards to this fact, the next sub-section presents a more detailed analysis of piezoelectric energy harvesting systems and their applications.

1.2. Piezoelectric energy harvesting

1.2.1. Piezoelectric effect and coupling modes

Piezo electrics is coupling between structural and electrical fields that occurs in certain crystalline materials. Applying voltage to a piezoelectric material creates displacement and vibrating piezoelectric material generates voltage. Direct piezo effect is known as the ability of piezoelectric material to generate electric field proportional to the strain applied to it. Inverse piezo effect entails the opposite – same material ability to strain when electric field is applied. In general, piezoelectric energy harvesting devices are based on direct piezoelectric effect [10].

Equations describing piezoelectric material properties are constructed under the assumption that the total strain on the material is the sum of strain caused by the mechanical stress and the controllable actuation strain caused by the applied electric voltage [12]:

$$\varepsilon_i = S_{ij}^E \sigma_j + d_{mi} E_m \quad (1.3)$$

$$D_m = d_{mi} \sigma_i + \zeta_{ik}^\sigma E_k \quad (1.4)$$

where subscripts *i,j* – values 1,2,…,6, *m,k* – 1,2,3 refer to different directions within the material coordinate system (explained below); σ – stress vector, N/m^2; ε – strain vector, N/m^2; *E* – vector of applied electric field, V/m; ζ – permittivity, F/m; *d* – matrix of piezoelectric strain coefficients, m/V; *S* – matrix of compliance coefficients, m^2/N; *D* – vector of electric displacement, C/m^2.

Piezoelectric materials have anisotropic properties, which means that their properties depend on both the direction of the applied mechanical or electric force and the directions perpendicular to the applied force. Therefore, the indexes in equations (1.3) and (1.4) are identified by numerals and show the direction of applying properties. Fig. 1.3 presents these numerals [12].

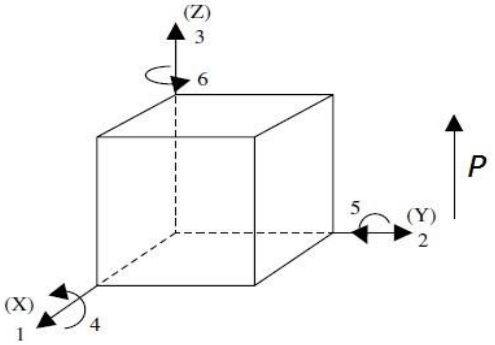

Fig. 1.3 The directions of forces affecting a piezoelectric element [16]

In Fig. 1.3, the arrow P shows the polarization direction of the piezoelectric element, 1 refers to the positive direction of x axis, 2 and 3 to the positive directions of y and z axes, accordingly. Numbers 4, 5 and 6 correspond with the shear of the x, y and z axes, accordingly [12].

As mentioned above, piezoelectric materials have built-in polarization and, therefore, respond differently to stresses depending on the direction. There are two basic modes of electromechanical coupling for piezoelectric materials used in energy harvesting areas: modes 31 and 33 [13]. These coupling modes are presented in Fig. 1.4.

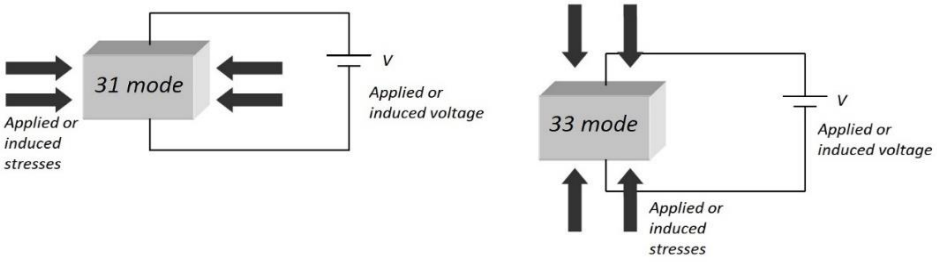

Fig. 1.4 31 and 33 electromechanical coupling modes of piezoelectric materials [13]

As Fig 1.4 shows, if piezoelectric element is coupled in the 31 mode, the electric field is produced on the axis perpendicular to the axis of applied strain. Most of beam configurations under base excitation work in this mode. When piezoelectric element is coupled in the 33 mode, the applied voltage and stress is generated on the parallel axis [13]. Most of the piezoelectric stacks, which can produce electric signal with higher frequency comparing with piezoelectric beams, work in the 31 mode.

1.2.2. Piezoelectric materials

Piezoelectric materials have three main types of piezoelectric coefficients: the piezoelectric coefficient d_{ij} which is the ratio of the strain in the j axis to the electric field applied along the i axis while all external stresses are constant, the electro-mechanical coupling coefficient k_{ij} which represents the ability of piezoelectric material to transform electrical energy to mechanical and vice versa, and the piezoelectric voltage constant g_{ij} which signifies the electric field developed along the i axis when the material is stressed along the j axis [12]. Different piezoelectric materials have different coefficients which means that by following these coefficients it is possible to indicate the piezoelectric properties of material. The piezoelectric properties of material also depend on material stress, age, and temperature.

The properties' dependency on time is known as the ageing rate and it significantly depends on the design methods ant material type. The changes are logarithmic with time and that is why the material properties stabilize with age; therefore, the manufacturers of piezoelectric materials tend to specify the constants of material after a certain period of time. The ageing process is significantly accelerated by the amount of stress applied to the material and this should be considered in cyclically loaded energy harvesting applications [14]. For example, "soft" piezoelectric ceramics, such as PZT-5A, are more susceptible to stress-induced changes than the "harder" piezo ceramic, i. e. PZT-4. Temperature is also a considerable factor with piezoelectric materials due to the Curie point. Above this limit, the piezoceramic material loses its piezoelectric properties effectively becoming de-polarized. It is noteworthy that stress application could reduce the Curie temperature [14].

The aforementioned piezoelectric coefficients and other properties of the most popular piezoelectric "soft" and "hard" lead zirconate titanate piezoceramics (PZT-5A and PZT-4), barium titanate ($BaTiO_3$) and polyvinylidene fluoride (PVDF) materials are presented in Table 2 [14].

Table 2. The piezoelectric coefficients of piezoelectric materials [14].

Piezoelectric coefficient	Unit	PZT-5A	PZT-4	$BaTiO_3$	PVDF
d_{33}	C/N	$420 \cdot 10^{-12}$	$250 \cdot 10^{-12}$	$149 \cdot 10^{-12}$	$-33 \cdot 10^{-12}$
d_{31}	C/N	$-180 \cdot 10^{-12}$	$120 \cdot 10^{-12}$	$78 \cdot 10^{-12}$	$23 \cdot 10^{-12}$
g_{33}	Vm/N	$24.8 \cdot 10^{-3}$	$26.1 \cdot 10^{-3}$	$14.1 \cdot 10^{-3}$	$330 \cdot 10^{-3}$
g_{31}	Vm/N	$-11.4 \cdot 10^{-3}$	$-11.4 \cdot 10^{-3}$	$5 \cdot 10^{-3}$	$216 \cdot 10^{-3}$

Piezoelectric coefficient	Unit	PZT-5A	PZT-4	$BaTiO_3$	PVDF
k_{33}	-	0.71	0.63	0.48	0.15
k_{31}	-	0.31	0.32	0.21	0.12
Permittivity	-	1700	1700	1700	12
Density	g/cm^3	7.75	7.45	6.02	1.78
Young's modulus Y_{33}	GPa	66	75	67	2
Mechanical quality factor Q_m	-	80	700	1300	3-10

1.2.3. Piezoelectric energy harvesters

The typical scheme of a piezoelectric energy harvester used to convert mechanical vibrations to electrical energy is presented in Fig. 1.5 [15].

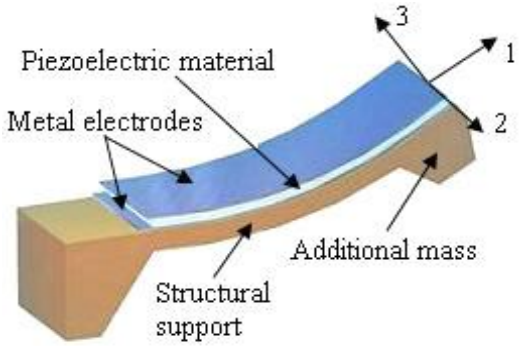

Fig. 1.5 The scheme of a typical piezoelectric energy harvester used to convert mechanical vibrations to electrical energy [15]

The piezoelectric energy harvester shown in Fig. 1.5 consists of a passive layer – the structural support which is covered with the active layer, the piezoelectric material, from one or both sides. In order to decrease the resonant frequency of such a harvester and to increase the deformation of piezoelectric material, additional concentrated mass is mounted at the tip of the cantilever (structural support). When such a harvester is excited by ambient vibrations, both the structural support and the piezoelectric material is deformed and thus electric energy is generated [15].

The dependency of the generated power on the input vibration amplitude is defined [16]:

$$P = \frac{V^2}{2R} = \frac{1}{2R} \cdot \frac{\left(\frac{2k_{31}t_c}{k_2}\right)^2 c_p}{\left[\frac{\omega_n^2}{\omega RC_b} - \omega\left(\frac{1}{RC_b} + 2\zeta\omega_n\right)\right]^2 + \left[\omega_n^2\left(1+k_{31}^2\right) + \frac{2\zeta\omega_n}{RC_b} - \omega^2\right]^2} A_{in} \tag{1.5}$$

where ω – frequency of excitation, ω_n – resonance frequency of the harvester, c_p – elastic constant of the piezoelectric material, k_{31} – piezoelectric coupling coefficient, t_c – thickness of one layer of the piezoelectric material, k_2 – geometric

constant that relates the average piezoelectric material strain to the tip deflection, ε – dielectric constant of the piezoelectric material, A_{in} – magnitude of excitation acceleration,R – the load resistance, V – voltage across the load resistance, C_b – the capacitance of the piezoelectric material, ζ – harvester damping factor.

Such types of harvesters, as most of those reported in literature, are based on resonant behaviour [17]. This means that the majority of energy harvesters based on piezoelectric principle generate the maximum amount of energy when they are excited with a harmonic excitation signal, the frequency of which corresponds with the first resonant frequency of the harvester. Thus, if ambient vibrations frequency does not correspond with the resonant frequency of the harvester, the amount of energy generated significantly reduces. With regards to this, most of such energy harvesters could not be applied in practice because the frequency of excitation in ambient vibrations is accidental.

Moreover, conventional energy harvesters using the resonance characteristic are not necessarily suitable from the viewpoint of power efficiency because ambient vibration widely spreads and is allocated at the low range of frequency which is below 200 Hz [18]. Thus, the impact energy harvesters which are excited by impact have been developed during the last decade.

1.3. Piezoelectric impact energy harvesting

The typical piezoelectric harvester, presented in Fig. 1.5, could be also used for impact energy harvesting. Two situations in which a piezoelectric harvester can operate – under a shock and impact are presented in Fig. 1.6 [15].

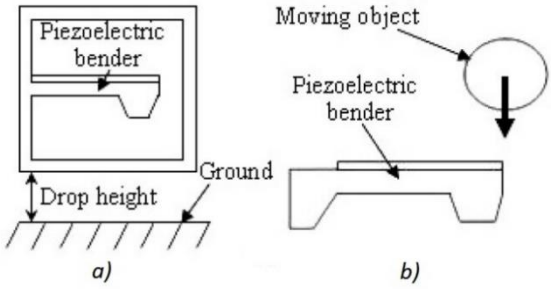

Fig. 1.6 The scheme of a piezoelectric energy harvester used with: a) shock b) impact excitation [15]

In the first situation, the piezoelectric energy harvester undergoes a shock, i.e. it is dropped from a certain height and falls to the ground, as shown in Fig. 1.6 a). In the second one, a certain moving object impacts the bender initially at the rest, as is shown in Fig. 1.6 b). The behaviour of the piezoelectric energy harvester under a shock could be defined by the solution of the free vibration problem: if the duration of the shock and the corresponding impulse of energy is very short compared to the natural oscillation period of the structure, after the shock the system behaves as if it had been given an initial velocity and becomes unforced, i.e. the system is in its free oscillation state [15]. The second situation (Fig. 1.6 b).), when a moving object

impacts the harvester, could be represented in the same way by using the method of the Newton coefficient of restitution to describe the impact between the two colliding bodies, i.e. the velocities of the two bodies after an impact can be expressed as simple functions of the velocities before the impact. As in the case of the shock excitation, if the duration of the impact and of the corresponding exchange of energy is very short compared to the natural period of the harvester, it can be considered that the oscillating structure after impact is in a free oscillation state [15]. This free oscillation state could be considered as input vibration and the working principle of the energy harvester could be further researched as traditional piezoelectric energy harvester described above.

One of the earliest impact energy harvesters, called a piezoelectric vibrator was presented in 1996 [19]. The scheme and working principle of the piezoelectric vibrator are presented in Fig. 1.7.

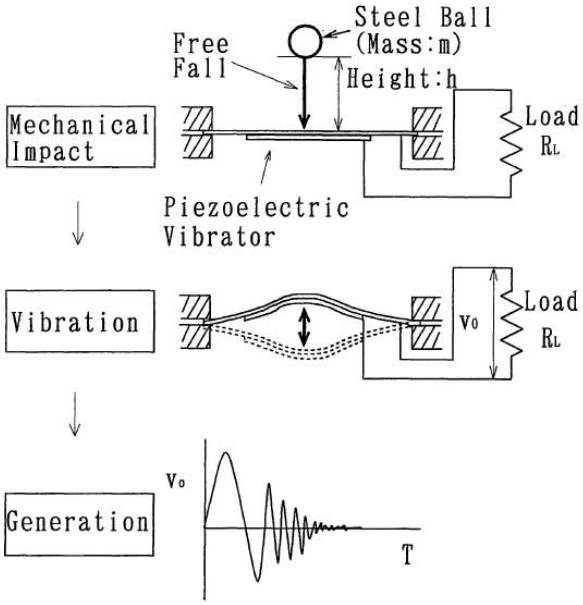

Fig. 1.7 The scheme and working principle illustration of piezoelectric vibrator [19]

Such a piezoelectric vibrator consists of a 27 mm diameter, 0.25 mm thick bronze disk and 19 mm diameter, 0.25 mm thick piezoelectric ceramic fixed to the holder at its edge. The electric output is generated from disk bending vibrations caused by the impact of falling from height h 5.5 g steel ball. The electric output of the vibrator is connected to the load resistance RL [19]. As Fig. 1.7 shows, the impact energy harvester has three main stages of impact energy harvesting – the mechanical impact, in this case caused by the free fall of mass m steel ball, the bending vibrations, excited by the impact of the steel ball to the piezoelectric vibrator, and the electric energy generation, which relies on the piezoelectric effect.

The results of experimental and theoretical research show that the piezoelectric vibrator (Fig. 1.7.) could operate at a frequency up to 4 kHz.

Based on the principle of the piezoelectric vibrator(Fig. 1.7.), the scheme of one of the impact energy harvesters which at present exist in market, called the ball-impact type lead-free (K,Na)NbO_3 (KNN) researched by Japanese scientists, is presented in Fig. 1.8 [20].

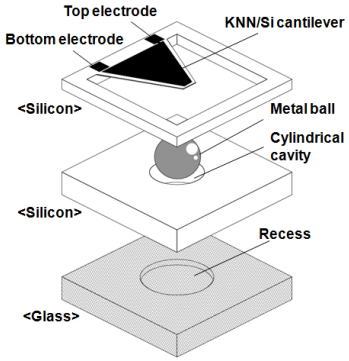

Fig. 1.8 The scheme of the ball-impact type KNN-based energy harvester [20]

This harvester consists of three-layer cavity; two of the layers are made of made of silicon and the third is made of glass. A KNN/Si cantilever is located in the top layer of silicon. Beneath this cantilever, a cylindrical cavity is integrated, and the metal ball is built in this cavity. The metal ball is guided by the cylindrical cavity and can always perpendicularly impact the cantilever. Fig. 1.9 presents the illustration of the harvester of power generation [20].

As shown in Fig. 1.9, when external force is applied, the metal ball moves up and strikes the cantilever. As a result, free oscillation is induced and the cantilever can vibrate at its natural frequency. In such a way, the electric power is generated from piezoelectric KNN film and deposited on the vibrating cantilever [20].

Such type of harvester is suitable for harvesting energy from ambient vibrations and can operate at low and wide frequency range of 20-190 Hz. The maximum power of such a harvester can be obtained at 190 Hz shaking frequency and reached 44 nW.

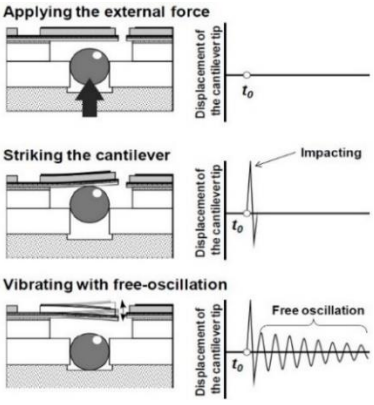

Fig. 1.9 An illustration of the harvester of power generation with free oscillation [20]

Another example of impact energy harvester could be the piezoelectric water drop energy harvester. The scheme and experimental stand view of such an energy harvester are presented in Fig. 1.10 [18].

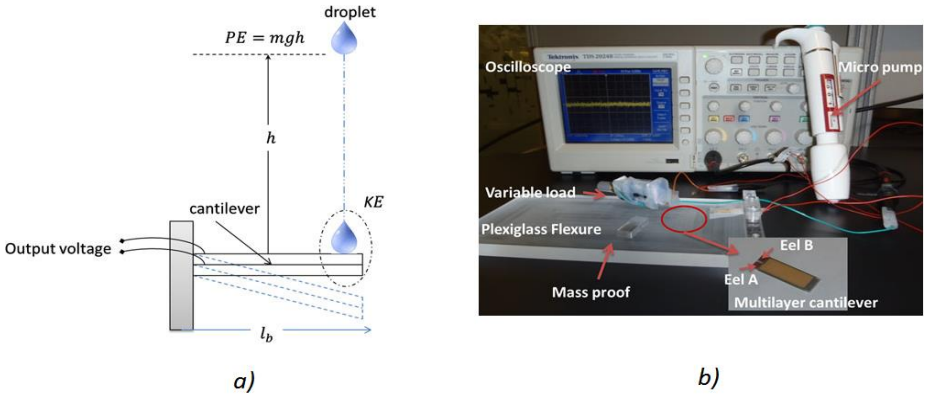

Fig. 1.10 The piezoelectric water drop energy harvester: a) scheme b) experimental stand [18]

As shown in Fig. 1.10 a) the electric energy in such harvester is generated from piezoelectric cantilever bending, which is affected by the water dropping (impact) on it [18]. The water drops are adjusted to fall freely from a fixed height (60 cm). The potential energy of the water drops gradually decreases, being converted into kinetic energy through the acceleration due to gravity. After a certain time, the drop reaches the top surface of the piezoelectric cantilever and impacts it, causing the piezoelectric structure to bend down which transfers the kinetic energy of the drop to piezoelectric mechanical deformation energy. During the experimental research, a PZT cantilever of the width, length, and thickness of 3 mm, 25 mm, and 0.58 mm, respectively, was used. The cantilever was fabricated from thick piezoelectric layers, each of them 65 μm thick, and a 0.25 mm thick carbon-fibre supporting layer. The total mass of the cantilever was 0.73 g [18]. As Fig. 1.10 b) presents, the drops were created and controlled artificially in the laboratory using tap water and a micro pump. The piezoelectric cantilever was fixed on one side and was free to move on the other. The cantilever output was connected to a variable resistance that could be varied from 50 Ω to 100 kΩ. The generated energy was measured using an oscilloscope [18].

The experimental results show that such an energy harvester can generate an output peak to-peak voltage of 0.8 V across the optimum load of 10 kΩ and produces 23 μW energy generated by a water drop of 0.23 g falling at a speed of 3.43 m/s. The experimental results show that this energy harvester can operate in the rainfall which has a number of drops up to 200 drops per second, corresponding to an output energy of 111 mW/cm^{-3} per second [18].

Another example of impact energy harvesting from natural sources could be an impact-based flow-induced-vibration wind energy harvesting system [21]. The scheme and prototype of such a system are presented in Fig. 1.11; it has a MEMS piezoelectric energy harvesting element fixed onto one end of the metal sheet and a

fixture where another side of metal sheet with MEMS is clamped. These elements form a flexible cantilever. The system also has a rigid stop fixed under the flexible cantilever and the bluff body fixed in front of the cantilever with respect to the wind direction [21].

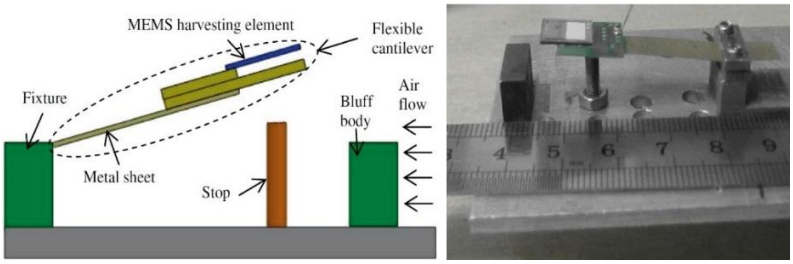

a) b)

Fig. 1.11 An impact-based wind energy harvesting system: a) scheme, b) prototype view [21]

Such a system operated on the following principle: wind blows by the bluff body and disturbs the flow field; the dynamic wind load on the flexible cantilever is enlarged. When the wind speed reaches a certain value, the so-called critical wind speed, the frequency of the dynamic wind load is close to the first natural frequency of the cantilever, which causes the cantilever to vibrate dramatically and impact the rigid stop repeatedly. These impacts generate force impulse and cause the MEMS piezoelectric energy harvesting element to vibrate dramatically with a frequency higher than the first natural frequency of the cantilever [21].

The impact-based wind energy harvesting system works in a frequency range from 20 Hz up to 750 Hz which corresponds to the critical wind speed from 3.2 m/s up to 15.9 m/s and generates the output power up to 1.6 μW.

The so-called Vibro-Impacting Piezoelectric Energy Harvester (VIPEH), developed by Lithuanian scientists V. Ostaševičius, R. Daukševičius, R. Gaidys et al operates on a similar principle. It consists of a cantilever beam of stainless steel covered by a piezoelectric layer operating in transversal (d_{31}) mode and a stopper beneath it which is located at certain distance from the fixture of the cantilever [22]. The principal scheme and experimental setup view of the VIPEH are presented in Fig. 1.12.

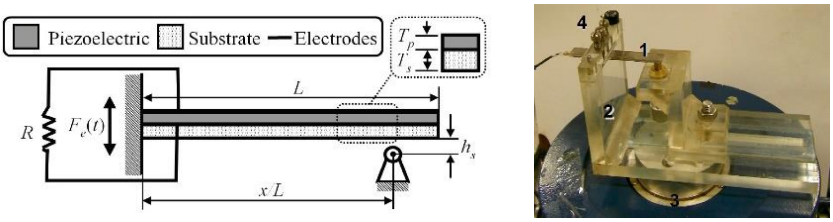

a) b)

Fig. 1.12 The Vibro-Impacting Piezoelectric Energy Harvester: a) the principal scheme [22], b) the experimental setup view [23]: 1 – vibration energy harvester prototype, 2 – harvester clamp, 3 – electromagnetic shaker, 4 – accelerometer

The VIPEH (Fig. 1.12) is excited with harmonic excitation and due to the cantilever impacting the stopper, it starts to vibrate at the third resonant frequency. Therefore, the efficiency of such an impact energy harvester rises from 16% to 90% at lower resonant frequencies when comparing them to traditional energy harvesters without a stopper. Moreover, such design of the cantilever energy harvester allows scavenging the energy independently from the frequency of the excitation [23].

Impact energy harvesters from various human motion are also widely researched [24-26]. One of them is used for impact-driven energy harvesting from human motion – a walking scheme and the prototype view are presented in Fig 1.13 [24].

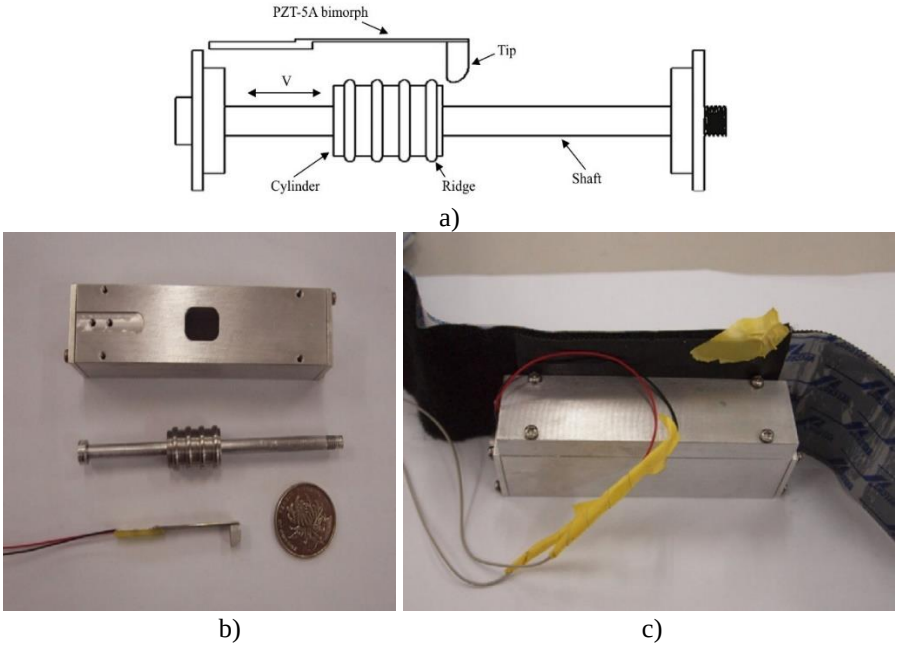

Fig. 1.13 Impact-driven piezoelectric energy harvester from human motion [24]: a) the scheme b) the prototype view c) the prototype mounted on a human's leg view

This harvester consists of a ridged cylinder which can slide freely on a shaft and PZT bimorphs with a tip which can be fixed in parallel with the cylinder. For protection from ambient conditions, the system is placed in a protection box, in this case, made of aluminium. When the cylinder (the entire system) is driven by external excitation, in this instance, the movement of a person's leg, the ridge on it impacts the tip and the PZT bimorph vibrates with its resonant frequency after they separate. This way, the stored mechanical energy is converted into electrical energy and transferred to the external circuit. The asymmetric design of the tip increases the vertical impulse force when the cylinder is moving backwards [24].

The impact-driven piezoelectric energy harvester from human motion generates the maximum power of 51 μW when it is mounted on the leg of a person walking at a speed of 5 km/h and has 265.5 Hz resonance frequency.

Another example of an impact energy harvester from human motion is the triaxial ball-impact piezoelectric converter (BIPC) for autonomous sensors harvesting energy from vibrations and human motion and is presented in Fig 1.14 [26].

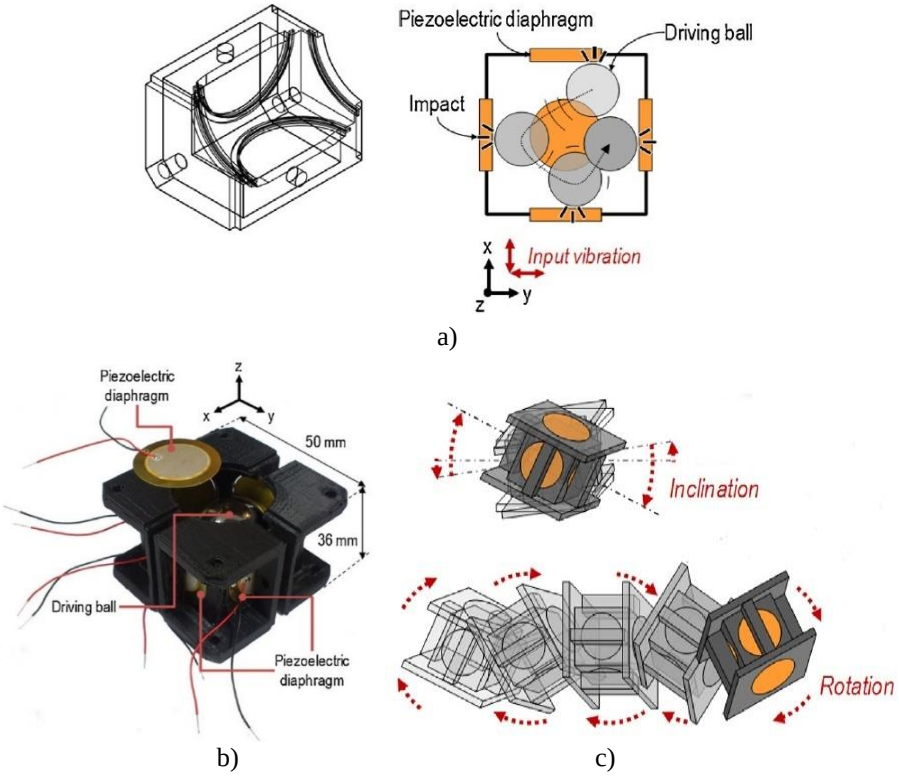

Fig. 1.14 Triaxial BIPC [26]: a) cross-section view b) fabricated prototype view c) excitations to which the converter is sensitive

In general, the working principle of the triaxial BIPC is based on the working principle of the piezoelectric vibrator [19]. The harvester has a stainless steel ball which can move inside a 3D structure, fabricated by using a rapid-prototyping 3D printer, bounded by multiple piezoelectric elements into the slots of the 3D structure (see Fig. 1.14). The ball is not rigidly or elastically connected to the structure, thus it impacts the piezoelectric elements as soon as the input excitation causes the ball to move by rolling or jumping. It is important that such a system does not limit the kinds of mechanical excitation which can generate impacts against the piezoelectric elements, as opposed to what happens when using resonant driving elements. In addition, rebounds of the ball against the piezoelectric elements can divert the path of the ball and generate unpredictable subsequent impacts [26].

The triaxial BIPC operates in a frequency range from 10 to 100 Hz; the device has been tested tied to the ankle of a person during walking and running activities. The maximum power is generated when the person runs at 7 km/h; the generated power reaches 16 mW.

Rotational piezoelectric wind energy harvesting using an impact-induced resonance [27] is also based on a typical impact energy harvester scheme (see Fig. 1.5). Such a harvester is called a piezoelectric windmill. Its scheme and prototype view is presented in Fig. 1.15.

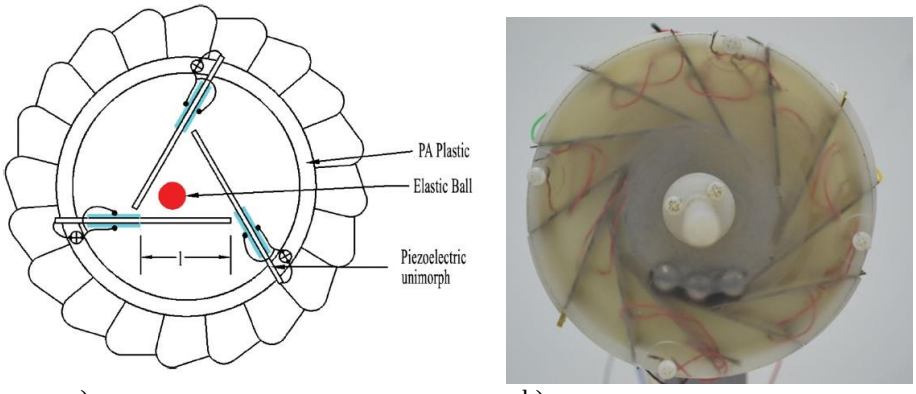

a) b)

Fig. 1.15 A piezoelectric windmill [27]: a) scheme b) prototype view

As Fig. 1.15 demonstrates, such a piezoelectric energy harvester uses impact-induced resonance to enable effective excitation of the intrinsic vibration mode of piezoelectric cantilevers and thus obtain the optimum deformations, which are beneficial for the piezoelectric transduction. The impact force is introduced through the formation of a piezoelectric bimorph cantilever polygon, which is fixed at the circumference of the internal surface of the rotating fan. The elastic balls are placed inside the polygon. When wind rotates the device, the balls impact the piezoelectric cantilevers and they start to vibrate at their first resonance mode; thus electricity is generated by the piezoelectric effect [27]. As in most piezoelectric energy harvesters [15, 18, 21, 24], piezoelectric bimorphs were chosen to be the energy-harvesting units in this harvester.

Such an impact energy harvester generates output power of up to 613 μW at the rotation speed of 200 rpm with an inscribed circle diameter of 31 mm. This means that it can operate at a frequency range up to 3.33 Hz. The generated electricity can be stored in a super capacitor and can be used to power wireless sensors in remote locations [27].

Impact excitation could also be observed in various metal machining techniques. One of them is described in Lithuanian researchers' V. Ostaševičius, V. Markevičius, V. Jūrėnas et al. work and is called cutting tool vibration energy harvesting for wireless sensors applications [28]. With this energy harvesting technique, the impact is obtained from the unavoidable flexibility between the cutting tool and the workpiece. This is related to the cutting force action which is dependent on the regimes of manufacturing as well on the tool wear. The energy harvester – the circular piezo bimorph with resonant frequency of ~ 4 kHz was integrated into the structure of the cutting tool and experimentation showed that such a technique works properly in 3.9-4.5 kHz frequency range of cutting tool vibrations [28].

As a literature review of energy harvesting systems and piezoelectric impact energy harvesting systems shows, traditional energy harvesters which are used for energy harvesting from the surroundings are based on resonant behaviour. This means that they generate the maximum power when they are excited with a harmonic excitation signal, at a frequency close to the resonant frequency of the harvester. Thus if the frequency of ambient vibrations does not correspond with the resonant frequency of the harvester, the amount of generated energy significantly reduces. That is why most of them could not be used in practice since the excitation frequency of ambient vibrations is accidental. Because of this and the fact that impact can excite resonance under any operating conditions, energy harvesters which are excited by impact are developed over the last decade. The next section presents the methods of mechanical impact generation and areas of their usage.

1.4. Mechanical impact generation methods

Nowadays mechanical impact, or in other words – mechanical shock phenomena are rather diverse due to the fact that collisions of moving bodies are inherent on all levels of the universe – from microcosm up to space [29]. There are two basic types of impacts – harmful, e.g. transport accidents, etc. and useful – those, which are involved in a lot of technical processes, e.g. in the field of non-destructive evaluation of concrete [30], for diagnostic system of composite materials [31], for structure borne sound analysis, for shockwave generation [32], for impact energy harvesting [9, 12-16, 18-21, 24-27], nano-positioning devices [33], etc. These facts show that the problem of impact is very important for designers, engineers, sportsmen, etc.

All the aforementioned processes require a well-defined mechanical impact (or shock). In general, a shock could be defined as a complex physical phenomenon which occurs when two or more bodies collide with each other; some of its characteristics include a very short duration, high force levels reached, rapid dissipation of energy and large accelerations and decelerations present [34]. For this purpose, a wide variety of shock generators are developed. There are two basic types of impact generators: mechanical and non-mechanical. The first ones can be operated by a machine (e.g. pneumatic, hydraulic) or by a person. The latter type of shock generators is usually based on the hammer-anvil principle [35].

The most commonly used generator is a simple impact hammer with feedback, usually used for testing structural behaviour. An impact from such a hammer imparts to the test structure a smooth excitation spectrum over a broad frequency range. The impact force is measured with the built-in force transducer and the structural response is measured with an additional accelerometer fitted to the test object. The frequency bandwidth of the first lobe of an impact spectrum is inversely proportional to the width of the impulse. This is determined by the duration of the impact force, which depends on factors such as the mass and structure of the hammer, and the hardness of the contacting surfaces – the hammer tip and the impact area [36]. Therefore, most of impact hammers have changeable tips of different hardness in order to obtain the required impact spectrum. An illustration of one of such impact hammers with changeable tips of different hardness are presented in Fig. 1.16.

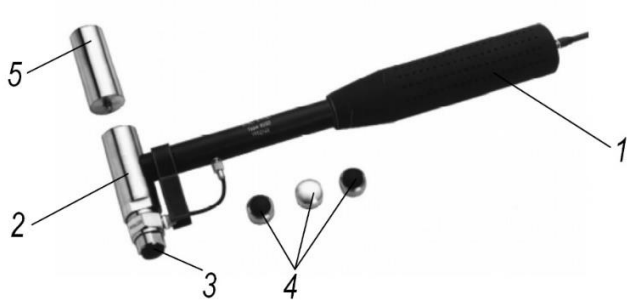

Fig. 1.16 An impact hammer with changeable tips of different hardness [36]: 1 – handle, 2 – impacting mass, 3 – mounted plastic tip, 4 – extra plastic, steel and rubber tips, 5 – additional mass

Fig. 1.17 presents the impulse shapes for the variety of the hammer tips of different hardness.

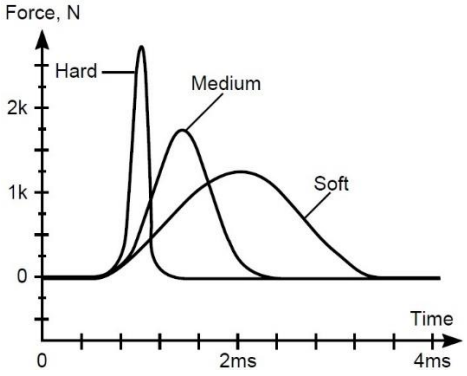

Fig. 1.17 Impulse shapes for various hardness of the hammer tip [36]

As Fig. 1.17 shows, when the hammer tip is soft, the generated impulse duration is long and amplitude is low in comparison with tips which are medium and hard when the impacting area is the same. Using such a hammer, the generated impact parameters of amplitude and duration could also be changed by using additional mass. It can also be concluded that the highest amplitude and frequency is generated when the hammer has a hard tip.

Despite their simple design and usage, mechanical shock generators have some disadvantages. Since they are based on the hammer-anvil principle, they allow only limited control of the shock amplitude and pulse width with a limited repeatability of the applied shocks. For instance, depending on how the operator releases the hammer pendulum, the shock amplitude can change up to 10% and more. Moreover, because the impact between the hammer and impact area is not completely elastic, a certain wear of both parts can be observed; it means that even if such parameters like the kinetic energy of the hammer were well-controlled, the shock amplitude and width would change from shock to shock [35]. The final disadvantage of mechanical shock

generators could be the need to change hammer tips every time when different impact parameters, such as the generated impulse width and amplitude are desired.

The non-mechanical shock generators are usually based on the piezoelectric principle, where a piezoelectric actuator is used as generator [32]. A scheme of one such shock generator is presented in Fig. 1.18. It shows that this shock generator (see Fig. 1.18) has a built-in piezoelectric stack made of several piezoelectric layers, usually rings. The impact is generated by applying a high-power electrical pulse to the piezoelectric layers where the it is instantaneously converted into potential mechanical energy; this way, the piezoelectric stack resembles a compressed spring, which starts its rapid expansion towards the elongated state which causes mechanical shock on the impact area [37].

In a configuration without the seismic mass (see Fig. 1.18 a)), the piezoelectric stack expands symmetrically to its centre of mass and only the forward impulse is directed onto the impacting area, thus the recoil impulse is not further used.

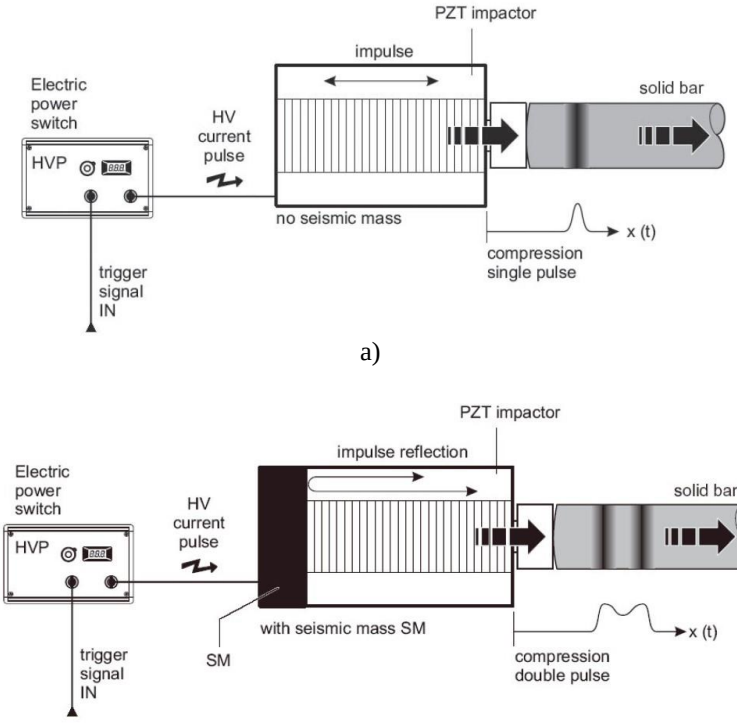

Fig. 1.18 A scheme of a piezoelectric shock generator: a) configuration without any seismic mass b) configuration with seismic mass [37]

The configuration with seismic mass is derived from the one without seismic mass by simply adding the mass to the bottom of the piezoelectric shock generator (Fig. 1.18 b)). In such configuration, the recoil impulse is reflected at the seismic mass into a forward direction what causes the double-impulse generation. This

configuration generates a content of impact energy nearly double than the configuration without any seismic mass [37].

Another scheme of a piezoelectric impact hammer of similar configuration, used for shock generation for non-destructive testing of concrete structures is presented in Fig. 1.19. It is composed of three basic parts: the PZT stack, the waveguide, and the flying head [30]. The operating principle of such a hammer is the following: a high voltage pulse generates voltage to the PZT stack and causes its displacement. The displacement amplitude is amplified by the wave guide and transmitted to the flying head, which directly impacts the testing surface.

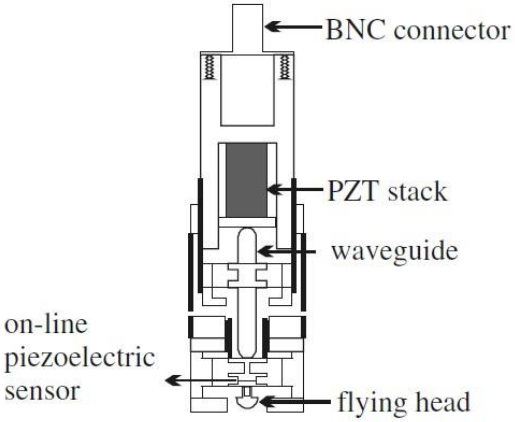

Fig. 1.19 A scheme of a piezoelectric shock generator used in non-destructive testing of concrete structures [30]

Both piezoelectric shock generators have a common disadvantage – the impacting surface impacts the testing area with a not completely elastic shock which causes both the shock head and the testing surface to wear. This disadvantage is non-existent in the "Spektra Hop-Ms" shock generator developed by "SPEKTRA Schwingungstechnik und Akustik GmbH" and used in Hopkinson-Bar [35] – a system which can be used to generate shocks with very high amplitudes up to 1000000 m/s^2 and more. A scheme of "Spektra Hop Ms" shock generator is presented in Fig 1.20 [35].

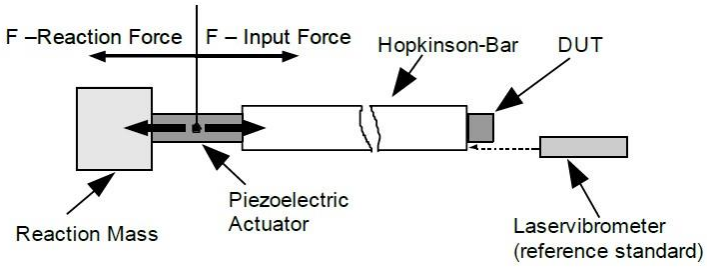

Fig. 1.20 A scheme of "Spektra Hop-Ms" piezoelectric shock generator [35]

In this type of shock generator, the piezoelectric stack is attached with one end directly to the front surface of the bar and has additional reaction mass attached on its other end. Such a construction creates the ability to completely control the shock parameters with electrical signals and does not have any parts which would mechanically wear [35].

One more type of non-mechanical shock generator is based on explosion. Such shock generators cause impact by the power of explosion [38, 39]. A scheme of explosively driven shock generator is presented in Fig. 1.21.

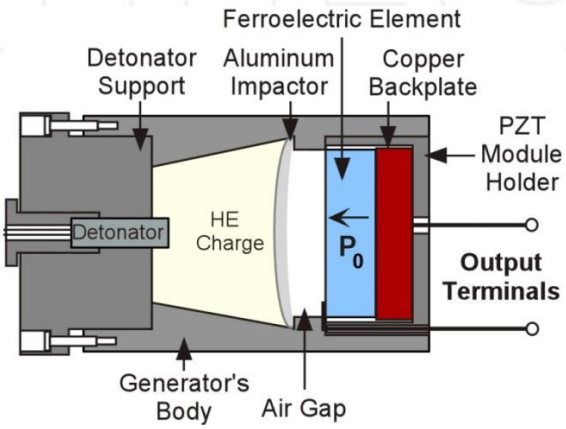

Fig. 1.21 A scheme of explosively driven shock generator [39]

Such a shock generator (Fig 1.21) consists of a ferroelectric element, an explosive chamber, a metallic impactor (a flyer plate), and output terminals. Here, a metallic impactor (flyer plate) is accelerated to high velocity by the detonation of a high explosive charge and impacts the face plate of the ferroelectric element; this initiates a shockwave towards the body of the ferroelectrics [35]. This impactor can generate extremely high impacts, however its construction is rather complicated with regards to the manufacture and usage – explosions are dangerous and difficult to control. This means that using this type of shock generators, it could be rather complicated obtaining repeated equal explosion and the same shock.

As a review of previous literature on the methods of mechanical impact shows, such phenomena could be used for impact energy harvesting as well as in other areas of application. On the other hand, one of the disadvantages of conventional impact energy harvesting systems [9, 12-16, 18-21, 24-27] is the fact that the piezoelectric material is poorly protected from impact. This is especially relevant when speaking of systems which directly impact the piezoelectric material. This means that after a few energy generation cycles the piezoelectric material could crack or totally shatter. This demonstrates the need for protecting the piezoelectric material.

In order to obtain a higher resonant frequency of the energy harvester, protect piezoelectric materials from impact, and to increase excitation impact energy, it is possible to use horn-type waveguides, which are an important part of the piezoelectric transducer, as resonators.

1.5. Types of horn-type waveguides and their areas of application

In recent years, the use of various piezoelectric transducers is increasing. Based on their operating frequency, piezoelectric transducers can be categorized into sonic, ultrasonic, and megasonic and the devices can vary significantly with regards to their design and function.

The sonic transducers operate at an audible frequency range, normally, less than 20 kHz, and can be designed to operate in a bending mode; examples of such transducers are the bimorph cantilever systems or buzzer transducers [40]. The ultrasonic transducers usually operate at a frequency range between 20 kHz and 200 kHz. Such transducers could be designed in both bending [41] and longitudinal [42, 43] modes and could be used in a wide variety of applications, i.e. ultrasonic machining technologies [44], ultrasonic welding [43], etc. The megasonic transducers operate in the frequency range of MHz and they are mostly designed to operate in thickness mode. The most popular area of use for such transducers is megasonic cleaning systems [44], since they offer such advantages as gentle and controllable cavitation, which will incur less damage on the cleaned surface if compared with other categories of transducers; therefore, megasonic transducers are more suitable for precision cleaning [40].

The capabilities of any horn-type piezoelectric transducer is closely related with the operating frequency, the vibration mode, and the wavelength. As a result, different types of transducers can achieve perform differently in a wide range of applications. When all three categories of piezoelectric transducers are compared, only the ultrasonic transducer with longitudinal operating mode is able to simultaneously achieve both a large vibration amplitude and a high energy density (power) [40]. For this reason, ultrasonic transducers designed for operating in the longitudinal mode, which usually uses a certain type of waveguides, the so-called horn-type waveguides (or ultrasonic horns), are nowadays the most popular in various areas of application and are called horn-type piezoelectric transducers.

A typical scheme of a horn-type piezoelectric transducer is presented in Fig. 1.22. The main principle of such a horn-type ultrasonic piezoelectric transducer is converting high frequency electric power to mechanical vibration power with the vibrator; then, a steady amplitude of mechanical vibration is reached [45].

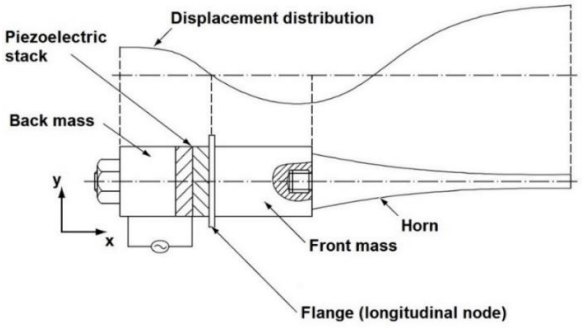

Fig. 1.22 A typical scheme of horn-type piezoelectric transducer [46]

In general, a typical horn-type piezoelectric transducer consists of four parts (see Fig. 1.22): the back mass, the piezoelectric stack, the front mass, and the horn-type waveguide (horn). The piezo stack in this scheme operates as the vibration generator and is clamped between the back and front masses. The horn, which is coupled to the front mass, amplifies vibrations by increasing the wave density of the energy generated from the piezoelectric stack [40]. This is achieved by reducing the cross-section along the length of the horn [47].

Since the output amplitude of the vibrator, usually the piezo stack, is very small, the horn-type waveguide is usually designed and operated in harmonization to amplify the output amplitude. It is very important that the horn-type waveguide resonant frequency should correspond or be close to the excited transducer frequency; otherwise, this will cause the vibration modal change, affecting the energy transfer and leading to a decline in amplification [45].

Depending on applications for which the horn-type piezoelectric transducers are designed, the horn-type waveguides could vary in shape and be made from a wide variety of materials, usually, metals that have high fatigue strengths and low acoustic losses [48]. Titanium has the best acoustical properties of all high-strength alloys. Aluminium has excellent acoustical properties but because of its lower strength and hardness, it is subjective to wear and fracture when used for highly stressed designs. Usually, it is preferred for making horn-type waveguides of simple geometry with low stress [47]. Moreover, in order to maximize the vibration amplitude of horn-type piezoelectric transducer, the horn can be designed with multiple sections. Each section could have the same or different shapes. Despite the shapes and applications of the horn-type waveguide, its total length should be usually integer multiple of the resonant wavelength [48].

Ultrasonic horn-type waveguides are used in various atomizers [49], ultrasonic welding devices [43, 50, 51], parts machining technologies such as grinding, drilling, cutting, etc. [52-54], polymer sheet formatting [55], automatic systems for beverage pasteurization [56], in the medical field, such as ultrasonic surgery [57-58], for the construction of ultrasonic motors [59], etc.

Ultrasonic horn-type waveguides with different shapes have been proposed and investigated by many researchers. For example, a planar Bezier-profiled shape horn-type waveguide was used for reducing penetration force in ultrasonic cutting [54]. Catenoidal shape horn-type waveguide was used in a spot welding system for thin metal strips in order to strengthen the welding seam [43]. Arc linked stepped shape horn was applied for driving the tool motion for machining metal or cutting tissue [45]. The simpler stepped horn was used in the system for pasteurization of sour cherry juice [56], ultrasonic welding [50], fine atomization of liquids [9]; the planar stepped horn was used in the ultrasonic scalpel for the dissection and coagulation of tissue [58]. Gaussian, as well as cylindrical, Bezier, catenoidal and stepped shape horn-type waveguides were used in a system for polymers joining processes [47]. Exponential shape horn-type waveguide was used in ultrasonic welding of dissimilar metals by vibrations [60] and for grinding difficult-to-cut materials [52]. The

sinusoidal shape horn-type waveguide was designed for impedance transformation [54].

Despite the wide variety of horn-type waveguide shapes, the most commonly used horns are conical, exponential, catenoidal, stepped, and Gaussian [54]. Numerous researches [47, 54] showed that the stepped horn-type waveguide provides the greatest displacement amplification, the catenoidal produces less and the exponential and conical ones show the lowest displacement amplification.

The horn-type waveguide amplifies vibrations by increasing the wave density of energy by reducing the cross-section along the length of the horn-type waveguide. All investigations were carried out when the horn-type waveguide was excited with harmonic excitation on a surface with greater cross-sectional area and the output displacement was obtained on a smaller cross-sectional area [40-60].

The literature review presented above reveals that all impact energy harvesters generate an electric signal in a relatively low frequency range and the signal is transmitted to traditional "power banks", such as batteries, capacitors, etc. In order to introduce a novel piezoelectric impact energy harvester which could generate ultrasonic frequency range burst-type signal and transmit the generated signal directly to some kind of receiver, the need of such technique should be determined. Hence, the next section reviews the basic features and traditional control techniques of an ultrasonic motor.

1.6. Basic features and control techniques of an ultrasonic motor

The application of USM in ultra-precision devices has been gradually increasing in various technical fields such as robot joints, high precision devices, micro robots developed by Lithuanian scientists R. Bansevičius et al. [61], automated focusing systems of cameras, MEMS [62, 63], and mass-consumer devices [64].

There are two basic types of ultrasonic piezoelectric motors: the rotary motor [62-63, 65-66] and the linear motor [67-69, 70]. Piezoelectric motors have many advantages over conventional electromagnetic motors, including a high torque at low speed, a large holding force without a power supply, silent operation, simple structure, and no electromagnetic noise generation [69]. Piezoelectric motors produce linear or rotary motions by their resonance vibrations excited via converse piezoelectric effect of the piezoelectric elements [61, 65]. Due to this fact the frequency of piezoelectric motors excitation signal should correspond with the resonant frequency of the motor vibrator (stator), usually made from PZT, which generates a standing or travelling wave [71]. In order to obtain constant rotation or a linear operating mode of the piezoelectric motor, the excitation signal should be harmonic, and in order to obtain step motion, the excitation signal should be burst-type [72]. The driving speed of the motor depends on both the amplitude and frequency of the excitation signal, thus the maximum speed or step size is obtained when the frequency of the burst-type excitation signal corresponds with the resonant vibration frequency of the piezoelectric motor [72, 73].

Most of piezoelectric motors used for various purposes are excited with signals, which are generated by signal generators [65, 67-69, 71-73]. This kind of control

requires electric power supply. Therefore, the piezoelectric motors could not be used in areas where traditional power supplies or grid are unavailable.

1.7. Conclusions of the section

This section has presented a literature review regarding vibrational and impact energy harvesters, mechanical impact methods, horn-type waveguides, and techniques for controlling an ultrasonic motor control.

The following conclusions are formulated from the literature review:

- Vibrational energy harvesters used for energy harvesting from the surroundings are based on resonant behaviour. They generate maximum energy power when they are excited with a harmonic excitation signal, the frequency of which is close to the resonant frequency of the harvester. Thus if the frequency of ambient vibrations does not correspond with the resonant frequency of the harvester, the amount of energy generated significantly reduces.
- Some common energy harvesters are based on a cantilever structure and others use impact directly to the piezoelectric material. The main disadvantage of the existing impact energy harvesters is that they generate the signal in a low frequency range – up to 4 kHz. Another disadvantage, especially of the harvesters which directly impact the piezoelectric material, is that the piezoelectric material is poorly protected from the impact.
- There are two basic types of impact generators: mechanical and non-mechanical. The first type is commonly based on the hammer-anvil principle, and allows only limited control of the generated shock amplitude and pulse width with limited repeatability of the applied impacts. The second type is usually based on the piezoelectric principle, where a piezoelectric actuator is used as a generator, or driven by explosion.
- The main purpose of a horn-type waveguide is to amplify the displacement amplitude by increasing the wave density of energy by reducing the cross-section along the length of the horn. Due to this, all of horn-type waveguides were investigated when the vibrations which should be amplified were harmonic signals. They were applied on the surface of the horn with greater cross-sectional area while the amplified displacement was obtained on the surface with a smaller cross-sectional area of the horn-type waveguide.
- The majority of piezoelectric motors used for various purposes are excited with signals, which are generated by signal generators. This kind of control requires electric power supply. Therefore, the ultrasonic motors could not be used in areas, where traditional power supplies or grid are unavailable.

Overall, this section has introduced a need of a novel piezoelectric impact energy harvester for burst-type signal generation which should have a certain shape resonator – a horn-type waveguide between the impact generator and the piezoelectric transducer in order to protect it from damage. Moreover, a novel piezoelectric impact energy harvester could produce the electric signal directly to a receiver, in this case, an ultrasonic motor. Such an impact energy harvester could operate as an alternative method for ultrasonic motor control when traditional methods, such as signal

generators, are unavailable or damaged. Therefore, the aim of this research is to design and develop a piezoelectric impact energy harvester for burst-type signal generation and adapt it for the drive of the ultrasonic motor.

The following objectives are set in order to reach the aim:

1. to design and theoretically investigate a novel piezoelectric impact energy harvester for burst-type signal generation by modelling a mechanical impact and horn-type waveguide with harmonic and impulse excitation when it is applied on a surface with a smaller cross-sectional area.
2. to experimentally investigate a piezoelectric impact energy harvester for burst-type signal generation, including experimental research of mechanical impact, horn-type waveguides, and ultrasonic motor control.
3. to create and investigate a methodology for designing an impact energy harvester for a certain ultrasonic motor.

2. THEORETHICAL INVESTIGATIONS OF A PIEZOELECTRIC IMPACT ENERGY HARVESTER FOR BURST-TYPE SIGNAL GENERATION

2.1. The structure and operating principle of a piezoelectric impact energy harvester for burst-type signal generation

A novel piezoelectric impact energy harvester is intended for burst-type signal generation and is applied for direct driving of an ultrasonic motor (USM). The principal scheme of the investigated piezoelectric impact energy harvester fort burst-type signal generation which could operate as an alternative method for ultrasonic motor control when traditional methods, such as signal generators are unavailable or temporarily damaged, is presented in Fig. 2.1.

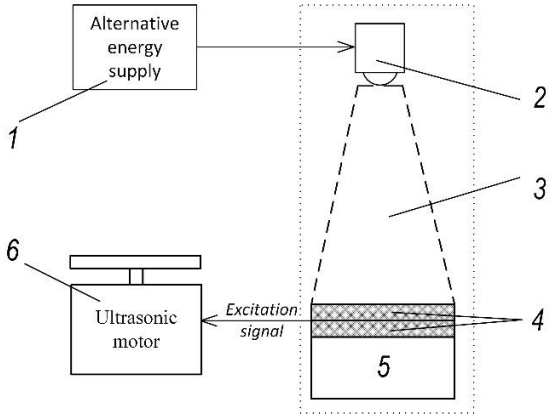

Fig. 2.1 The principal scheme of the investigated piezoelectric impact energy harvester for burst-type signal generation: 1 – power supply, 2 – shock generator, 3 – horn-type waveguide, 4 – piezoelectric transducer, 5 – backing mass, 6 – USM

Such piezoelectric impact energy harvester for burst-type signal generation consists of an energy supply 1, e.g. thermoelectric, solar cells, human muscle force, etc., a shock generator 2, e.g. a hammer-type impactor, a piezoelectric shock generator, etc., a horn-type waveguide 3 designed for a particular piezoelectric motor, a Langevin-type [45] piezoelectric transducer 4 made of piezoelectric rings, a backing mass 5, and a controlled USM 6.

In the presented piezoelectric impact energy harvester, the energy is generated by a mechanical shock on the surface of a horn-type waveguide with a smaller cross-sectional area. The energy is transmitted onto a surface with a greater cross-sectional area of the horn-type waveguide, thus the energy from the excitation shock is dispersed and surface displacement (with greater cross-sectional area) is obtained. This surface transmits displacement and energy throughout the entire surface area to the Langevin-type piezoelectric transducer. The surface area corresponds with the piezoelectric transducer dimensions, thus the piezo electric transducers can generate an electric signal for USM control with the highest amplitude and a certain impulse duration. Moreover, the horn-type waveguide used in such a piezoelectric impact

energy harvester operates as protection from impact-induced crash or damage of the piezoelectric rings.

Another advantage of such an energy harvester is that it operates as an alternative method for ultrasonic motor control when traditional methods, such as signal generators are unavailable or temporarily damaged. This decreases the risk of ultrasonic motor exploitation failure when traditional systems are damaged or unavailable in areas such as nature, space, etc. Since the presented piezoelectric impact energy harvester for burst-type signal generation can drive both rotational and linear USMs, such a control method allows to increase the reliability of precision positioning drive exploitation.

In order to obtain the desired excitation signal for certain USM control, the generated signal parameters can be adjusted in two ways: by altering the mechanical shock parameters, such as the shock amplitude and the duration or by altering the shape of the horn-type waveguide, e.g. geometrical structure, length, etc.

2.2. The theory of modelling and simulation of impact mechanics

Analytical models for impact mechanics can be classified into four categories [74]:

1. Models based on rigid-body dynamics;
2. Models for propagation of stress waves in perfectly elastic materials;
3. Models for propagation of stress waves through solids which are not perfectly elastic, such as shock and plastic waves;
4. Nonlocal or non-classical models which can describe spallation and fragmentation upon impact.

From the point of computing the solutions of initial and boundary value problems generated by the analytical models mentioned previously, the numerous methods used in literature fall under the following classifications: element-based (e.g., finite-element methods), finite-difference methods, and mesh-free methods (e.g., smooth particle hydrodynamics, element-free Galerkin, Peridynamics). Depending on the referential, they can be Lagrangian (the computational grid follows the material), Eulerian (the computational grid is fixed and the material flows through it), or arbitrary Lagrangian-Eulerian codes [74].

Rigid-Body dynamics model. In rigid dynamics, one assumes that when a force is applied to a point in a body, all the points in that body are set in motion instantaneously and the relative distances between any two material points never change. This rigid-body dynamics model is based on the impulse-momentum law for rigid bodies, adjusted with phenomenological observations of elastic and inelastic restitution. The loss of energy that takes place between two bodies at impact is taken into account by means of the coefficient of restitution. The principal calculation scheme of this model is presented in Fig. 2.2. The coefficient of restitution e is defined [74]:

$$e = \frac{(v_{2f} - v_{1f})}{(v_{20} - v_{10})}; \tag{2.1}$$

where v_{1f}, v_{2f} – velocities of the colliding masses m_1 and m_2 after impact, v_{10}, v_{20} – velocities of the colliding masses m_1 and m_2 before impact, m_1 and m_2 – masses of colliding bodies.

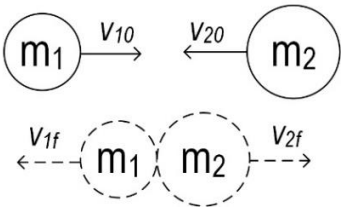

Fig. 2.2 The principal calculation scheme of Rigid-Body dynamics model

The rigid-body dynamics model for impact has serious limitations. It cannot describe transient stresses, forces, or deformation produced. When the forces of contact are applied over very short periods of time and local deformation is significant, the effect of stress waves propagating inside the body must be considered for a better approximation of the reality [74].

Stress Wave Propagation in Perfectly Elastic Media. Impact generates stress waves that propagate strain energy away from the region of impact. If the energy transformed into elastic vibrations amounts to a large fraction of the total energy, the rigid-body dynamics model is not applicable any more, and the approach based on wave propagation (or the transient model) is more suitable [74].

Using this model, the longitudinal impact of two rods, the transverse impact of a mass on a beam, the tensile impact of a mass on a rod, and the effect of viscoelasticity on impact behaviour is investigated. The principal calculation scheme for this model is presented in Fig. 2.3.

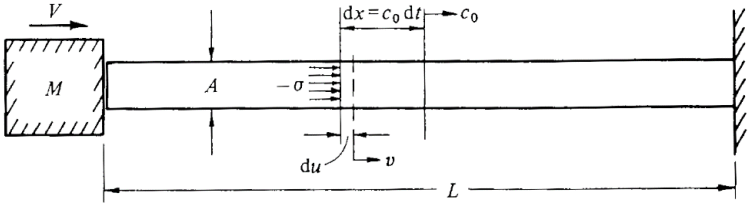

Fig. 2.3 The principal calculation scheme of stress wave propagation in perfectly elastic materials model [58]

For example, the displacements of a rod produced by an impulsive load can be expressed in a form representing standing waves as [74]:

$$u = -\left\{\frac{\sigma_0 t^2}{2\rho L} + \frac{2\sigma_0 L}{\pi^2 E}\sum \frac{(-1)^i}{i^2}\cos\left(\frac{i\pi x}{L}\right)\left[1 - \cos\left(\frac{i\pi c_0 t}{L}\right)\right]\right\}, \qquad (2.2)$$

with the initial and boundary conditions as:

$$v = \frac{\partial u}{\partial t} = 0, \quad t = 0, \quad 0 \le x \le L; \qquad (2.3)$$

$$v = \frac{\partial u}{\partial x} = 0,\ x = 0,\quad t \geq 0;\ \frac{\partial u}{\partial x} = -\frac{\sigma_0}{E}, x = L,\ t \geq 0; \tag{2.4}$$

where L – length of the bar, σ_0 – compressive stress applied at $x = L$ at $t \geq 0$, E – Young's modulus, ρ – density of the bar, v – velocity, t – time.

For high velocity impacts, the transient model must be used in order to capture the real time stress wave history. However, the transient model, which does not consider contact deformation, cannot capture the local deformation due to projectile impact. The contact stresses generated at the impact of two bodies allow for determining the contact duration and local deformation [74]. Hertz theory has been used to determine the dependence of force on deformation and to predict the contact duration and the maximal indentation [75]. Normal contact force is defined as:

$$F = K_c \alpha^{\frac{3}{2}}; \tag{2.5}$$

where K_c – contact stiffness, α – normal deformation between colliding bodies, F – normal contact force.

Combining equation (2.5) with the equation of motion of the corresponding beams or plates, the contact force history and contact duration can be solved.

Stress Wave Propagation in Solids That Are Not Perfectly Elastic: shock and plastic Waves. The elastic contact impact model (Fig. 2.3) can be extended to the cases where the plastic deformation occurs in a contained area. The force–deformation equation is often modified by adding a damping term to reflect dissipation in the contact area, thus allowing to effectively model the contact area as a spring-damper system [74]:

$$F = F_c(\alpha) + F_v(\alpha, \dot{\alpha}) + F_p(\alpha, \dot{\alpha}); \tag{2.6}$$

where F_c – elastic or conservative part of the contact force, F_v – viscous damping part, F_p – dissipation due to plastic deformation, α and $\dot{\alpha}$ – accordingly, deformation and the deformation rate between the target and projectile.

Kinematic and mechanical constraints must be satisfied at the contact surface between the colliding bodies. The mechanical constraints are defined using the laws for normal and tangential forces generated during the contact process. The Lagrange multiplier method and penalty method are the two methods most frequently used for implementing contact-impact algorithms and analysing contact-impact problems. Friction is most often modelled using the Coulomb's law, and the normal contact force is mostly modelled using the Hertz contact law [74].

When the plastic strains become large and prevalent in the target, the elastic wave propagation model can no longer be applied to analyse such impact problems. There are two options in such situations: the hydrodynamic theory of the behaviour of solid bodies, and the theory of plastic wave propagation. In the hydrodynamic theory, the permanent deformation takes place with a sudden change of density. An equation of state which relates pressure to density changes and temperature or entropy is needed in addition to the laws of conservation of momentum, energy and mass [76].

The theory of plastic strain propagation, considers the material incompressible in the plastic domain and a temperature-independent equation of state [74].

Nonlocal models. Nonlocal models can capture size effects, adjust the strain softening problems and avoid mesh sensitivity in numerical computations. Hence, a large variety of these models have been introduced over the past years [74].

Peridynamic formulation is one of nonlocal methods developed specifically for dealing with fracture and dynamic failure. One of the main features of peridynamics is the spontaneous formation of discontinuities, which can be effectively used to capture material behaviour at impact, e.g. spallation and fragmentation processes. Peridynamics replaces the spatial derivatives from the equations of motion of classical mechanics with an integral of force density over a certain volume, thus eliminating the mathematical and practical difficulties of treating strong discontinuities, such as cracks [74]:

$$\rho\ddot{u} = \int_R f(u(x',t) - u(x,t), x' - x)dV_{x'} + b\,; \tag{2.7}$$

and f is defined as:

$$f(\eta,\xi) = \frac{\partial w}{\partial \eta}(\eta,\xi), \text{ here } \eta = u' - u,\ \xi = x' - x; \tag{2.8}$$

where f – pairwise particle force (per volume squared), w – pair wise elastic potential for micro elastic materials, u – displacement vector, b- body force, ρ – density.

In the peridynamic model, as in other nonlocal continuum theories, all forces are long-range [74].

In order to simulate impact phenomena, a wide variety of computational techniques have been developed. One of the most widely used computation methods is finite-element method (FEM). This method uses the most popular computational software such as ANSYS, ABAQUS, LS-DYNA, SOLIDWORKS, etc. Other methods which could also be used for impact simulations are Finite-difference method (FDM), Mesh-Free Methods, Peridynamics, etc. [77-79].

2.3. Modelling the mechanical impact

To investigate mechanical impact parameters, such as the dependency of amplitude and duration (frequency) on different material properties of colliding bodies, a mechanical impact 2D-axis symmetry computational model was created using ANSYS explicit dynamics software. The impacting body was simulated as a sphere, made of steel 1006, which impacts the plate with initial velocity; the plate is fixed at the bottom and is made of different materials – steel 1006 and aluminium AL6061-T6. It should be noted that when boundary conditions are the same, different material properties produce different impact parameters, such as impact shock duration and amplitude.

The computational model with boundary conditions and gauge points consists of 420 finite elements with 481 nodal points; it is presented in Fig. 2.4.

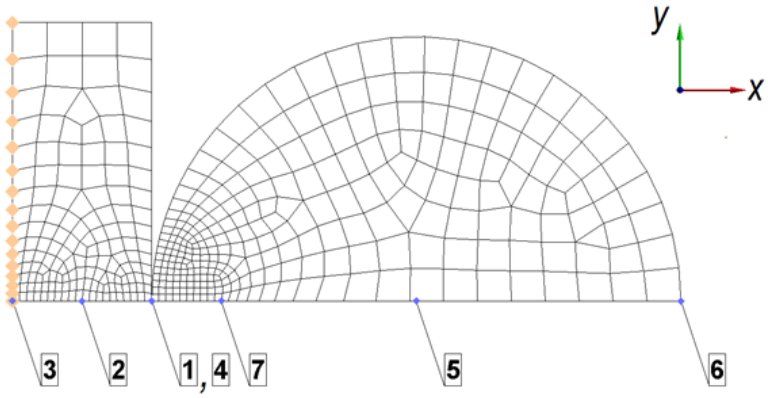

Fig. 2.4 Computational model of mechanical impact created using ANSYS explicit dynamics software. Here 1-7 gauge points located accordingly on the impacting plate and the sphere.

The modelling was carried out twice: the first modelling was carried out with a sphere and a plate, both made of Steel 1006. The second modelling was done with Steel 1006 sphere, and plate made of aluminium AL6061-T6. Table 3 shows the geometric dimensions and characteristics of elements which were used in both calculations. The properties of materials used in modelling are presented in Table 4.

Table 3. The characteristics and geometric dimensions of elements used for both calculations

Parameter	Measurement unit	Value
Radius of impacting sphere	mm	19
Length x width impact plate	mm	20x10
Initial velocity of impacting sphere v_x	m/s	-1.1
Initial distance between impacting sphere and impact plate	mm	0.05

Table 4. Properties of materials used in modelling

Parameter	Measurement unit	Steel 1006	Aluminium AL6061-T6
Density	kg/m^3	7896	2703
Gruneisen coefficient	-	2.17	1.97
Shear modulus	GPa	81.8	27.6
Yield stress	MPa	350	290

Fig. 2.5 presents the– directional (x direction, see Fig. 2.4) displacement of gauge point 1, which is located on the edge of the impact plate (see Fig. 2.4).

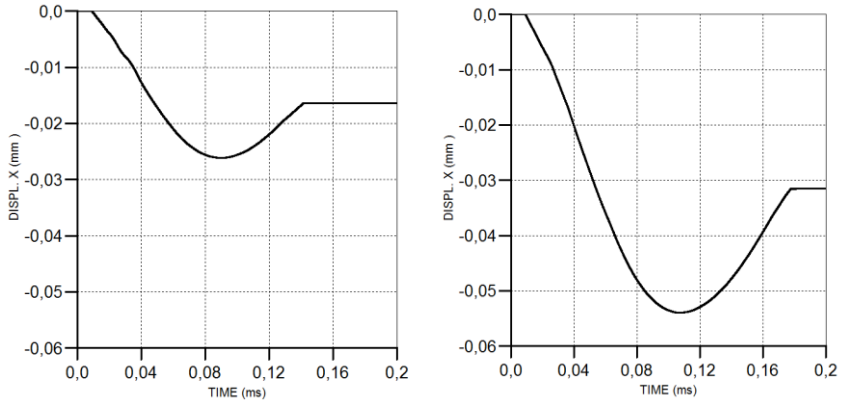

a) b)

Fig. 2.5 Directional displacement of gauge point 1: a) the first modelling, sphere and plate made of steel 1006, b) the second modelling, sphere made of steel 1006, plate made of aluminium AL6061-T6.

Fig. 2.6 shows the directional (x direction, see Fig. 2.4) velocity of gauge point 2, which is located on the edge of the impacting sphere (see Fig. 2.4).

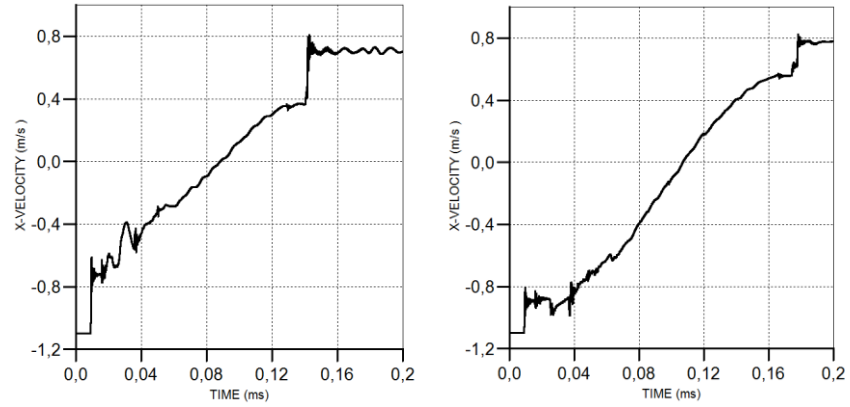

a) b)

Fig. 2.6 Directional velocity of gauge point 2: a) the first modelling, sphere and plate made of steel 1006, b) the second modelling, sphere made of steel 1006, plate made of aluminium AL6061-T6.

The results of modelling show that maximum displacement of the impact plate when the colliding parts are made from steel 1006 is 0.025 mm; the maximum displacement of impact plate when the colliding parts are made from Steel 1006 and aluminium AL6061-T6 is 0.055 mm. The time of directional velocity change from -1.2 mm/s to ~ 0.8 m/s is shorter when the sphere impacts the steel plate (0.13 ms) than the aluminium plate (0.17 ms).

Since the time of the directional velocity change of the impacting sphere (Fig. 2.6) corresponds with the generated shock duration, and the displacement of impact plate (Fig. 2.5) corresponds with the generated shock amplitude, the modelling results

imply that the generated shock parameters significantly depends on the material of the colliding parts. These facts show that the parameters of the shock generator in the developed piezoelectric impact energy harvester must be chosen very carefully, taking into account the parameters of drive, which should be controlled.

2.4. Basic design principles of horn-type waveguides

The presented novel piezoelectric impact energy harvester has another part which significantly influences the generated signal parameters (amplitude and frequency) – the horn-type waveguide (see Fig. 2.1). Therefore, it is important to theoretically research the horn-type waveguides.

As mentioned in section 1.5, the most important aspect of horn-type waveguide design is its resonant frequency and the determination of the correct horn resonant wavelength. The resonant frequency of horn-type waveguide which has a simple geometrical shape (i.e. cylindrical shape) can be determined analytically. For a complicated geometrical shape, the resonant frequency is usually determined numerically using the finite element method (FEM) [48].

The required performance of a conventional horn-type waveguide is determined with an amplification factor [48]:

$$\vartheta = \left|\frac{A_1}{A_0}\right|; \tag{2.9}$$

where ϑ – amplification factor, A_0 – vibration amplitude of input end of horn-type waveguide, A_1 – vibration amplitude of output end of horn-type waveguide.

The basic requirement for the amplification factor is that it should be more than 1.

Analytical solution of the horn-type waveguides vibrations

The governing equation of a longitudinally vibrating horn-type waveguide (principal calculation scheme is presented in Fig. 2.7) with a variable circular cross-section $S(x)$ which is valid for one-dimensional wave continuum (thin elastic bar), is expressed in the following form [48]:

$$\frac{\partial^2 u(x,t)}{\partial t^2} = c_p^2 \left[\frac{1}{S(x)}\frac{\partial S(x)}{\partial x}\frac{\partial u(x,t)}{\partial x} + \frac{\partial^2 u(x,t)}{\partial x^2}\right]; \tag{2.10}$$

where x – coordinate in the axial direction, $u(x,t)$ – axial displacement of cross-section, $S(x) = \pi(r(x))^2$ – cross-section area, $r(x)$ – radius of circular cross-section, $c_p = \sqrt{\frac{E}{\rho}}$ – velocity of axial waves in one-dimensional continuum, E – Young's modulus of horn material, ρ – density of horn material.

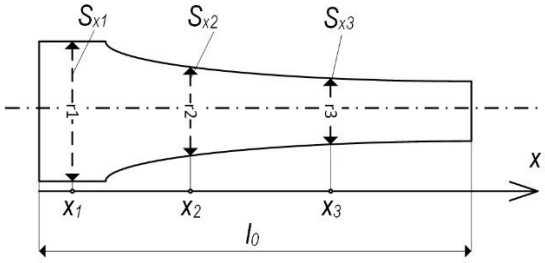

Fig. 2.7 The principal calculating scheme of a longitudinally vibrating horn

The free vibration of a cylindrical horn-type waveguide shape (r(x)=r) can be determined by the following equation:

$$\frac{\partial^2 u(x,t)}{\partial t^2} = c_p^2 \frac{\partial^2 u(x,t)}{\partial x^2} \tag{2.11}$$

If the solution of (2.11) equation is expressed in the form $u(x,t) = U(x)T(t)$, then the partial differential equation is divided into two differential equations as follows:

$$\frac{d^2U(x)}{dx^2} + \frac{\omega_0^2}{c_p^2} U(x) = 0; \tag{2.12}$$

$$\frac{d^2T(t)}{dt^2} + \omega_0^2 T(t) = 0; \tag{2.13}$$

where ω_0 – natural frequency of the horn-type waveguide.

By inserting the non-dimensional values of coordinate in the axial direction $\xi = \frac{x}{l_0}$, $\xi \in \langle 0; 1 \rangle$, and axial displacement of cross-section $\psi(\xi) = \frac{U(x)}{l_0}$ into the first of equations (2.12), the non-dimensional equation is obtained:

$$\frac{d^2\psi(\xi)}{d\xi^2} + \beta^2 \psi(\xi) \tag{2.14}$$

which is solved as:

$$\psi(\xi) = A\cos(\beta\,\xi) + B\sin(\beta\xi); \tag{2.15}$$

where β is the frequency parameter and can be expressed as:

$$\beta = \frac{\omega_0}{c_p} l_0; \tag{2.16}$$

where l_0 is the length of the horn-type waveguide.

Both input and output ends of horn-type waveguide have the possibility to move in the axial direction. The input end of the horn is attached to the vibration generator, usually a piezoelectric stack, which generates axial vibrations, and the output end is usually attached to a vibrating tool or the end itself operates as the vibrating tool. Then the boundary conditions for free vibration of horn-type waveguide are assumed to be free-free end on both sides as follows [48]:

$$\left.\frac{d\psi(\xi)}{d\xi}\right|_{\xi=0} = 0, \qquad \left.\frac{d\psi(\xi)}{d\xi}\right|_{\xi=1} = 0 \tag{2.17}$$

Then, after inserting the boundary conditions (equation (2.9)) into the solution (equation (2.7)), the modal parameters of the horn-type waveguide, such as natural frequency and wave length are obtained and expressed below. The natural frequency (in Hz) of the k^{th} mode shape:

$$f_{0k} = \frac{k}{2l_0}\sqrt{\frac{E}{\rho}} \tag{2.18}$$

Non-dimensional wave length of the k^{th} mode shape:

$$l_k = \frac{2\pi}{\beta_k} = \frac{2}{k}; \tag{2.19}$$

where β_k is k^{th} the root of the characteristic equation and $k = 1,2, \ldots$

In order to achieve the desired effect on the horn-type waveguide operating process, usually only the first two mode shapes of the horn are used. If $k = 1$, the horn-type waveguide has the so-called half wave shape and if $k = 2$, the horn-type waveguide has the full wave shape. Illustrations of both half wave and full wave shapes are presented in Fig. 2.8 [45].

NAME OF SHAPE	PARAMETERS	MODE SHAPE OF SONOTRODE VIBRATION
$\lambda/2$ – *"half wave"* shape	$k = 1$ $\lambda_1 = 2$ $f_{01} = \frac{1}{2l_0}\sqrt{\frac{E}{\rho}}$ $\vartheta_1 = 1$	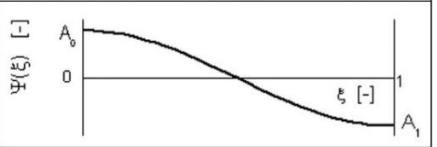
λ – *"wave"* shape	$k = 2$ $\lambda_2 = 1$ $f_{02} = \frac{1}{l_0}\sqrt{\frac{E}{\rho}}$ $\vartheta_2 = 1$	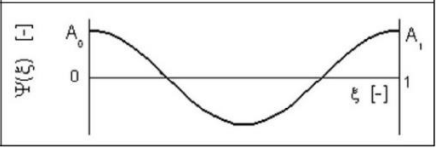

Fig. 2.8 Mode shapes of cylindrical cross-section horn-type waveguide vibrations [45]

As mentioned above, the calculations (2.10-2.19 equations) were relatively simple and based on the assumption that the horn-type waveguide was rotationally symmetric. However, the desired horn-type waveguide could have rotationally asymmetric characteristics, such as the convex features on the horn outlet and planar faces on the horn shank [55], which means that analytical determination of these parameters for such a non-cylindrical shapes is more complicated. Therefore, the numerical FEM instead of the analytical model is typically used to determine the modal properties of the more complicated geometrical horn-type waveguide shapes [45].

Finite element method for analysing the vibrations of the horn-type waveguides

The basic equation for describing free vibration motion which defines the modal properties of the horn-type waveguide FEM, is expressed as follows [45]:

$$M\ddot{u} + B\dot{u} + Ku = 0; \tag{2.20}$$

where M – mass matrix, B – damping matrix, K – stiffness matrix, $\ddot{u}$ – vector of nodes acceleration, $\dot{u}$ – vector of nodes velocity, and u – vector of nodes displacement.

In consideration to the fact that the horn-type waveguide materials have a low damping value from the dynamical aspect, the damping in equation (2.20) can be taken to zero, thus the equation of motion can be rewritten as:

$$M\ddot{u} + Ku = 0 \tag{2.21}$$

Moreover, the modal properties of the horn-type waveguide are determined by the solution of the eigenvalue problem:

$$\left(K - \omega_i^2 M\right)\phi_i = 0; \tag{2.22}$$

where ϕ_i - i^{th} – mode shape (eigenvector), ω_i – natural frequency of i^{th} mode shape.

The FEM modelling and calculations of modal properties of horn-type waveguides is usually done using various FEM software packages, i.e. ANSYS [46, 48], COMSOL Multiphysics [80], Elmer FEM [81], etc.

As both analytical and FEM calculations methods show, the efficiency and performance of horn-type waveguides depend on a specific design and a relatively large number of parameters. Due to this, the design of a geometric shape of the horn-type waveguide depends on the technological operation for which the horn-type waveguide will be used [48].

2.5. Theoretical research of horn-type waveguides

It should be noted that all previously mentioned theoretical research was carried out when the horn-type waveguide was excited with a harmonic excitation signal on the smaller cross-sectional area and the displacement was obtained on the surface with a greater cross-sectional area. Therefore, modelling both with harmonic excitation signal on a smaller cross-sectional area and with impulse excitation, which corresponds with impact, must be carried out on the same surface.

2.5.1. Modelling horn-type waveguides with harmonic excitation

The dependence of excitation signals amplitude on the shape of horn-type waveguide when excitation is on the surface with a smaller cross-sectional area was investigated theoretically. Fig. 2.9 shows a computational model with boundary conditions created using the ANSYS Harmonic response software.

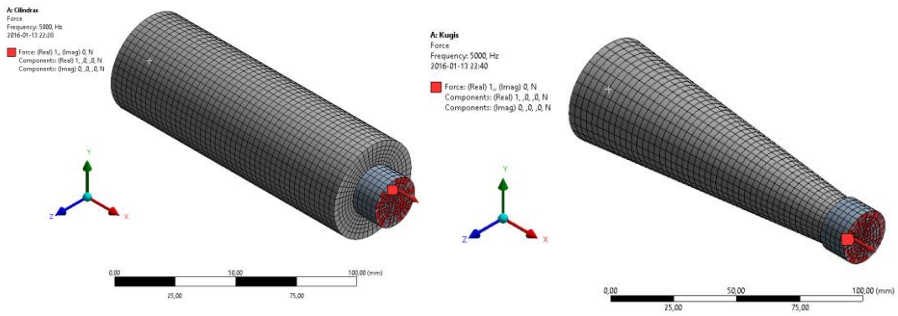

a) b)

Fig. 2.9 The computational model of waveguides: a) A type (cylindrical shape) b) B type (conical shape)

During the theoretical research, two types of waveguides were excited with a harmonic 1N force applied on the surface with the smaller cross-sectional area. The first type (A) was a cylindrical shape waveguide, 45 mm in diameter and 130 mm long, while the second type (B) was a conical waveguide, 45 mm and 20 mm in diameters and 130 mm in length. The dimensions of the force-applying body correspond with the dimensions of the cylindrical stack in the piezoelectric shock generator – 23 mm in diameter and 13 mm long. The computational model consists of 7,985 finite elements and 35,187 nodes with the A type waveguide, and of 22,925 finite elements and 96,491 nodes with the B type waveguide. The excitation frequency was between 5 kHz and 30 kHz and the solution had 125 interval for both simulations. The properties of the materials used in both simulations are presented in Table 5.

Table 5. The properties of materials used in simulations

Parameter	Measurement unit	Waveguide material	Excitation body material
Density	kg/m^3	2770	7100
Young's Modulus	GPa	71	110
Poisson's Ratio	-	0.33	0.34
Bulk Modulus	GPa	69.6	114.58
Shear Modulus	GPa	26.69	41.045

The deformation of waveguide surface with greater cross-sectional area in x direction and its frequency response in the same direction are presented in Fig.2.10 and Fig. 2.11, respectively.

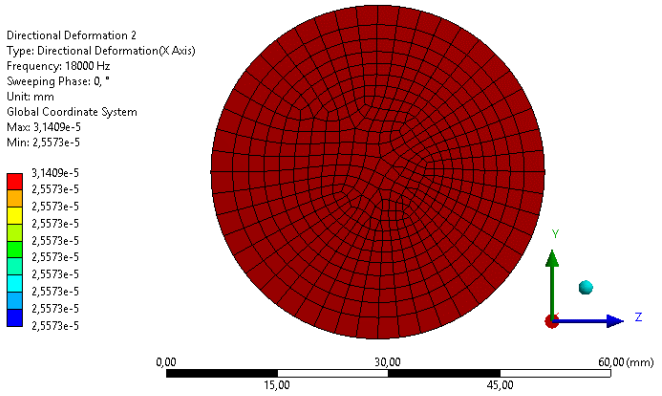

a)

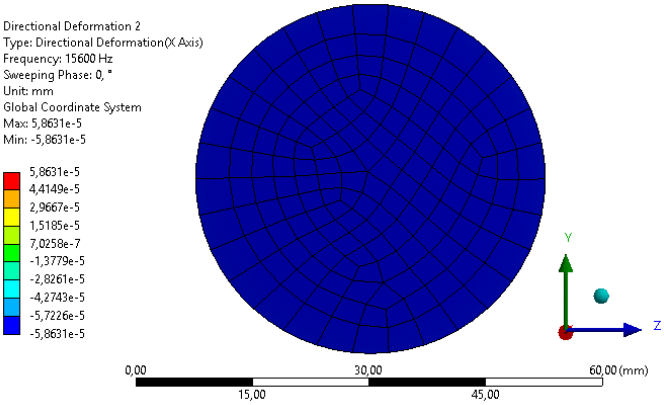

b)

Fig. 2.10 Deformation of surface with greater cross-sectional area of x direction: a) A type waveguide b) B type waveguide

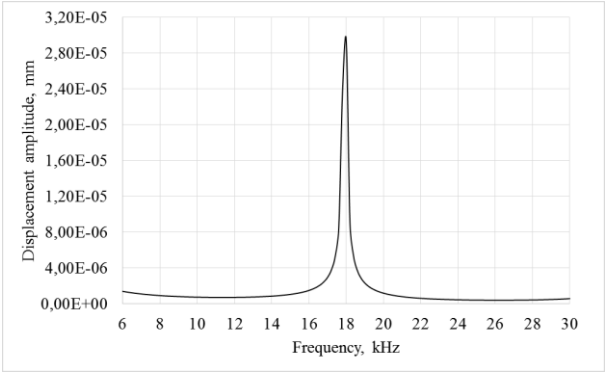

a)

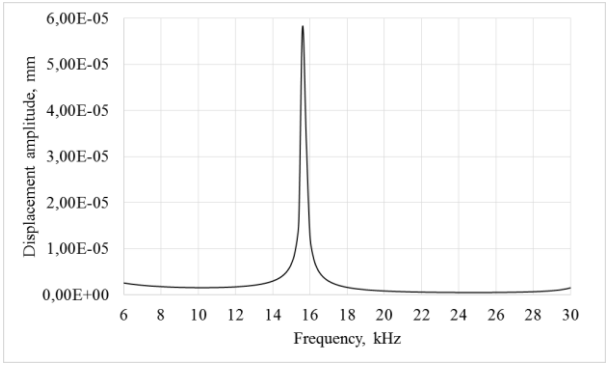

b)

Fig. 2.11 Frequency response of the displacement amplitude in x direction: a) A type waveguide b) B type waveguide

The results of the simulation show that the resonant frequency of longitudinal vibrations are 18.0 kHz of the type A waveguide and 15.8 kHz of the type B waveguide (see Fig. 2.11). The amplitude of longitudinal vibrations over the waveguide surface with greater cross-sectional area in x direction at resonant frequencies when the excitation conditions are identical is 0.314 μm when the waveguide is type A and 0.586 μm when the waveguide is type B. It could be concluded that the difference of longitudinal resonant frequency between the two types of waveguides is 2.2 kHz; the conical waveguide generates 1.87 times higher displacement of surface with greater cross-sectional area than the cylindrical waveguide. These results show that there is a need to theoretically investigate various shapes of horn-type waveguides when the excitation is on the smaller cross-sectional area. Since the presented piezoelectric impact energy harvester for burst-type signal generation involves impact-type excitation, further theoretical research is carried out with impulse excitation on the smaller cross-sectional surface of the horn-type waveguide.

2.5.2. A simulation of horn-type waveguides with impulse excitation

To investigate the dependence of mechanical impact parameters on different shapes of the horn-type waveguide, a computational model was created using ANSYS Explicit Dynamics software; it is presented in Fig. 2.12. Since the structure is symmetrical, only a quarter of the waveguide was modelled. During the simulation, the waveguides were made from Steel 1006, the excitation was by 1N force, applied for a certain period of time on surface B (20 mm diameter circle). Such excitation corresponds with an impact. Table 6 shows the properties of the material used in modelling.

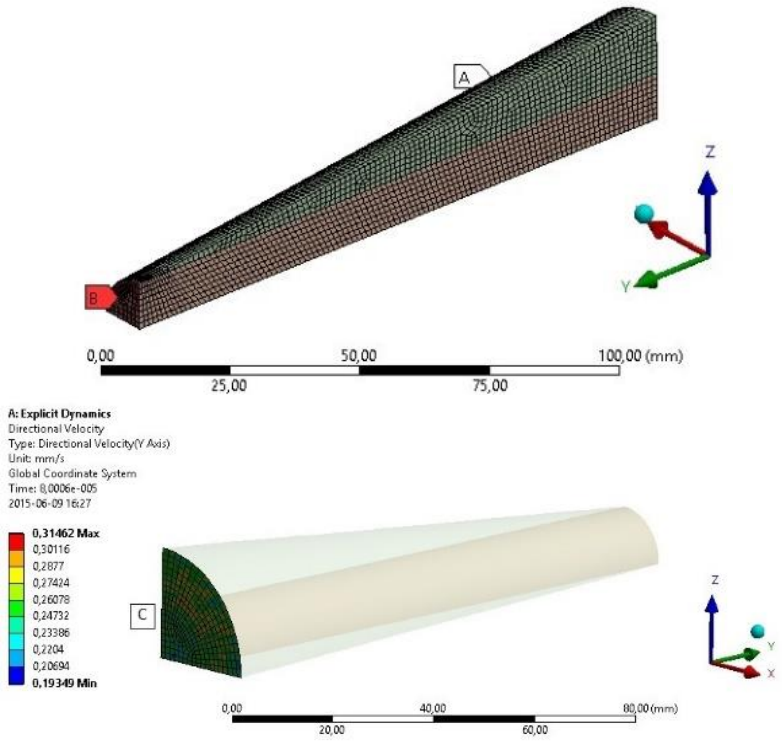

Fig. 2.12 A computational model with boundary conditions when the horn is conical

Table 6. The properties of the material (Steel 1006) used in modelling

Parameter	Measurement unit	Value
Density	kg/m^3	7896
Gruneisen coefficient	-	2.17
Shear modulus	GPa	81.8
Yield stress	MPa	350

The boundary conditions were identical in all simulations: the horn-type waveguides were fixed on edge A (a certain distance from surface C) at 0 mm/s velocity in y direction and on two section planes – at 0 mm/s velocity in x and z directions, accordingly (Fig. 2.12).

5 types of horn-type waveguides were modelled for this research. Their shapes and geometric dimensions are presented in Fig. 2.13.

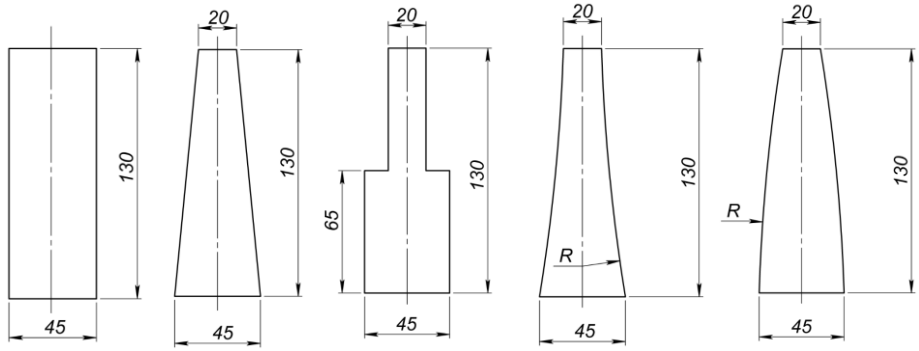

Fig. 2.13 The shapes and dimensions of the modelled waveguides: a) cylindrical, b) conical, c) stepped, d) close exponential, e) reverse close exponential

The first simulation was carried out with the conical waveguide to investigate how the shape of excitation impulse influences the amplitude of surface velocity. During the entire simulation, a constant force amplitude (of 1 N) of the waveguide excitation impulse was maintained and applied for five different periods of time. These impulse shapes were selected to determine how the resonant oscillations of the waveguide depend on the duration of the impulse. The modelled shapes of the excitation impulse are presented in Fig. 2.14.

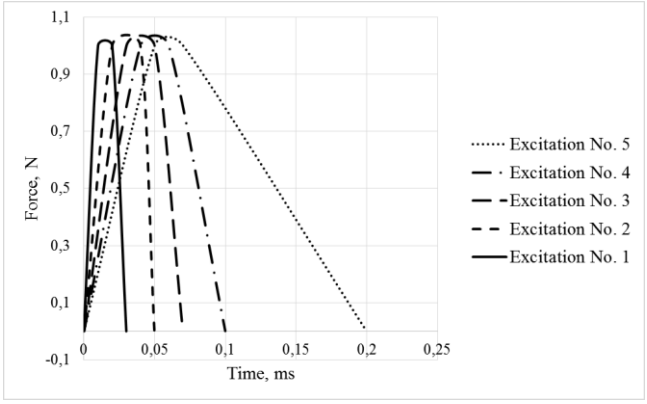

Fig. 2.14 The shapes of excitation impulse used in modelling with the conical waveguide

The maximum and minimum velocities in y direction of all surface C points were determined during the simulation. For example, Fig. 2.15 shows the maximum and minimum velocities in y direction of all surface C points when the waveguide has a conical shape. The green curve indicates the maximum directional velocity of the entire surface C while the red curve shows the minimum directional velocity of the entire surface C.

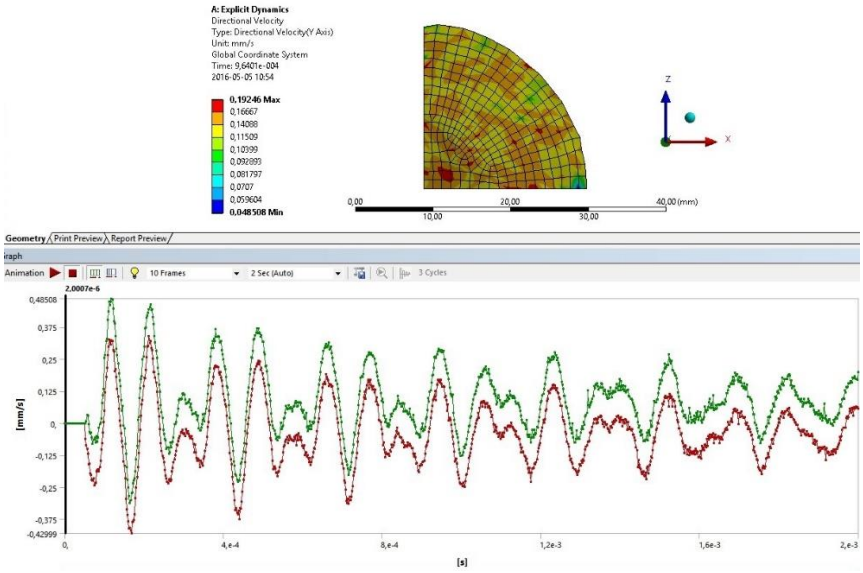

Fig. 2.15 Maximum and minimum velocities in y direction of all surface C points when the waveguide has a conical shape

Due to the discrepancy between the maximum and minimum velocities of the surface C points determined in Fig. 2.15, the results (Fig. 2.16, Fig. 2.18 and Fig. 2.20) are presented as an average velocity amplitude.

The dependence of the average velocity amplitude of surface C in y direction on the duration of the excitation impulse are presented in Fig. 2.16.

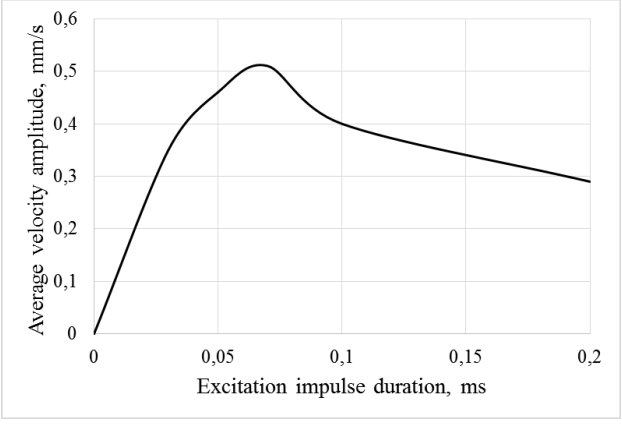

Fig. 2.16 Average velocity of surface C in y direction amplitude's dependency from excitation impulse duration

The results show that the highest amplitude of velocity (0.51 mm/s) is generated using the excitation shape no. 3 (0.07 ms excitation impulse duration) and the lowest amplitude of velocity (0.29 mm/s) is generated with the excitation shape no. 5 (0.2 ms excitation impulse duration). These results imply that velocity is the highest when the

excitation frequency (impulse duration) is close to a half of the resonant frequency period of the horn-type waveguide.

The second simulation investigated how the velocity amplitude depends on the location of the fixture in the conical waveguide. During the modelling the excitation shape was no. 3 (see Fig. 2.14), and the place of the fixture varied (the fixed edge distance *L*, mm from surface C). The modelling scheme is presented in Fig. 2.17.

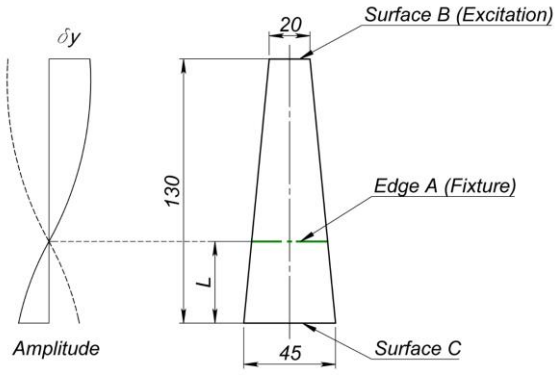

Fig. 2.17 The scheme of the second modelling

The relationship between the average velocity of the amplitude of surface C in y direction and the place of the fixture *L* are presented in Fig. 2.18.

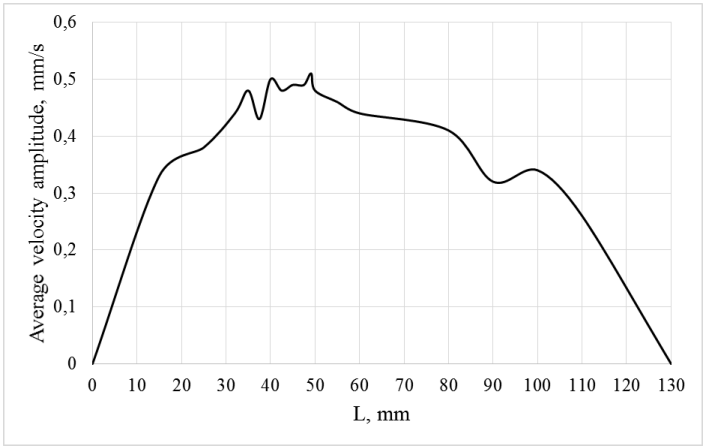

Fig. 2.18 The average velocity (y direction) amplitude, mm/s, of surface C. Conical waveguide, excitation shape No. 3

The analysis shows that velocity of y direction has the highest amplitude (0.51 mm/s) when fixture is 49.12 mm from surface C. This distance corresponds with the conical shape waveguide's centre of gravity.

The third simulation investigated the influence of the waveguide shape on the velocity amplitude. During this modelling, horn-type waveguides of all geometrical shapes (see Fig. 2.13) were fixed at the centre of their gravity. The designed close

exponential and reverse close exponential shape waveguide schemes are presented in Fig. 2.19, which also depicts the process of forming such horn-type waveguides; – arcs with variable centre were drawn between two parallel lines.

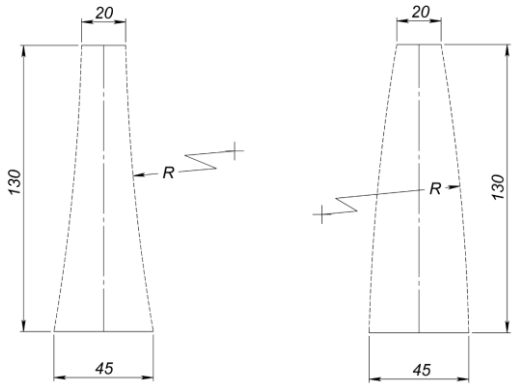

a) b)

Fig. 2.19 Schemes of forming waveguides –arcs with variable centre arc is drawn between two parallel lines: a) close exponential shape b) reverse close exponential shape

Fig. 2.20 shows how the average velocity amplitude of surface C in y direction depends on the shape of the waveguide.

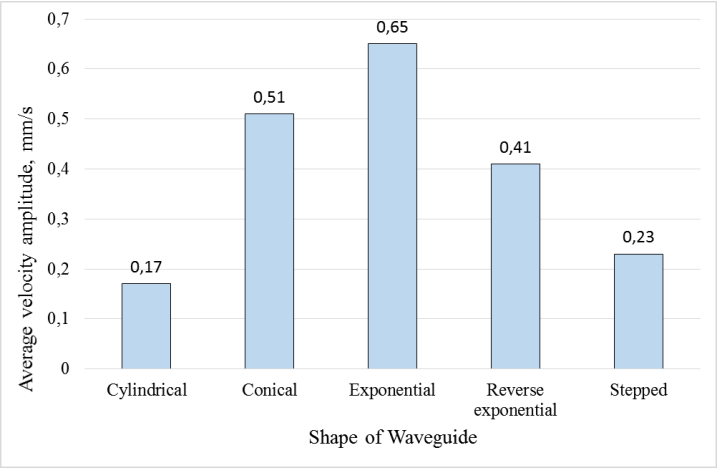

Fig. 2.20 Average velocity (y direction) amplitude, mm/s, of surface C

The results indicate that directional velocity has the highest amplitude (0.65 mm/s) when the waveguide has the close exponential shape, and the lowest (0.17 mm/s) when the waveguide is cylindrical.

Considering that movement uniformity of horn-type waveguide surface with greater cross-sectional area is an important aspect for a piezoelectric impact energy harvester, the discrepancies between the maximum and minimum velocities in y direction of all surface C points should be also determined. The lower the difference between the maximum and minimum velocities is, the more uniformly surface C

moves. Table 7 presents the discrepancy between maximum and minimum velocities of all surface C points for all modelled shapes, when the waveguides were fixed at the centre of their gravity and excitation was no. 3.

Table 7. Discrepancy between maximum and minimum velocities in y direction

Waveguide shape	Maximum velocity, mm/s	Minimum velocity, mm/s	Difference
Cylindrical	0.25	0.15	0.1
Conical	0.62	0.41	0.21
Stepped	0.26	0.20	0.06
Close exponential	0.75	0.56	0.19
Reverse close exponential	0.53	0.38	0.15

According to Table 7, the lowest difference between minimum and maximum directional velocities in y direction is when the horn-type waveguide has a stepped (0.06 mm/s) and cylindrical (0.1 mm/s) shapes. The largest difference between minimum and maximum directional velocities in y direction is when waveguide is conical (0.21 mm/s) and close exponential (0.1 mm/s). To verify the data, the simulation results of maximum and minimum velocities in y direction of all surface C points when waveguide is of the stepped shape, the fixture is at the centre of gravity and excitation is No. 3 (see Fig. 2.11) are presented in Fig. 2.21.

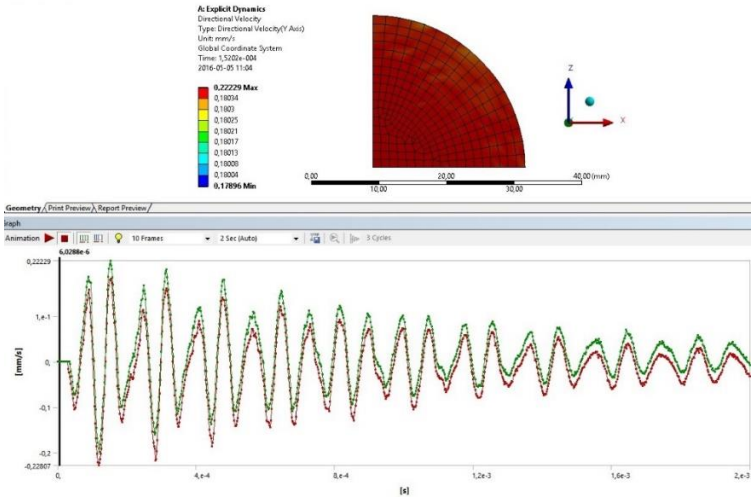

Fig. 2.21 Maximum and minimum velocities in y direction of all surface C points when waveguide has stepped shape

Comparing the results presented in Fig. 2.21 with those provided in Fig. 2.15, it is evident that the discrepancy is significantly lower when the horn-type waveguide has a stepped shape.

Despite the fact that the largest discrepancy between minimum and maximum directional velocities in y direction generates close exponential shape waveguide (0.19 mm/s), it generates the largest average amplitude (0.65 mm/s). The lowest

discrepancy generates the stepped shape waveguide (0.06 mm/s); on the other hand, it generates the average amplitude of only 0.23 mm/s. Therefore further research should combine these two shapes of horn-type waveguide; it could be called as stepped-exponential shape horn-type waveguide.

2.6. Conclusions of the section

In this section, theoretical researches of horn-type waveguides were carried out when the waveguide was excited on the surface with a smaller cross-sectional area and the displacement was obtained on the surface with a greater cross-sectional area. Because horn-type waveguides could have complicated geometry, the modal properties were determined using the FEM method with ANSYS Harmonic Response and Explicit dynamics software.

The following conclusions were formulated:

- Theoretical research of mechanical impact shows that the generated shock parameters, such as frequency and amplitude, significantly depend on the material of the colliding bodies. This indicates that in the developed piezoelectric impact energy harvester for burst-type signal generation, the parameters of the shock generator must be chosen very carefully, taking into account the parameters of the ultrasonic drive which should be controlled.
- The modelling of horn-type waveguides with harmonic excitation on the surface with a smaller cross-sectional area shows that the conical waveguide generates 1.87 times higher displacement of the surface with a greater cross-sectional area than the cylindrical waveguide under equal excitation conditions.
- The modelling of horn-type waveguides with impact excitation shows that the highest average velocity amplitude of the waveguide surface with a greater cross-sectional area is generated with a waveguide which is excited for 0.07 s, which should be close to or correspond to a half of the resonant frequency period of the horn-type waveguide.
- The modelling of horn-type waveguides shows that vibrational velocity amplitude is significantly influenced by the waveguide's fixture place; it is the highest when the horn-type waveguide is fixed at its centre of gravity. This modelling also shows that the velocity amplitude of a horn-type waveguide which has the close exponential shape is 3.8 times higher than that of a cylindrical horn-type waveguide shape, when boundary conditions are the same. It was also determined that that the stepped shape horn-type waveguide produces the lowest discrepancy between maximum and minimum velocities. Due to these results, further research combines the stepped and close exponential shapes of the waveguide and the new device is called stepped-exponential shape horn-type waveguide.

3. EXPERIMENTAL RESEARCH OF THE PIEZOELECTRIC IMPACT ENERGY HARVESTER FOR BURST-TYPE SIGNAL GENERATION

3.1. Experimental research of mechanical impact

In order to investigate the dynamic parameters of mechanical impact, experimental research was carried out on the basis of the theoretical modelling presented in section 2.3. The principal layout of the experimental setup is presented in Fig. 3.1.

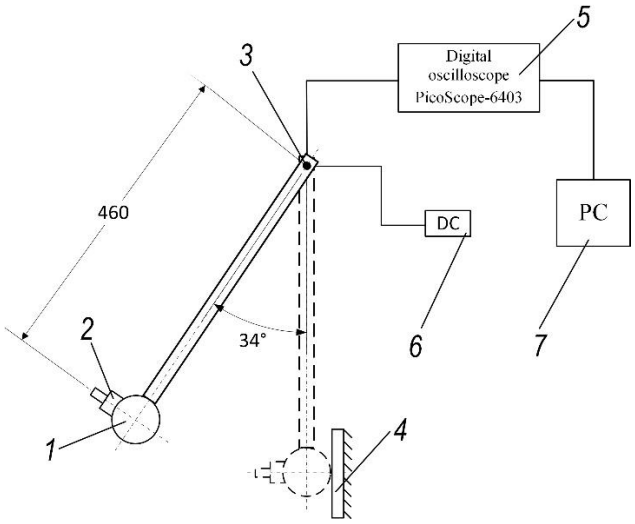

Fig. 3.1 The layout of mechanical impact experimental setup: 1 – impacting sphere, 2 – accelerometer, 3 – potentiometer, 4 – impact plate, 5 – digital oscilloscope; 6 – power supply, 7 – PC

During the experimental investigation, mechanical impact was created using an impacting sphere 1 (see Fig. 3.1) which was released from a certain height and impacted the impact plate 4 as a pendulum. Due to the measurement range of the accelerometer, the initial angle of the pendulum was $\alpha = 34^{\circ}$ in all experiments. Acceleration of the impacting sphere was measured with the accelerometer 2 and the duration of pendulum's movement was measured with the potentiometer 3. The data from the sensors was acquired and analysed using a PC and the experimental results were analysed with the MATLAB software package.

The experiment was carried out in three stages. The first experiment was carried out when the impacting sphere, made of hardened steel C45E impacted into plate, made of the same material; the second part involved the same impacting sphere impacting a plate made of steel AISI304, and during the last experiment, the impacting sphere (made of hardened steel C45E) impacted a plate made of aluminium AL6061-T6. The view of experimental setup is presented in Fig. 3.2.

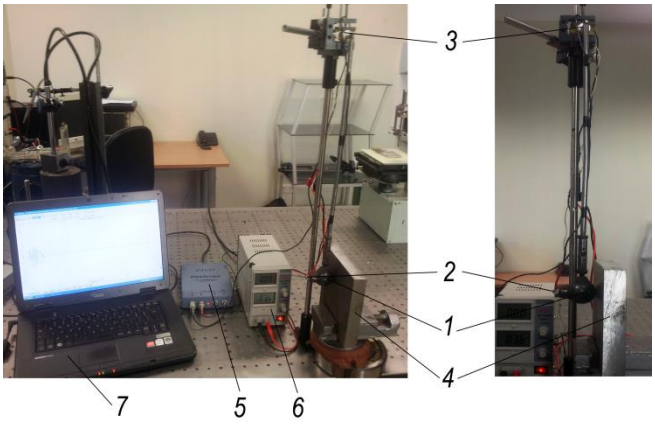

a) b)

Fig. 3.2 The experimental investigation of mechanical impact: a) setup view b) impacting pendulum view: 1 – impacting sphere of 295 g, 2 – accelerometer KD91, 3 – potentiometer, 4 – impact plate, 5 – digital oscilloscope PicoScope 3424, 6 – power supply Mastech HY1803D, 7 – PC.

The analysis shows that the voltage rate of the potentiometer is proportional to the velocity of the impacting sphere. These results are presented in Fig. 3.3 a). With regards to these results, the time of pendulum movement is determined – 0.1 s. The velocity change of a moving object could be defined as:

$$\Delta v = v - v_o = at \tag{3.1}$$

where v_o – initial velocity of a moving object, v – velocity of a moving body after time t, a – acceleration of a moving body.

In our case, a is considered as acceleration due to gravity and is equal 9.8 m/s^2. Due to the fact that during the start phase the movement of the pendulum $v_o = 0$ m/s, the velocity of impact could be calculated:

$$v = at = 9.8 \cdot 0.1 = 1 \text{ m/s} \tag{3.2}$$

These results imply that the impact velocity is ~ 1 m/s when the impacting sphere is released from a particular height and the initial angle of the pendulum is $\alpha = 34^{\circ}$. Since the material and the releasing height of the impacting sphere was not changed during the experiments, it is safe to conclude that the velocity and the initial conditions of the mechanical impact remained constant during all of the stages of investigation.

The accelerometer signals obtained under identical conditions of mechanical impact are given in Fig. 3.3 b), c), and d).

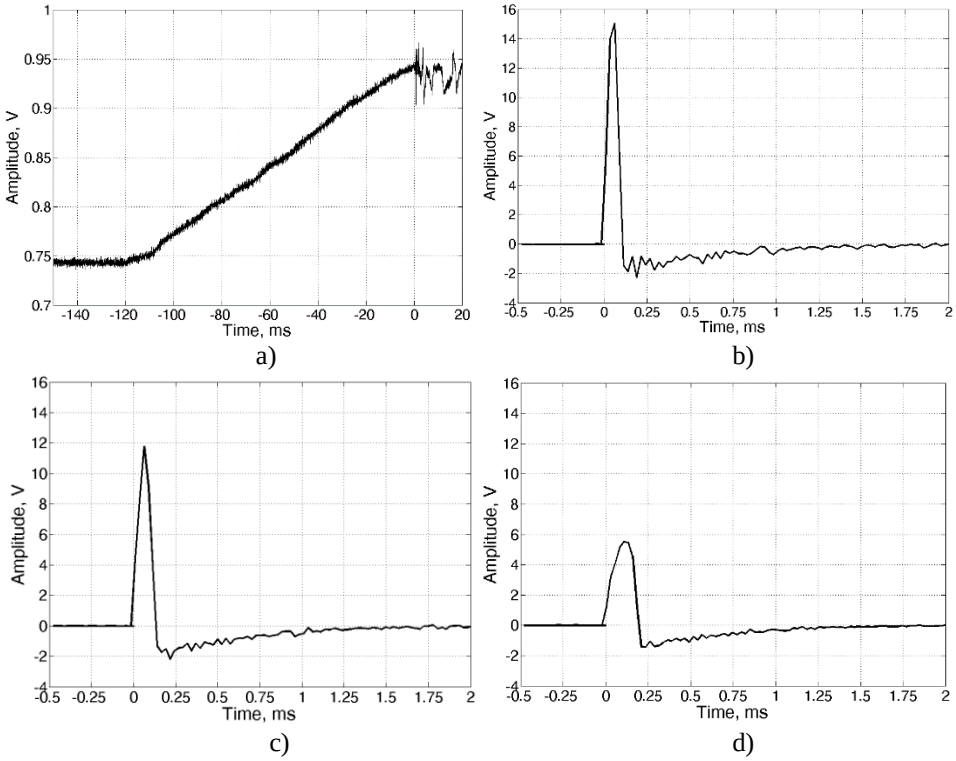

Fig. 3.3 The experimental results: a) potentiometer voltage change during experimental investigation, b) accelerometer signal, impact plate made of steel C45E, c) accelerometer signal, impact plate made of steel AISI304, d) accelerometer signal, impact plate made of aluminium AL6061-T6

The longest impact time (0.235 ms) is registered when the impacting sphere impacts with a plate made of aluminium, –and the shortest (0.105 ms) when the plate is made of steel. The highest impact amplitude is 15 V which is obtained when the impacting sphere impacts a steel C45E plate, and the lowest amplitude is 5.8 V which is registered when the plate is made of aluminium AL 6061-T9.

These experimental results are consistent with the theoretical results, which shows that it is essential to match the materials of the impacting surface when using a mechanical impact in order to obtain the desired shock amplitude and duration (frequency).

Despite the fact that such mechanical impact phenomena are rather simple, this method has some disadvantages, such as the repeatability of the impact parameters during some impacts. Another disadvantage of such a system is that the material of the impacting sphere or the impacting surface should be changed in order to obtain the desired shock parameters, what is rather complicated. Therefore, a piezoelectric shock generator could be used instead of a mechanical impact.

3.2. Experimental research of horn-type waveguides with harmonic excitation

First of all, in order to make sure that the surface of a horn-type waveguide with a greater cross-sectional area moves in different way depending on its shape when the excitation is based on the surface with a smaller cross-sectional area, experiments were carried out with a harmonic excitation signal.

Firstly, frequency responses of two horn-type waveguides (A and B types) with the same piezoelectric stack as the harmonic vibrations exciter (made of 19 piezo rings, dimensions of 23x13x0.5 mm, capacity 60 nF) located on the surface with a smaller cross-sectional area were obtained using an impedance meter Wayne Kerr 6500B. The principal layout of A and B horn-type waveguides, cylindrical and conical, respectively, with their dimensions and location of excitation are presented in Fig. 3.4, while Fig. 3.5 presents the measured impedances with phase angles

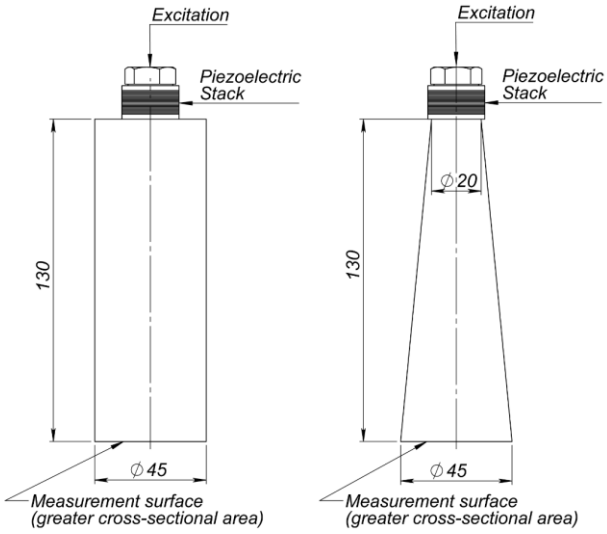

Fig. 3.4 The principal layout of horn-type waveguides with their dimensions and location of excitation: on the left – A type waveguide, on the right – B type waveguide

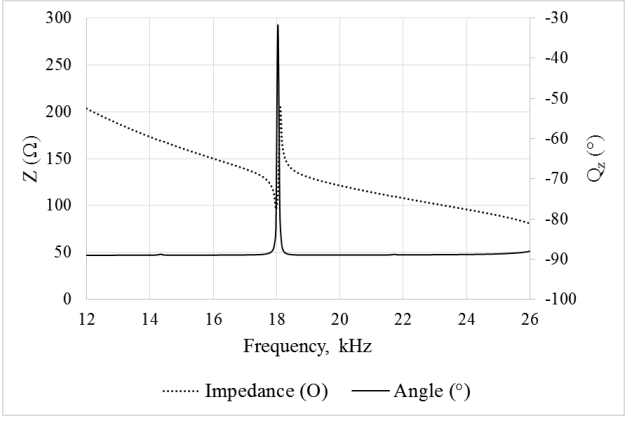

a)

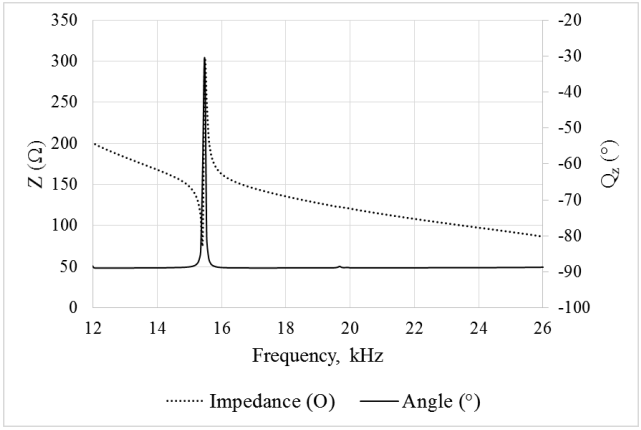

b)

Fig. 3.5 The impedance and phase angle of the piezoelectric stack attached to the waveguide: a) type A waveguide; b) type B waveguide

As the experimental results (Fig. 3.5) show, the longitudinal resonant frequency of type A waveguide with piezoelectric stack is approximately 18.1 kHz, when type B produces a frequency of approximately 15.6 kHz with the same piezoelectric stack; the phase angles are 305° and 290°, respectively.

The movement uniformity of the surface with a greater cross-sectional area was also analysed experimentally. First of all, holographic tests of the horn-type waveguides (Fig. 3.4) were performed using a holographic interferometry system PRISM 100 (HYTEC Inc., USA). During holographic tests, excitation was generated on the surface with smaller cross-sectional area and displacement of the surface with greater cross-sectional area was obtained. Both types of horn-type waveguides were fixes at the centre of their gravity and excited with the same harmonic excitation signal generated by the same piezoelectric stack as in the experiment with the impedance meter. During this experiment, the frequency ranged from 0 kHz to 100 kHz. Fig. 3.6 presents the holograms of cylindrical and conical horn-type waveguide surfaces with greater cross-sectional area when these surfaces move uniformly and non-uniformly.

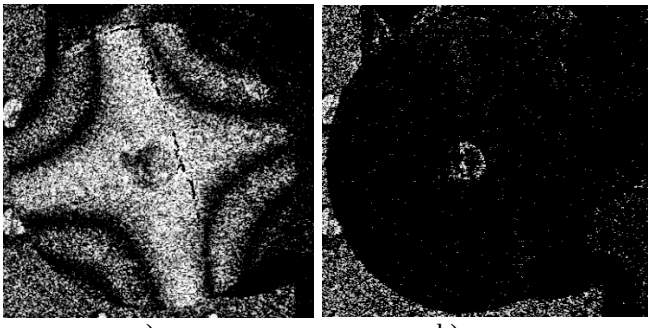

a) b)

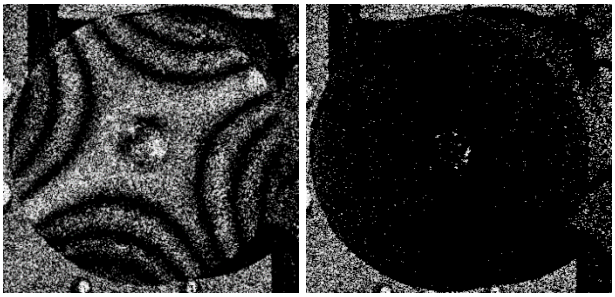

c) d)

Fig. 3.6 Holograms of waveguide surfaces with greater cross-sectional area – a) cylindrical waveguide, excitation frequency 60.55 kHz; b) cylindrical waveguide, excitation frequency 17.9 kHz; c) conical waveguide, excitation frequency 43.56 kHz; d) conical waveguide, excitation frequency 15.5 kHz

As the holograms show, the surface of the cylindrical waveguide with greater cross-sectional area moves uniformly when the excitation signal is 17.9 kHz (Fig. 3.6 b) and the surface of the conical waveguide with greater cross-sectional area moves uniformly when the excitation signal is 15.5 kHz (Fig. 3.6 d). Non-uniform movement of both cylindrical and conical waveguide's surfaces with greater cross-sectional area are presented in Fig. 3.6 a) and c), respectively. Also it should be noted that excitation frequency of waveguides when they move uniformly is close to their resonant frequencies of longitudinal mode, obtained both theoretically (2.5.1 section) and with the impedance meter (Fig. 3.5).

Next, the study investigates the quantity of surface's movement. For this investigation, excitation was generated using the same piezoelectric stack (made of 19 piezo rings of 23x13x0.5 mm dimensions, capacity 60 nF) located on the surface with a smaller cross-sectional area; surface displacement was measured with a laser vibrometer at 5 gauge points of the measured surface with a greater cross-sectional area. The principal scheme of measurement points is presented in Fig. 3.7, and the layout and stand view of the experimental setup are given in Fig. 3.8.

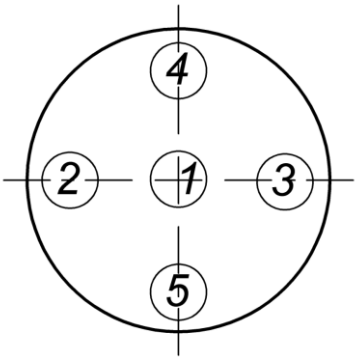

Fig. 3.7 The scheme of gauge point locations on the measured surface with a greater cross-sectional area

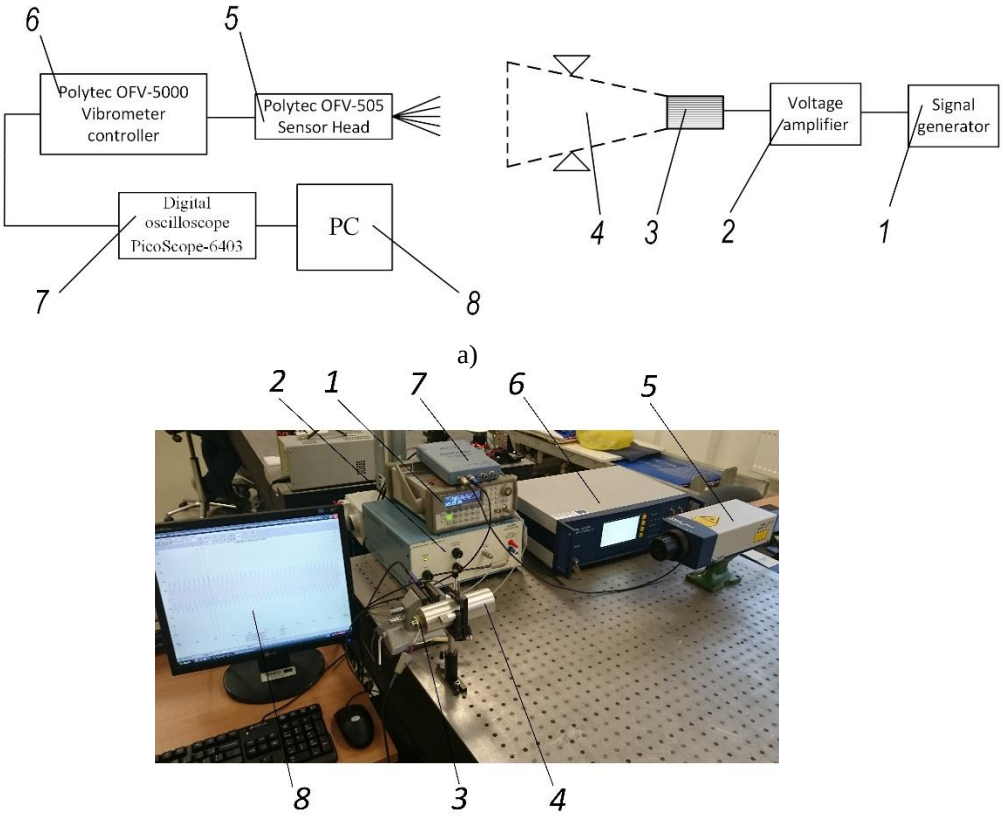

Fig. 3.8 Experimental setup for investigating the uniformity of waveguides surface movement: a) scheme b) stand view: 1 – signal generator, 2 – voltage amplifier, 3 – piezo stack, 4 – waveguide, 5 – laser sensor head, 6 – vibrometer controller, 7 – digital oscilloscope, 8 – PC

During this experimental investigation, the excitation of piezoelectric stack 3 (made of 19 layers 23x13x0,5 mm piezo rings, C = 68 nF) was generated by the signal generator 1 (Tabor WW5064) and amplified with the voltage amplifier 2. The same harmonic signal was used to excite both types of waveguides ($U_{p\text{-}p}$= 5V) and the frequency ranged from 0 to 34 kHz. The waveguide 4 was fixed at the centre of its gravity and the displacement of surface with greater cross-sectional area was measured with a laser sensor head 5 (Polytec OFV-505) and a laser Doppler vibrometer controller 7 (Polytec OFV-5000). The data were acquired and analysed with a digital oscilloscope 7 (PicoScope-6403) and a PC 8.

Fig. 3.9 presents the amplitude-frequency characteristics of type A and B waveguides obtained with a laser vibrometer and using the same excitation signal for both horn-type waveguides.

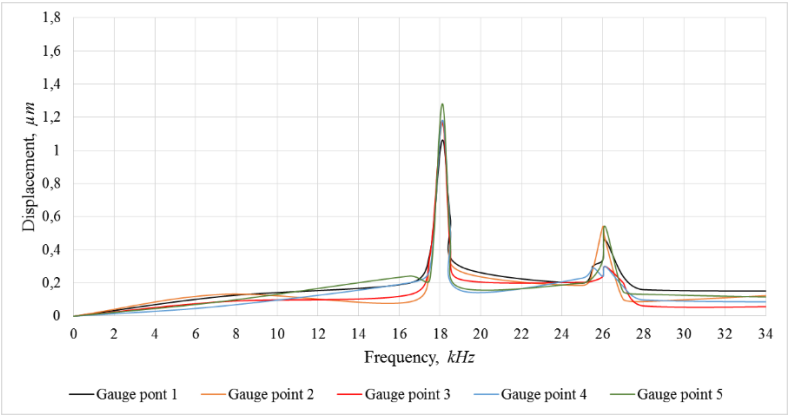

a)

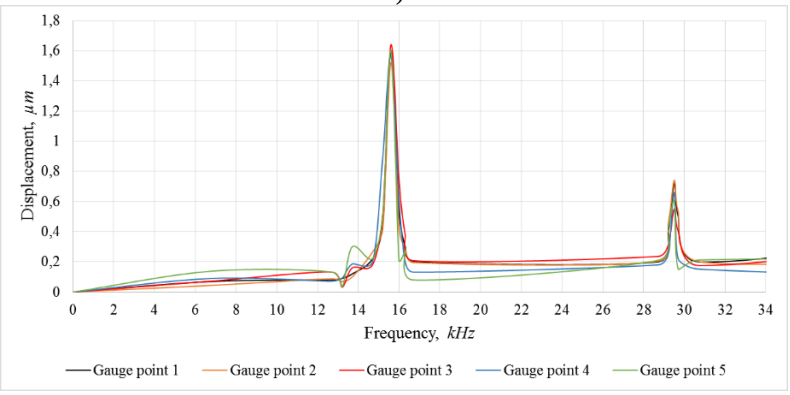

b)

Fig. 3.9 Amplitude-frequency characteristics obtained with a laser vibrometer: a) type A waveguide b) type B waveguide

Experiments (Fig. 3.9) show that the average maximum displacement of 5 gauge points of type A horn-type waveguide surface with a greater cross-sectional area are obtained at approximately 18.1 kHz resonant frequency; it reaches 1.3 μm when the harmonic signal with peak-to-peak amplitude of 5V is used for excitation. The average maximum displacement of 5 gauge points of type B horn-type waveguide surface with a greater cross-sectional area is obtained at approximately 15.6 kHz resonant frequency and reaches 1.65 μm under the excitation conditions as type A waveguide. These results also indicate that the surface movement of the conical shape waveguide (B type) is more uniform than that of the cylindrical waveguide (B type) because the discrepancy of the 5 gauge points is lesser with type B waveguide than with type A.

It could be concluded that the conical shape horn-type waveguide generates 1.27 higher displacement of the surface with a greater cross-sectional area than the cylindrical waveguide under the same excitation signal. Also it is seen that the entire larger surface moves more uniformly when the waveguide has a conical shape rather than a cylindrical one. Resonant frequencies are 18.1 kHz and 15.6 kHz when the waveguide is cylindrical and conical, respectively. These frequencies are similar to

the resonant frequencies at which the waveguides move uniformly (determined during the holographic tests and obtained with an impedance meter).

In order to confirm the results presented above, another experimental investigation was carried out using a different technique. The layout and the stand view of it are presented in Fig. 3.10.

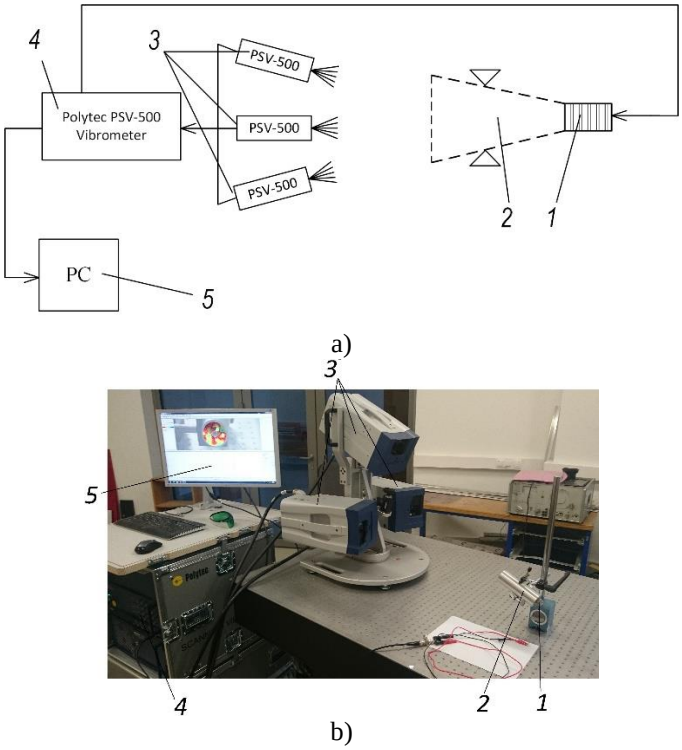

Fig. 3.10 Experimental setup for investigating the movement uniformity of horn-type waveguides: a) layout; b) stand view: 1 – piezo stack, 2 – waveguide, 3 – laser scanning heads, 4 – laser vibrometer, 5 – PC.

During this investigation (Fig. 3.10), the same cylindrical and conical waveguides (type A and B, respectively) were excited with the same periodic chirp-type signal on the smaller cross-sectional surface. The horn-type waveguide 2 which is fixed at the centre of its gravity is excited using the same piezoelectric stack 1 as in the experiments presented above (made of 19 layers 23x13x0,5 mm piezo rings, C = 68 nF). The movement of waveguide's larger cross-sectional surface is measured with three laser scanning heads (Polytec PSV-500 scanning heads) and a laser Doppler vibrometer 4 (3D Polytec PSV-500 vibrometer). The data were acquired and analysed using a PC 5.

The characteristics of the amplitude frequency obtained with a 3D Polytec vibrometer of both type A and B waveguides are presented in Fig. 3.11.

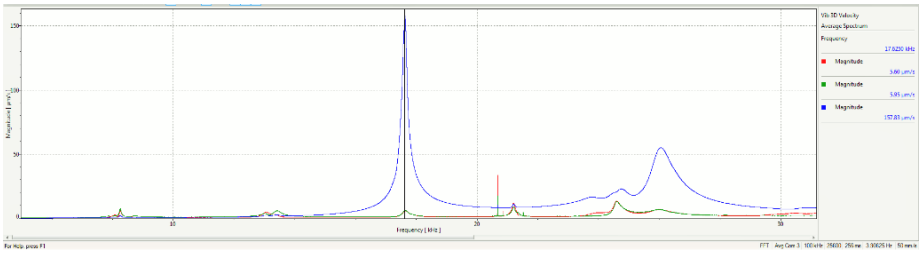

a)

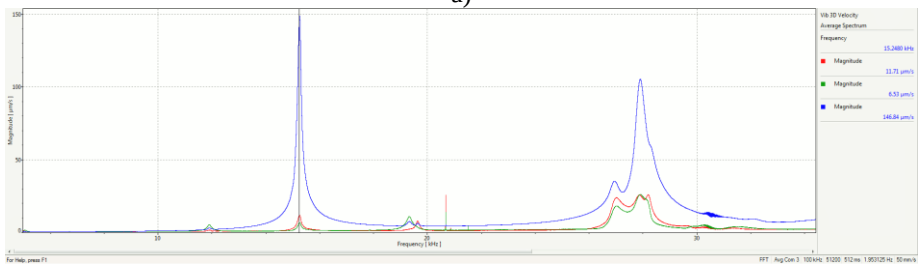

b)

Fig. 3.11 Amplitude-frequency characteristics obtained with a 3D laser vibrometer: a) type A waveguide b) type B waveguide

As these results show, the peak of velocities of the larger cross-sectional surface are obtained at frequencies of 17.63 kHz and 15.25 kHz, respectively, with the cylindrical (A) and conical (B) waveguides. The displacement of greater cross-sectional surface of both waveguides under the same excitation amplitude ($U_{p\text{-}p}$ = 5V) and frequencies of 17.63 and 15.25 kHz for type A and B waveguides, accordingly, are presented in Fig. 3.12.

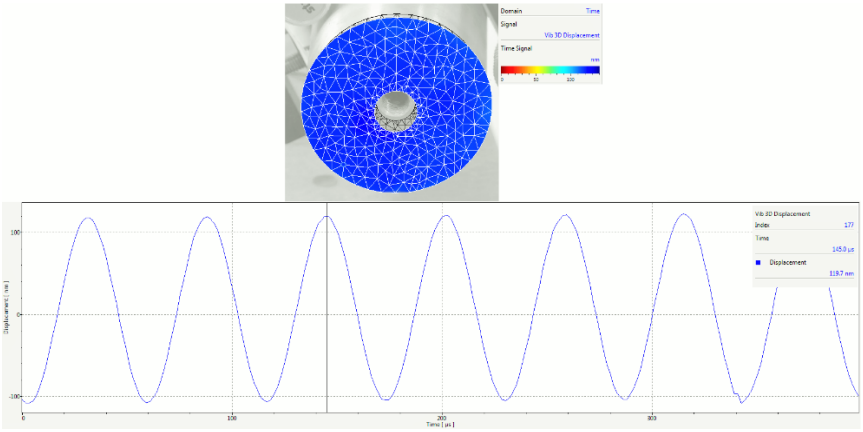

a)

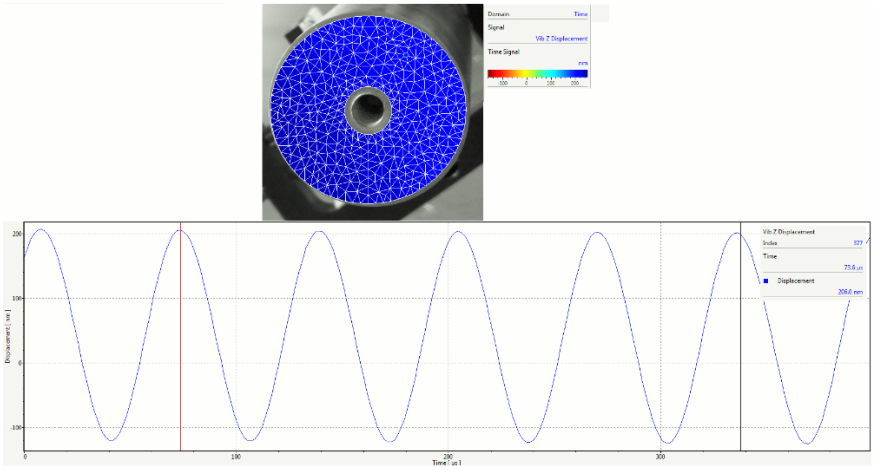

b)

Fig. 3.12 The greater cross-section surface displacement obtained with a 3D laser Doppler vibrometer: a) type A waveguide b) type B waveguide

Research shows that the displacement amplitude of larger cross-section surface is 119.7 nm when the waveguide is type A, and 206 nm when the waveguide is type B. These result also indicate that at resonant frequencies of 17.63 and 15.25 kHz, respectively, the larger cross-section surface of type A and B waveguides moves uniformly. Similar to the results obtained with the methods of another investigation (theoretically, with a laser vibrometer at 5 points), it is seen that the conical waveguide generates 1.72 higher displacement than the cylindrical waveguide when the fixture and excitation conditions are the same.

Table 8 compares the results of the cylindrical and conical (A and B, respectively) waveguide harmonic excitation on the smaller cross-sectional surface obtained using different methods, such as theoretical calculation using ANSYS Harmonic response software, experimental investigations using an impedance meter, a 1-point laser vibrometer, a 3D laser vibrometer and holographic tests.

Table 8. A comparison of harmonic excitation of waveguides on the smaller cross-sectional surface

Method	Resonant frequency of longitudinal mode		Displacement of surface with greater cross-sectional area	
	A type waveguide	B type waveguide	A type waveguide	B type waveguide
Theoretical calculation	18.0 kHz	15.8 kHz	0.314 μm	0.586 μm
Impedance meter	18.1 kHz	15.6 kHz	-	-
Holographic tests	17.9 kHz	15.5 kHz	-	-
1 point laser vibrometer	18.1 kHz	15.6 kHz	1.3 μm	1.65 μm
3D laser vibrometer	17.6 kHz	15.3 kHz	119.7 nm	206 nm

As presented in Table 8, resonant frequencies of both type A and B horn-type waveguides is similar to each other, regardless of the method used for investigation.

The displacement of the greater cross-sectional surface differs due to the excitation conditions; depending on the method used, the excitation amplitude varies. Even though excitation does not coincide in both research methods, it was identical for the analysis of both types of waveguides during each investigation. Therefore, it is easier to compare how many times the greater cross-sectional surface displacement of B type waveguide is higher than that of type A waveguide when the excitation conditions are equal. It should be noted that this factor varies from 1.27 times during investigation with 1-point laser vibrometer up to 1.87 times during theoretical calculation. This difference may be caused by the imperfectly steady fixture conditions during different investigations and is relatively small, so it can be concluded that the results are consistent and the shape of a horn-type waveguide has a very significant impact on the greater cross-sectional surface displacement. Therefore, the shape of a horn-type waveguide is important for piezoelectric impact energy harvester for burst-type signal generation and must be selected properly depending on its application.

3.3. Experimental research of ultrasonic motor control

3.3.1. Experimental research of piezoelectric materials generating voltage from impact

To compare how the amplitude of generated voltage depends on the properties of piezoelectric material, PZT-5A ("soft") and PZT-4 ("hard") were investigated experimentally. The properties of the two different piezoelectric materials –are presented in Table 2.

The experimental layout and the stand view are presented in Fig. 3.13. During this experiment, the impacting sphere 1 made of steel C45E, with a diameter of 14 mm and mass of 11.2g was released from a certain height and as a pendulum directly impacted the piezoelectric disk 2 (30 mm diameter, 10 mm height) at the initial angle of 50°. This angle of the pendulum was selected due to the geometric dimensions of the experimental stand. Data was acquired and analysed with a digital oscilloscope 3 (PicoScope-6403) and a PC 4.

The momentum of the impacting sphere could be described as:

$$p = mv; \tag{3.3}$$

where p – quantity of motion (moment), m – mass of impacting sphere, v – velocity of the impacting sphere at impact time, which could be expressed as:

$$v = \sqrt{2gL(1-\cos a)}; \tag{3.4}$$

where g – acceleration due to gravity, L – the length of the pendulum, a – angle of the pendulum, at which the impacting sphere is released. In this way, velocity at impact time is equal:

$$v = \sqrt{2 \cdot 9.81 \cdot 0.25 \cdot (1-\cos 51.3)} = 1.35 \text{ m/s} \tag{3.5}$$

And thus the quantity of motion in the experiment is:

$$p = 0.0112 \cdot 1.35 = 0.015 \text{ kg·m·s}^{-1} \tag{3.6}$$

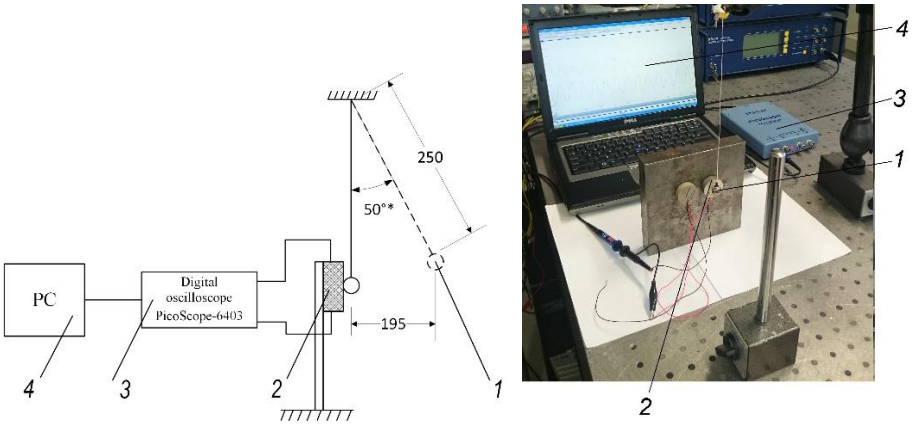

a) b)

Fig. 3.13 Experimental investigation of the voltage generated by the piezoelectric material: a) experimental layout, b) stand view

During this study, the sphere impacted each piezoelectric disc (the "soft" PZT-5A, and the "hard" PZT-4) three times with the same quantity of motion. The experimental results are presented in Table 9 , which shows that the "soft" piezoelectric material, PZT-5A, generates approximately 1.4 times higher voltage amplitude from the same impact. It should also be noted that the duration of the generated impulse is 1.14 times shorter when the piezoelectric material is the "hard" PZT-4.

Table 9. The voltage generated by the piezoelectric disks

Test no.	Generated voltage, peak to peak, V		Generated impulse duration, μs	
	PZT-4	PZT-5A	PZT-4	PZT-5A
Test No. 1	105.6	153.6	49.03	55.15
Test No. 2	116.7	160.9	49.02	56.38
Test No. 3	113.3	150.3	47.48	53.92
Average	111.9	154.9	20.62	18.14

Since the generated voltage amplitude is an important aspect for the piezoelectric impact energy harvester for burst-type signal generation, further research uses the "soft" PZT-5A piezoelectric material. Impulse duration is chosen by altering the parameters of the horn-type waveguide and impact.

3.3.2. Designing a piezoelectric impact energy harvester for burst-type signal generation

The ultrasonic motor should be controlled. The one used in this study is USM-50-3; it operates at 42.6 kHz frequency (more technical characteristics of the motor are presented in Table 10). A piezoelectric impact energy harvester for burst-type signal generation with longitudinal resonant frequency of 21.1 kHz, a stepped-

exponential horn-type waveguide and a piezoelectric shock exciter for impact generation was designed and fabricated.

The drawing and the 3D model view of the designed piezoelectric impact energy harvester are presented in Fig. 3.14. the impedance of this impact energy harvester measured with the impedance meter Wayne Kerr 6500B is presented in Fig. 3.15.

Table 10. The characteristics of ultrasonic motor USM-50-3

Characteristic	**Measurement unit**	**Value**
Motor type	-	Piezoelectric, rotational
Motor operating frequency	kHz	42.6
Rated RMS voltage	V	21.28
Rated torque	Nm	0.004608
Rated rotational speed	rpm	56.075
No-load maximum rotational speed	rpm	78.947
Maximum torque	Nm	0.006912
Resonance quality factor	-	300
Capacitance per phase	nF	13

The stepped-exponential shape (Fig. 3.14) of the horn-type waveguide is chosen based on previous theoretical research which has revealed that the close exponential shape waveguide has the highest amplitude magnification factor of the generated vibrations, when compared to the cylindrical, conical, stepped and reversed close exponential shapes. It has also been determined that the greater cross-sectional surface moves in the most uniform way in the longitudinal direction when the excitation conditions are the same as using a stepped horn-type waveguide.

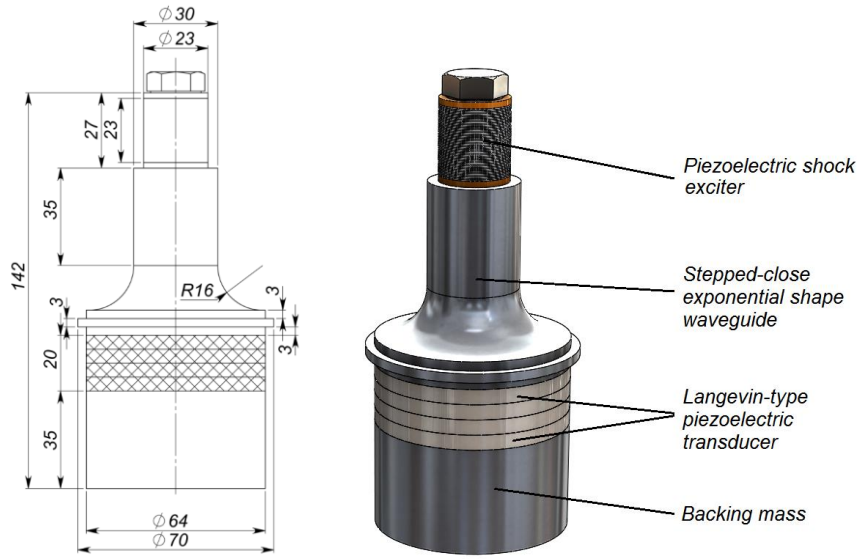

a) b)

Fig. 3.14 The fabricated piezoelectric impact energy harvester for burst-type signal generation: a) drawing b) 3D model view

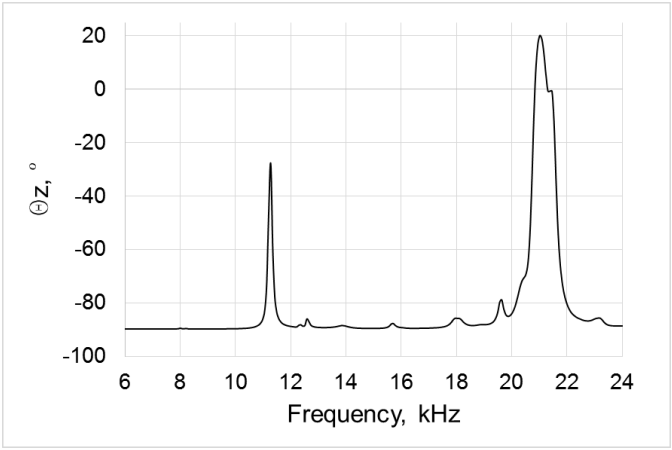

Fig. 3.15 The impedance of the designed piezoelectric impact energy harvester for burst-type signal generation

Resonant frequency of 21.1 kHz is determined considering that the ultrasonic motor which should be controlled operates at 42.6 kHz frequency. This frequency is close to the subharmonic frequency of 21.3 kHz, which resembles the resonant frequency of the designed piezoelectric impact energy harvester for burst-type signal generation.

A piezoelectric shock exciter made of 46 PZT-5A piezoelectric rings (dimensions Ø23x Ø13x0.5 mm, total capacity of 260 Nf) was used to generate shock. This piezo stack can be described as a solid bar of PZT ceramics and when it is electrically discharged sufficiently fast, the internal stress upsurges instantaneously. The initial pressure is the blocking pressure, which causes an accelerated expansion of the piezo stack and creates shock. By coupling the PZT stack to another solid body, in this case the waveguide surface, the shock impulse can be transferred and a shock wave is propagated. In such way, the piezoelectric stack is generating inherently mechanical shock pulses by electrical pulse excitation [32].

In general, such a piezoelectric shock generator could be charged by an alternative energy supply, e.g. solar or photovoltaic panels, and when needed, the shock could be generated by shortening the poles of shock exciter.

To convert mechanical energy into electric, this research uses a Langevin-type piezoelectric transducer made of 4 soft PZT-5A piezoelectric rings, with the total capacity of 6.56 nF. As shown in drawing (Fig. 3.14), the surface area of these piezo rings corresponds with the greater-cross sectional surface of the waveguide, thus the impact energy is transmitted to these piezoelectric rings from the entire surface.

3.3.3. Experimental investigation of the burst-type signal generated with the piezoelectric impact energy harvester

The dependence of the voltage generated with the piezoelectric impact energy harvester on the charging voltage of the piezoelectric shock exciter has been

determined experimentally. The principal scheme of the experiment is presented in Fig. 3.16.

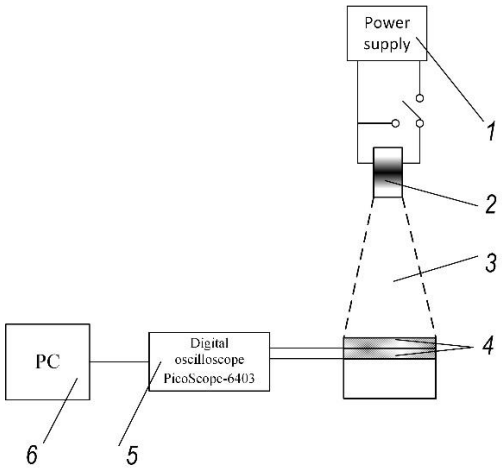

Fig. 3.16 The principal scheme of the experiment with the voltage generated with the piezoelectric impact energy harvester: 1 – power supply, 2 – piezoelectric stack–shock exciter: a piezoelectric ring made of 46 layers 23x13x0,5 mm piezo rings, 3 – stepped-close exponential horn-type waveguide, 4 – Langevin-type piezoelectric transducer, C = 6.56 nF, 5 – digital oscilloscope PicoScope-6403, 6 – PC

As Fig. 3.16 shows, the shock exciter (the piezoelectric stack made of 46 layers 23x13x0.5 mm piezo rings, with total capacity of 260 nF) was charged using DC from traditional power supply 1 (Mastech HY5003 with a laboratory voltage amplifier) with variable voltage in the range of 200–500V and shortened afterwards. Consequently, a shock was generated and the energy thrown into the stepped-close exponential waveguide 3 was transmitted to the Langevin-type piezoelectric transducer 4. Voltage generated by the piezoelectric rings 4 (Langevin-type piezoelectric transducer made of 4 piezoelectric rings, with the total capacity of 6.56 nF) was measured with a digital oscilloscope 5 (PicoScope-6403). Data was acquired and analysed with a PC 6.

The results of the experiment are provided in Fig. 3.17 a), as an example of voltage generated by the piezoelectric impact energy harvester when the piezoelectric shock exciter is charged with 400V. Fig. 3.17 b) shows how the voltage generated with the piezoelectric impact energy harvester depends on the charging voltage of the piezoelectric shock exciter in the range of 200-500 V.

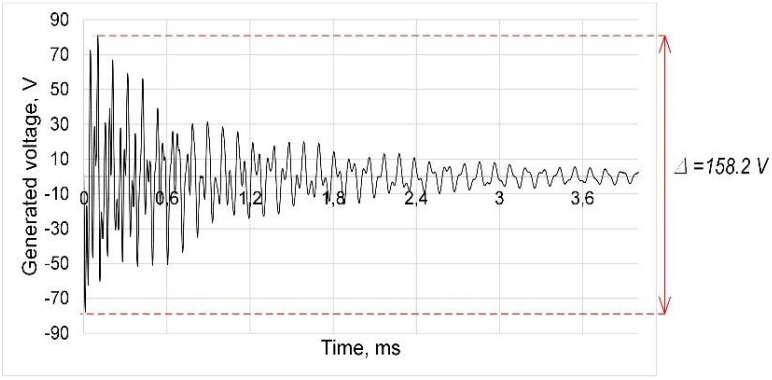

a)

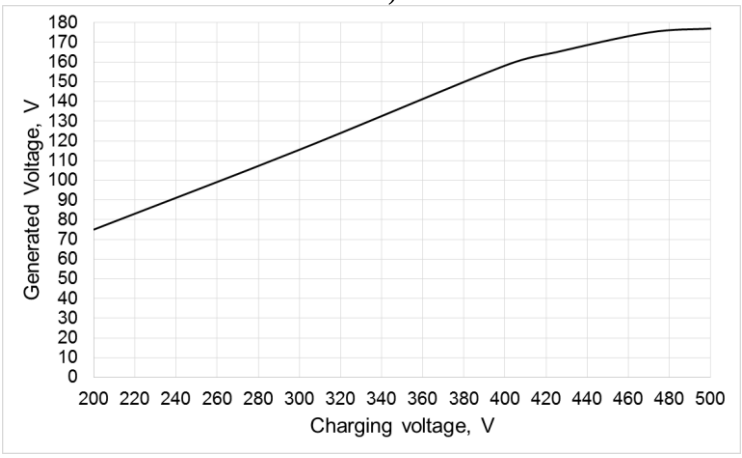

b)

Fig. 3.17 The voltage generated with the piezoelectric impact energy harvester: a) when the shock exciter is charged with 400 V, b) charging voltage in range 200-500 V

As experimental results show, the voltage generated with the Langevin-type piezoelectric transducer increases when the charging voltage of the shock exciter increases up to approximately 470 V. A When the charging voltage increases further over this limit, the voltage generated by the Langevin-type piezoelectric transducer varies only slightly. This is due to the geometric and technical characteristics of the piezoelectric shock-type exciter. Despite this fact, the generated voltage could be adjusted from 75V to 175V in the allowable range of shock exciter's charging voltage. It should provide an opportunity to control the motor steps on demand.

3.3.4. Experimental investigation of ultrasonic motor control using piezoelectric impact energy harvester

This dissertation also investigates the possibility of USM control using the designed piezoelectric impact energy harvester for burst-type signal generation. The experimental layout and stand view are presented in Fig. 3.18. During the experiment, the shock exciter 2 (a piezoelectric stack made of 46 piezo rings, dimensions Ø23x Ø13x0.5 mm, material PZT-5, total capacity of 260 nF), was charged with DC power

supply 1 (Mastech HY5003 with a laboratory voltage amplifier) in a voltage range 315-470 V. Then shock was generated by shortening the contacts of the shock exciter 2, and the stepped-close exponential horn-type waveguide 3 transmitted the generated shock energy to the piezoelectric Langevin-type transducer 4 which consisted of 4 PZT-5 piezoelectric rings, with the total capacity of 6.56 nF. The generated electrical energy was directly transmitted to the USM 5 and a discrete step movement of the rotor was obtained. The USM movement was measured with a laser vibrometer 6, 7 (Polytec OFV-5000/505), data were acquired with a digital oscilloscope 8 (PicoScope-6403) and a PC 9. The sensitivity of the Polytec vibrometer was 2 μm/V during the experiment.

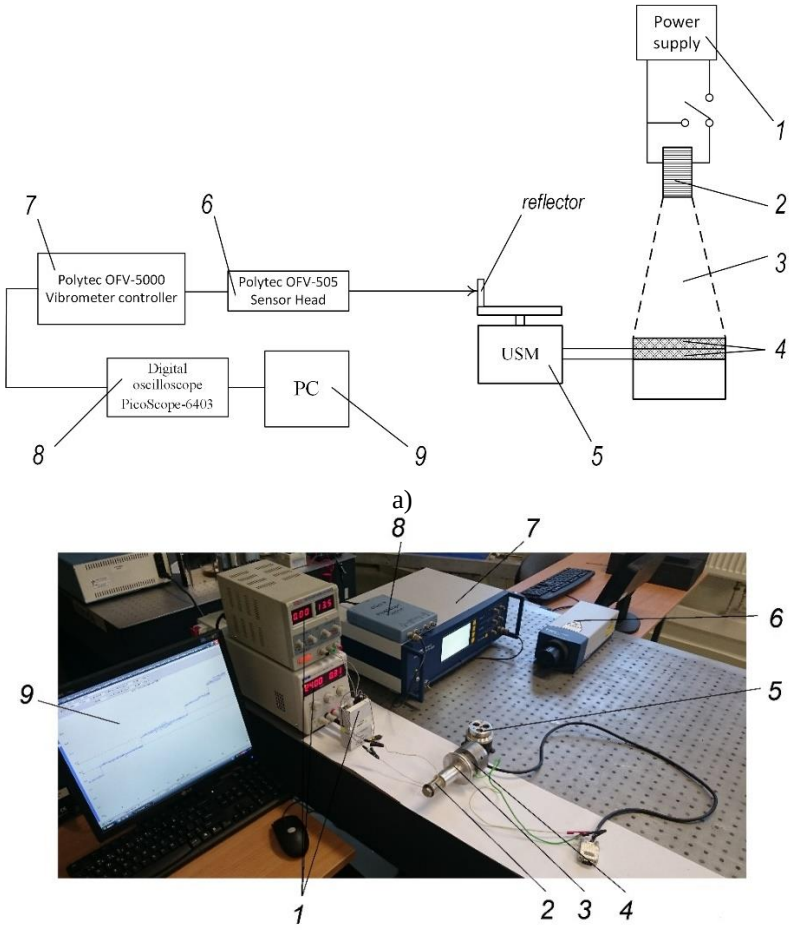

Fig. 3.18 Experimental setup of piezoelectric impact energy harvester for burst-type signal generation: a) layout b) stand view: 1 – power supply, 2 – shock exciter, 3 – stepped-exponential shape horn-type waveguide, 4 – Langevin-type piezoelectric transducer, 5 – USM, 6, 7 – laser Doppler vibrometer, 8 – Digital oscilloscope, 9 – PC

The results of the experiment, i. e. the rotational steps of the motor when the shock exciter was charged with 370 V and 470 V before shortening them are presented in Fig. 3.19.

These investigation (Fig. 3.19) shows that there is direct correlation between the charging voltage of the shock exciter and the height of the motor steps; higher charging voltage results in higher motors steps. The lowest rotational step (1.55 µrad) is obtained at the lowest charging voltage used in the study (315V). The highest rotational step (10.4 µrad) is produced when the charging voltage is 470 V. As mentioned above, higher charging voltage is not allowed due to the technical characteristics of the shock exciter.

The research has also analysed the dependence of the motor step on the charging voltage of the shock exciter and the results are presented in Fig. 3.20.

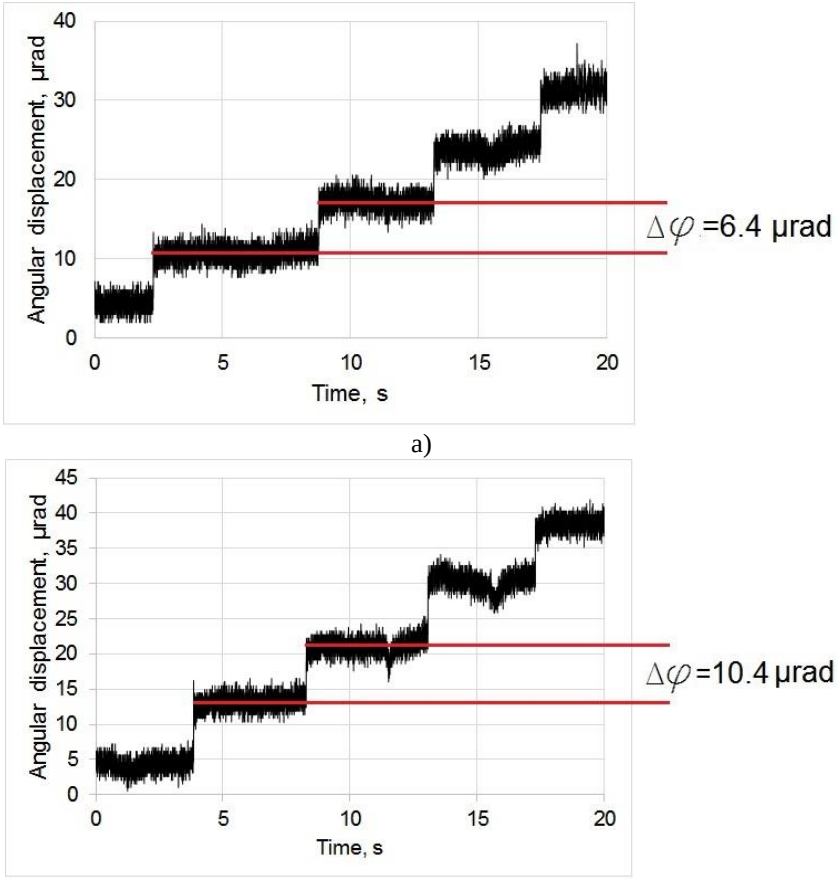

Fig. 3.19 The rotational steps of the motor: a) shock exciter before shortening charged with 370 V, b) shock exciter before shortening charged with 470 V

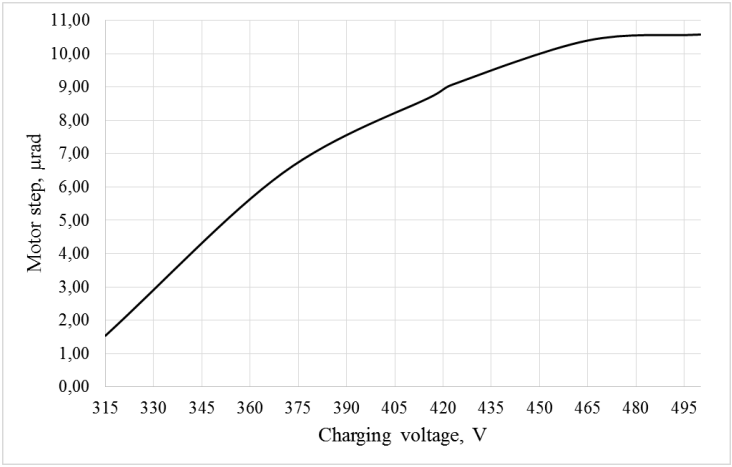

Fig. 3.20 The dependence of the motor rotational steps on the charging voltage of the shock exciter

Based on the graph presented in Fig. 3.20, the appropriate charging voltage can be chosen based on the desired USM step.

In real conditions, i.e. when power supply voltage is 450 V, but only 400 V are needed, the required charging voltage could be obtained by using additional resistance in the power circuit of piezoelectric shock exciter.

3.3.5. Experimental investigation of the shock exciter's power circuit using an additional capacitor

In order to obtain more than one ultrasonic motor step from one charge of the shock exciter, the stud proposes a new technique for the power circuit of the shock exciter. The scheme of the proposed power circuit for the shock exciter and the experimental setup are presented in Fig. 3.21.

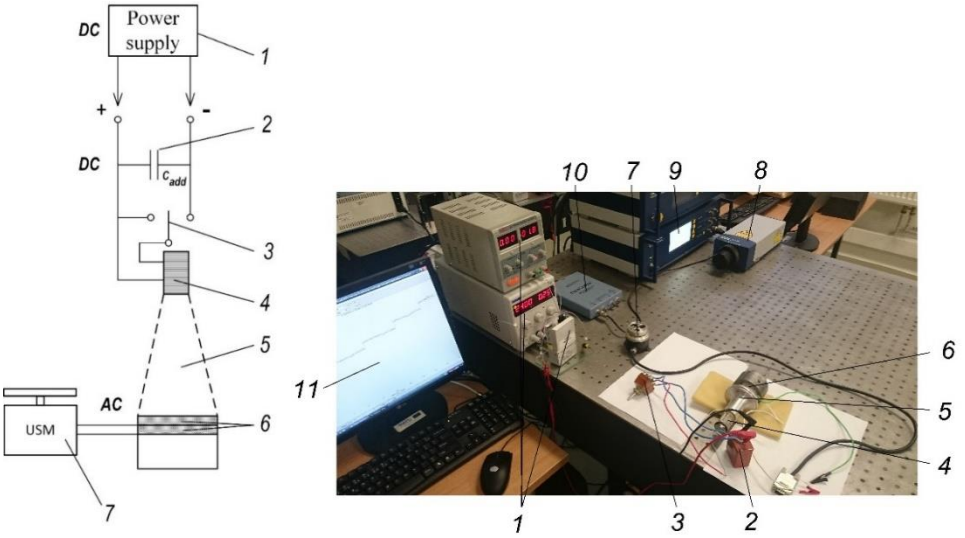

a) b)

Fig. 3.21 The power circuit of the shock exciter: a) layout of the piezoelectric impact energy harvester with an additional capacitor, b) experimental setup: 1 – power supply, 2 – additional capacitor, 3 – switch, 4 –shock exciter, 5 – stepped-close exponential horn-type waveguide, 6 – Langevin-type piezoelectric transducer, 7 – USM, 8,9 – laser vibrometer, 10 – digital oscilloscope, 11 – PC

This power circuit of the shock exciter (Fig. 3.21) involves a DC power supply 1 (e.g. solar panels, thermoelectric panels, etc.), an additional capacitor of 100 μF 2, a switch 3, a shock exciter 4, a stepped-close exponential waveguide 5, a Langevin-type piezoelectric transducer 6 with the total capacity of 6.56 nF, a USM 7 (operating frequency 42.6 kHz), a laser Doppler vibrometer 8, 9 (Polytec OFV-5000/505), a digital oscilloscope 10 (PicoScope 6403) and a PC – 11.

Such power circuit operates as follows: at the beginning, the additional capacitor which is located between the power supply and the shock exciter is charged up to 470 V with a DC power supply; this research used the Mastech HY5003 with a laboratory voltage amplifier. Then the contacts of the shock exciter are shortened in different directions after every motor step and shock is obtained from one charge of the additional capacitor.

Experimental results show that the presented technique for controlling the shock exciter (Fig 3.21) works correctly and generates up to 30 ultrasonic motor steps from one electric charge of the additional capacitor C_{add}=100μF. As in the experiment without the additional capacitor, the highest step is obtained at the first step (10.4 μrad) and is the same until the 21st. The lowest is the 30th step – 2.5 μrad.

The last 10 motor rotational steps of the total 30 obtained during the experiment from one electric charge of the additional capacitor (up to 470 V) are presented in Fig. 3.22.

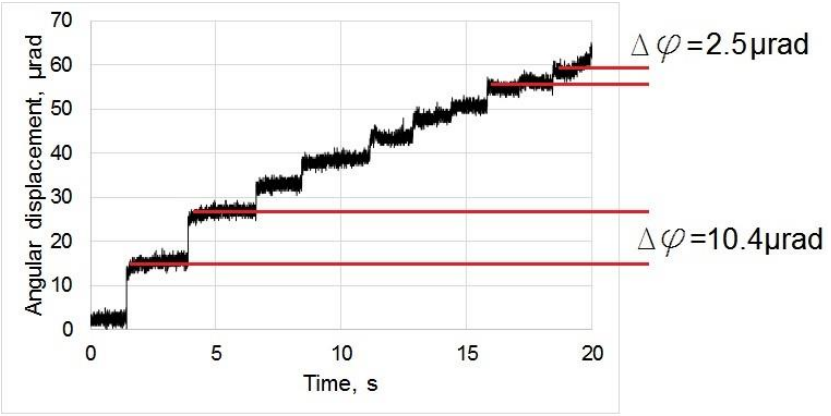

Fig. 3.22 The last 10 motor rotational steps (of 30) from one electric charge of the additional capacitor up to 470 V

Such power circuit could be especially helpful in areas where traditional DC power supply is unavailable, e.g. in space or nature, where alternative energy supply, such as solar etc. could be used. For example, solar panels could charge the additional capacitor through a certain control circuit, and after that, the ultrasonic motors steps could be obtained without a recharge after every step.

3.4. The dependence of motor resolution on the burst-type excitation signal

In order to investigate how parameters, such as amplitude and duration (frequency) of the burst type signal influence the USM steps additional experiment was carried out. The principal scheme and setup of the experiment are presented in Fig. 3.23.

The excitation signal, as damped oscillation with variable frequency and amplitude, was formed using a signal generator 1 (Rigol DG103Z) and amplified with an amplifier 2 (EPA-104). Then this signal was transmitted directly to the ultrasonic motor 3 (USM-50-3, for more details see Table 10) and its movement – the rotational steps were measured with a laser Doppler vibrometer 4, 5 (Polytec OFV-5000/505), the data was acquired with a digital oscilloscope 6 (PicoScope-6403) and a PC 7.

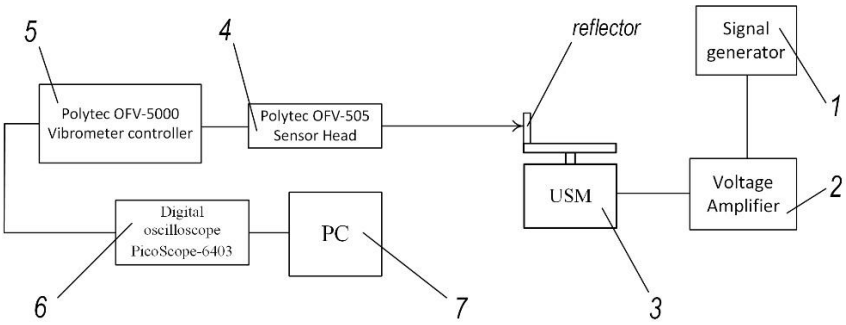

a)

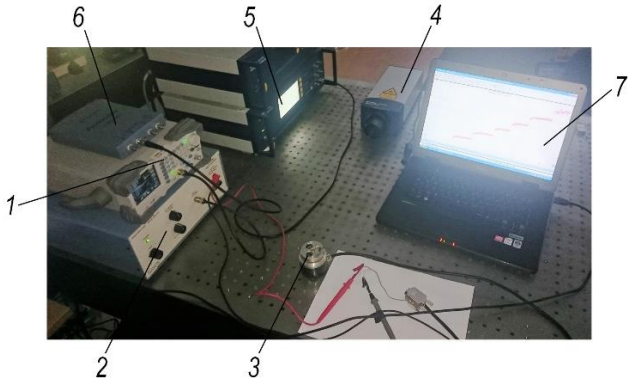

b)

Fig. 3.23 The experimental setup for analysing the influence of the excitation signal parameters on the USM steps: a) scheme b) setup: 1 – signal generator; 2 – voltage amplifier; 3 – USM; 4, 5 – laser vibrometer; 6 – digital oscilloscope; 7 – PC

The excitation signal generated with the signal generator under the frequency of 21.3 kHz and voltage of 150 V peak-to-peak is presented in Fig. 3.24.

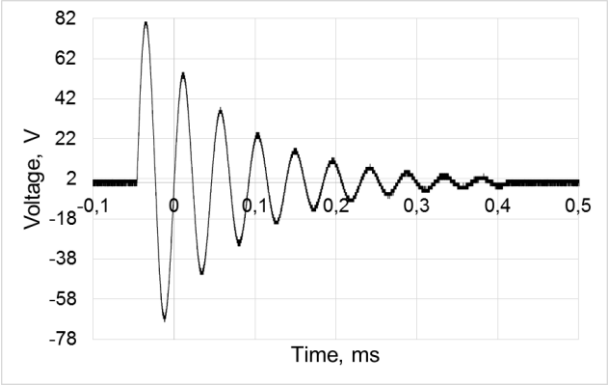

Fig. 3.24 The excitation signal generated with a signal generator – voltage 150 V peak-to-peak, frequency – 21.3 kHz

The first stage of the experiment was carried out under the same amplitude of the excitation signal (150 V), only the excitation frequency differed. Fig. 3.25 shows how the size of USM step is influenced by the excitation signal when the excitation frequency is between 9.8 and 56.4 kHz.

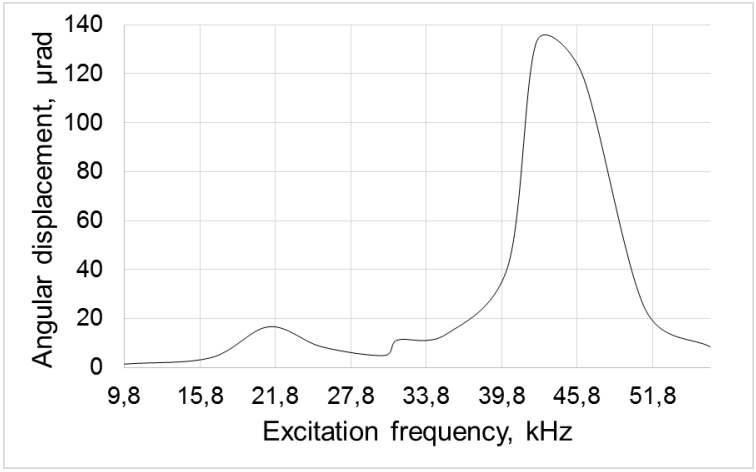

Fig. 3.25 The influence of the excitation signal frequency on the ultrasonic motor step when the excitation amplitude is 150 V peak-to-peak

The results indicate that the size of the motor step increases to 16.7 µrad at the excitation frequency of 21.3 kHz, which is the subharmonic operating frequency of the USM (42.6 kHz). Besides this increase, a very significant peak is noticed at the excitation frequency of 42.6 kHz, which corresponds to the operating frequency of USM; the motor step increases up to 133.3 µrad. This step is 7.98 times higher than the step obtained at the subharmonic frequency of 21.3 kHz when the voltage is the same. This implies that in order to increase the efficiency and obtain the highest possible USM step, the frequency of the piezoelectric impact energy harvester must correspond with the operating frequency of the USM. If the maximum step is not necessary, the piezoelectric impact energy harvester could also be used with the frequency which corresponds the subharmonic USM operating frequency.

Moreover, the research has also investigated if and how the USM step is influenced by the excitation signal voltage peak to peak. During this experiment, the frequency of the excitation signal corresponded to the USM operating frequency (42.6 kHz) and the voltage peak-to-peak varied in range from 0 up to 150V.

The relationship between the motor step size and the excitation signal amplitude when the excitation frequency is 42.6 kHz and the amplitude varies from 0 to 150V is presented in Fig. 3.26.

The results show that the minimum amplitude at which motor step is obtained when the excitation signal frequency corresponds with the USM operating frequency is approximately 25 V peak-to-peak. When the excitation amplitude increases to 75 V, the motor step varies insignificantly, but when the excitation voltage rages between 75 V and 150 V, the motor step size increases proportionally to the excitation amplitude and the dependency becomes linear.

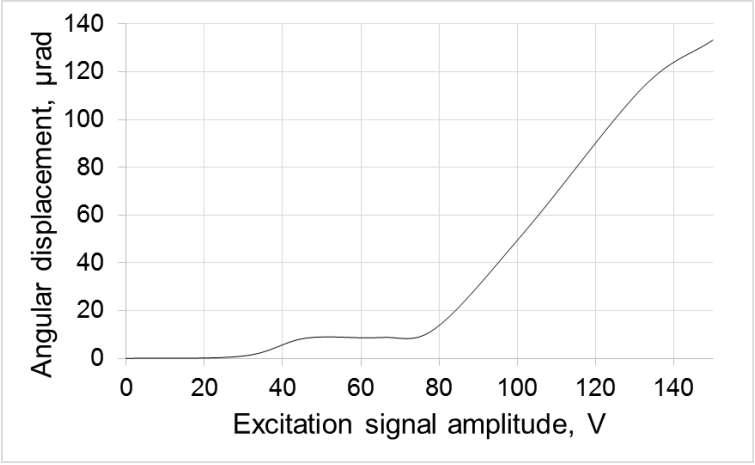

Fig. 3.26 The relationship between the motor step and the excitation signal amplitude when the excitation frequency is 42.6 kHz

It could be concluded that the minimum voltage amplitude of the excitation signal should be 25 V, and when it exceeds 75 V, the motor step increases linearly along the excitation signal amplitude while the excitation frequency is the same and corresponds with the operating frequency of the USM.

3.5. Conclusions of the section

This section has presented the experimental studies of the piezoelectric impact energy harvester for burst-type signal generation, which include experimental research of mechanical impact, horn-type waveguides and ultrasonic motor control. The experiments used 1D and 3D scanning laser Doppler vibrometers (Polytec Inc.), the holographic interferometry system PRISM 100 (Hytec Inc.), the impedance meter Wayne Kerr 6500B and high frequency accelerometers (Bruel and Kjaer).

The following conclusions are formulated:

- The results of the experimental investigation of mechanical impact are similar to results the obtained during theoretical calculations; they have shown that it is very important to match the surfaces of the impacting materials when using mechanical impact in order to obtain the desired shock amplitude and duration.
- Experimental research of horn-type waveguides with harmonic excitation indicates that the displacement of greater cross-sectional surface of the conical horn-type waveguide is from 1.27 to 1.87 times higher than that of a cylindrical waveguide depending on the method used for investigation when the excitation conditions are the same.
- The “soft” piezoelectric material (PZT-5A) provides 1.4 times higher amplitude of generated voltage than the “hard” piezoelectric material PZT-4 when the motion impact quantity is the same for both materials – 0.015 $kg \cdot m \cdot s^{-1}$.
- A piezoelectric impact energy harvester for burst-type signal generation with a resonant frequency of 21.1 kHz and stepped-close exponential horn-type

waveguide was designed and fabricated. Such a harvester generates rotary USM-50-3 steps from 1.55 μrad up to 10.4μrad.

- In order to obtain more than one ultrasonic motor step from one charge of the shock exciter, a power circuit for the shock exciter was proposed and investigated. Research shows that this circuit allows to drive the USM for up to 30 steps from one electric charge of the additional capacitor. The steps obtained from one charge vary from 10.4μrad (the first step) to 2.5 μrad (the thirtieth step).
- The USM step increases when the frequency of the excitation signal corresponds with the subharmonic operating frequency of the USM when the driving voltage is the same. The highest USM step – approximately 8 times higher than the step generated by the excitation with a subharmonic frequency – is generated with the excitation signal with a frequency which corresponds with the operating frequency of the USM when the amplitude is the same. These results suggest that in order to increase the efficiency of the harvester and obtain the highest possible USM step USM, the frequency of the piezoelectric impact energy harvester for burst-type signal generation must correspond to the operating frequency of the USM. To produce the higher USM-50-3 step, it is essential to design and manufacture the new piezoelectric impact energy harvester for burst-type signal generation with its resonant frequency close to 42.6 kHz.

4. DESIGN METHODOLOGY FOR CERTAIN ULTRASONIC MOTOR CONTROL

Experimental results showed that in order to increase the efficiency of the harvester and obtain the highest possible step of the USM, the excitation signal frequency should correspond to the USM operating frequency. Therefore, a new piezoelectric impact energy harvester for burst-type signal generation must be designed, fabricated and tested. Moreover, since the piezoelectric shock-type exciter cannot be used where traditional or alternative energy sources are unavailable, a new type of shock exciter is needed. A novel piezoelectric impact energy harvester must be designed to control the USM-50-3; it should be human-operated thus eliminating the need for any type of energy sources.

Using the methodology presented below, a piezoelectric impact energy harvester for USM with any operating frequency could be designed and investigated.

4.1. Design and theoretical investigation of a piezoelectric impact energy harvester for burst-type signal generation

The theoretical investigation is divided into two stages. First, the piezoelectric impact energy harvester for burst-type signal generation without a shock exciter is investigated, then only the shock exciter is analysed.

To begin with, a new piezoelectric impact energy harvester without a shock exciter was designed, and its resonant frequency of the longitudinal mode was determined using the FEM computational software. The drawing including the dimensions and the 3D model of the impact energy harvester are presented in Fig. 4.1.

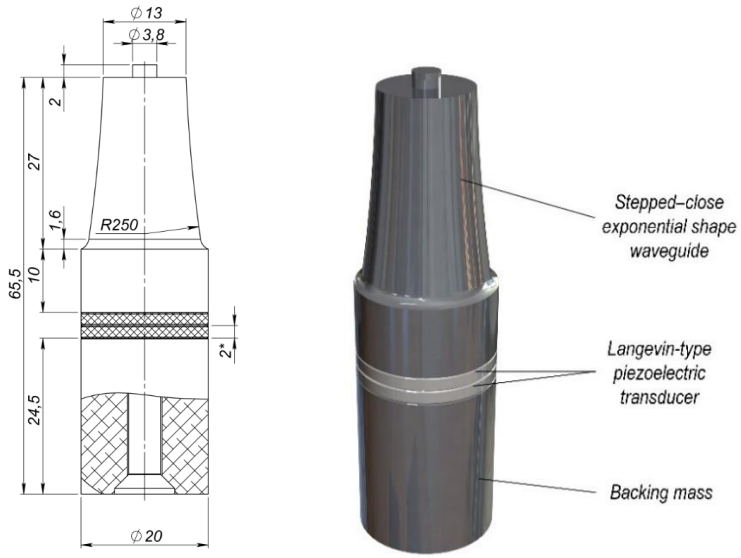

a) b)

Fig. 4.1 A new piezoelectric impact energy harvester for burst-type signal generation without a shock exciter: a) drawing b) 3D model

As Fig. 4.1 indicates, such an impact energy harvester consists of a stepped-close exponential horn-type waveguide and a Langevin-type piezoelectric transducer made of two PZT-5A piezoelectric rings, the surface area of which equals the greater cross-sectional surface of the horn-type waveguide.

The theoretical investigation applied the Solidworks frequency analysis software. The stepped-close exponential horn-type waveguide and the backing mass material is Aluminium 6061-T6; its properties are presented in Table 4. The piezoelectric rings have been made of custom material of 7.75 g/cm^3 density, what corresponds to the density of the "soft" PZT-5A material. The screw was made of steel 1006 (see Table 4). The contact between all parts – the waveguide, piezoelectric rings, the backing mass and the screw – was bonded. The computational model which consists of 50382 finite elements and 72962 nodes is presented in Fig. 4.2 a).

The displacement of piezoelectric impact energy harvester at longitudinal mode which was obtained at the resonant frequency of 42.607 kHz is presented in Fig. 4.2.

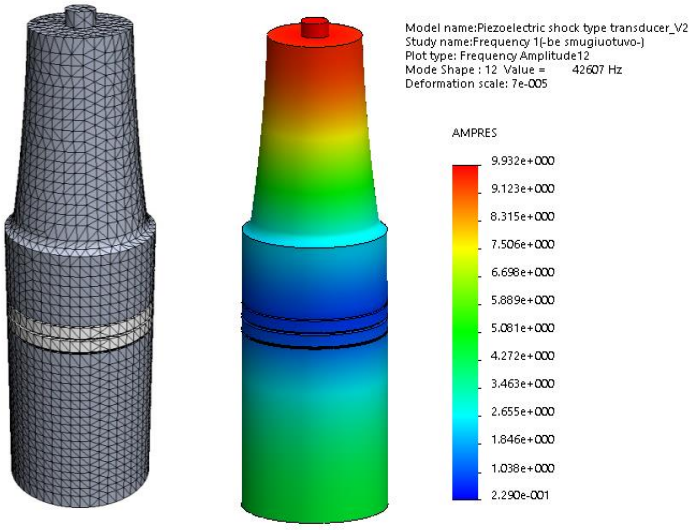

a) b)

Fig. 4.2 Theoretical investigation of a piezoelectric impact energy harvester without a shock exciter: a) computational model b) longitudinal mode at resonant frequency of 42.607 kHz

So far, the modelling results show that the resonant frequency of the longitudinal mode of such a harvester is very similar to the operating frequency of the USM-50-3. Therefore, it is suitable for USM-50-3 control.

To develop a shock exciter which could be used in areas where traditional or alternative energy sources are unavailable, a mechanical shock exciter operated by human force is designed. A drawing with dimensions and a 3D model of it are presented in Fig. 4.3.

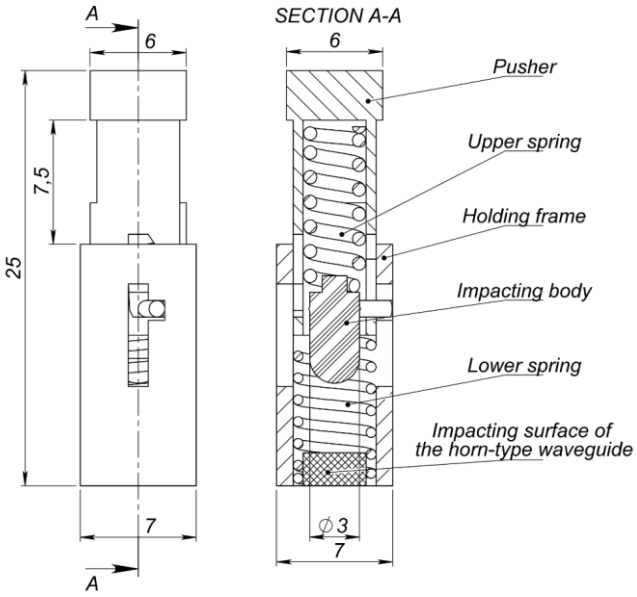

a)

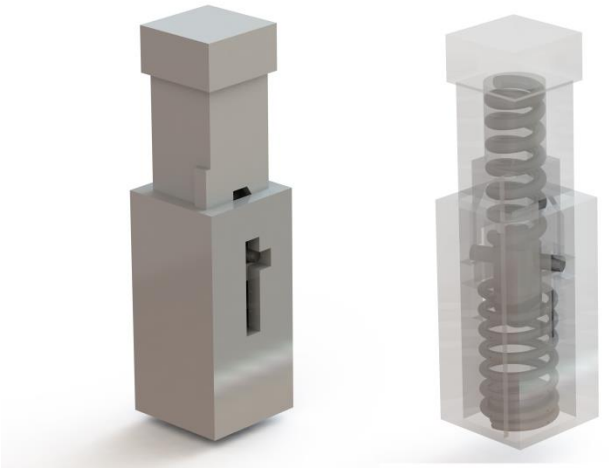

b)

Fig. 4.3 Human-operated mechanical shock exciter: a) drawing b) 3D model view

Fig. 4.3 presents the components which make this shock exciter; it is composed of two springs, an impacting body, a holder frame and a pusher. The working principle is illustrated in Fig. 4.4; at the initial condition (Fig. 4.4 a) the pusher 1 is pushed down by human force, in this case, a finger, until the upper spring 2 is compressed and the maximum energy of this spring is generated. Then, the pusher 1 releases the impacting body 3 by chamfer and generating shock to the impacting surface of the horn-type waveguide 5 (Fig. 4.4 b). After the shock, the lower spring 4, which at this

time is fully compressed by the edge of the pusher (Fig. 4.4 c), pushes the impact body up to the initial condition.

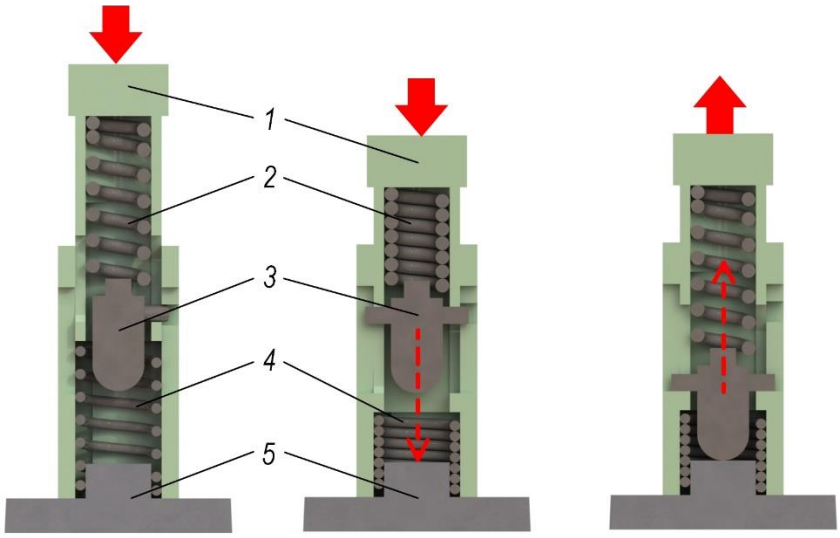

a) b) c)

Fig. 4.4 The operating principle of the mechanical shock exciter: a) initial condition b) shock beginning stage c) aftershock stage – return to the initial condition. Here, 1 – pusher, 2 – upper spring, 3 – impacting body, 4 – lower spring, 5 – impacting surface

The parameters of impact significantly depend on the materials used both for the impacting body and the surface, but mostly on the parameters of the upper spring.

With regards to the fact that the USM generates the highest step when the excitation signal frequency corresponds to the operating frequency of the USM, the shock exciter should generate an impulse with approximately 23.5μs duration, which corresponds to 42.6 kHz frequency. For this purpose, three theoretical investigations of mechanical shock exciter were carried out. First of all, the influence of dimensions on the stiffness of the spring was investigated with the aim to determine the lowest and the highest stiffness of the upper spring according to the dimensions of the designed mechanical shock exciter. The possible extreme geometrical dimensions of upper spring are presented in Table 11.

Table 11. Possible extreme dimensions of the upper spring

Characteristic	Value
Minimum inner diameter	1.6 mm
Maximum outer diameter	3.8 mm
Number of active coils	7
Non-compressed spring length	10.5 mm
Compression stroke	4 mm

In general, the stiffness of the spring is determined as [82]:

$$k = \frac{Gd^4}{8D^3N}; \quad (4.1)$$

where k – spring stiffness, N/mm; G – shear modulus of the spring material, N/mm^2; d – wire diameter, mm; D – mean coil diameter, mm; N – number of active coils.

The shear modulus of the spring steel used for the calculation is 81500 N/mm^2. The wire diameter could be between 0.4 mm and 0.6 mm according to the geometrical dimensions. Therefore, the mean diameter of the coil is between 2.2 mm and 3.2 mm. Seven active coils were used for all theoretical investigations.

The relationship between the stiffness of the spring and the mean diameter of the coil when the wire diameter is 0.4, 0.45, 0.50, 0.55 and 0.6 mm, respectively, is presented in Fig. 4.5.

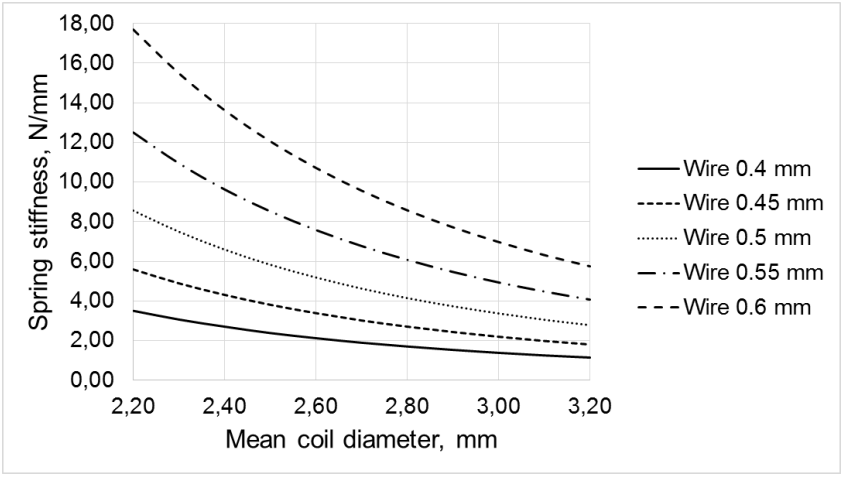

Fig. 4.5 The relationship between spring stiffness and mean coil diameter

According to the geometrical dimensions of the designed piezoelectric impact energy harvester for burst-type signal generation the lowest spring stiffness is 1.14 N/mm when the upper spring wire diameter is 0.4 mm and mean coil diameter is 3.2 mm. The highest spring stiffness is 17.71 N/mm when the spring wire diameter is 0.6 mm and mean coil diameter is 2.2 mm.

The second theoretical investigation determined the velocity of the designed mechanical shock exciter's impacting body (during impact with waveguide's surface) from the upper spring stiffness. For this purpose, a computational model presented in Fig. 4.6 was created using SolidWorks Motion analysis software.

For the computation, the initial distance between the impacting body and the waveguide's surface was 4 mm, which coincides with the real distance in the designed mechanical shock exciter. The spring force expression was linear – 1. The velocity of the impacting body was determined as the it hit the surface of the waveguide due to compressed spring stiffness, which varied from 1.14 N/mm up to 17.71 N/mm.. As an example, the velocity of the impacting body when the spring stiffness is 1.14 N/m is presented in Fig. 4.7.

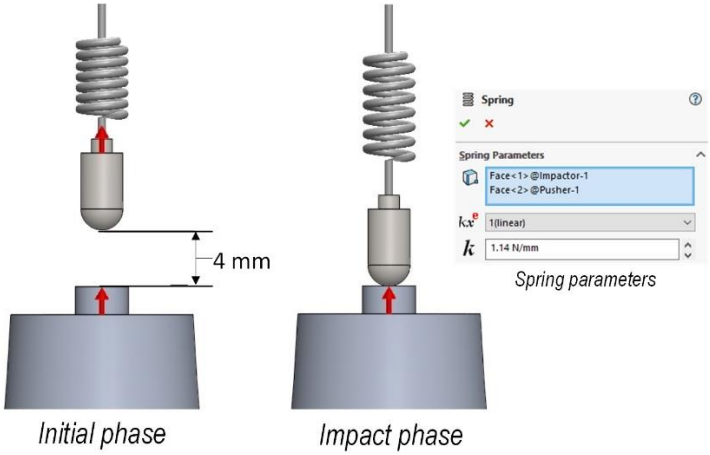

Fig. 4.6 Computational model created using SolidWorks motion analysis software

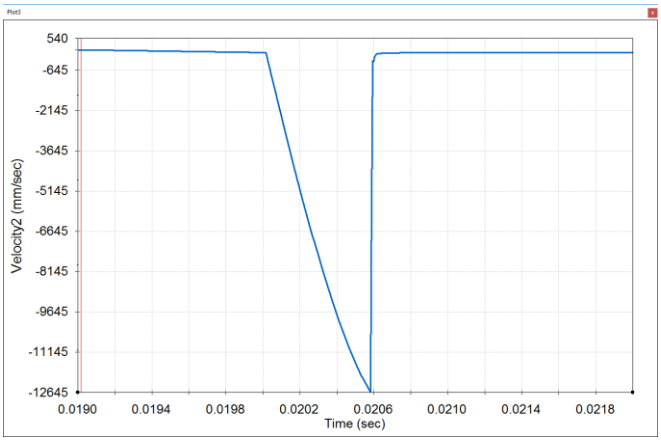

Fig. 4.7 Impacting body velocity when upper spring stiffness is 1.14 N/mm

The theoretical influence of the upper spring stiffness on the velocity of the impacting body is presented in Fig. 4.8.

These results (Fig. 4.8) show that the lowest possible impacting velocity is 12.5 m/s, when the upper spring stiffness is 1.14 N/mm, and the highest is 47.5 m/s, when upper spring stiffness is 17.71 N/mm.

With reference to the results presented in Fig. 4.5 and Fig. 4.8, it is possible to determine what impact velocity is generated by springs of different dimensions.

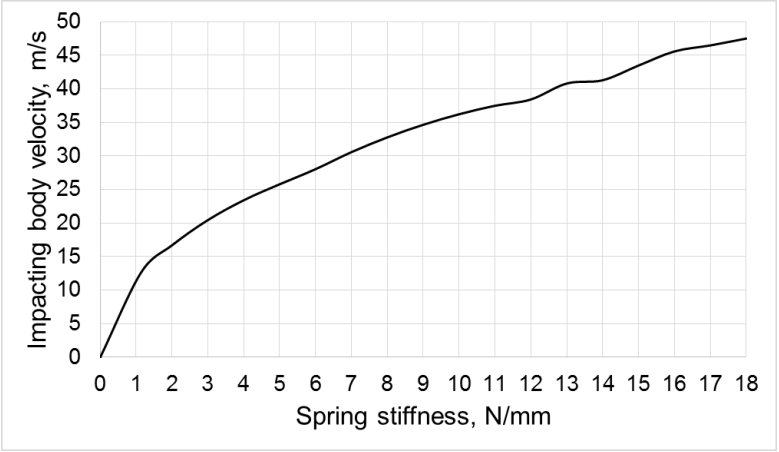

Fig. 4.8 The influence of upper spring stiffness on the velocity of the impacting body

The third theoretical investigation determined the velocity and displacement generated by different springs. A computational model was created using the ANSYS Explicit dynamics software with AUTODYN solver. Since the horn-type waveguide is a symmetrical device, only a quarter of it and the impacting body were modelled. The computational model with boundary conditions and gauge points consists of 93,472 finite elements with 87,775 nodal points; it is presented in Fig. 4.9. Gauge points 1 and 2 are located on the surface of the waveguide while gauge points 3 and 4 are located on the surface of the impacting body.

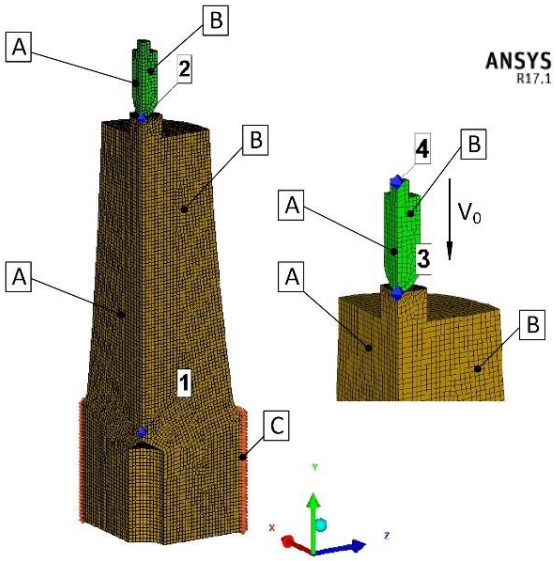

Fig. 4.9 The computational model with boundary conditions: A, B – section planes, C – waveguide's surface, v_0 – direction of initial velocity, 1, 2 – gauge points on the waveguide, 3, 4 – gauge points on the impacting body

The geometrical dimensions of the impacting body and horn-type waveguide are the same as those of the designed piezoelectric impact energy harvester for burst-type signal generation presented in Fig. 4.1. The boundary conditions are as follows: both the waveguide and the impacting body are fixed by two section planes A and B (see Fig. 4.9) by 0 m/s velocity in z and x directions, respectively. The waveguide is fixed on surface C by 0 m/s velocity in y direction. The impacting body has the initial directional velocity in y direction, which, according to previous results (Fig. 4.8), varies from 0 m/s to 50 m/s. Due to this, the initial velocity impacting body impacted the surface of the horn-type waveguide and generated impact.

This investigation was carried out in four different variations, and in all of them the impacting body was made of Steel 1006. The waveguide material varied: Al6061-T6, Steel 1006, Al2024-T4 and steel SS304 were used in the four experiments, respectively. The properties of the materials used in this modelling are presented in Table 12.

Table 12. The properties of materials used in modelling

Parameter	Measurement unit	Steel 1006	Aluminium AL6061-T6	Aluminium AL2024-T4	Steel SS304
Density	kg/m^3	7896	2703	2785	7900
Gruneisen coefficient	-	2.17	1.97	2.0	1.93
Shear modulus	GPa	81.8	27.6	28.6	77.0
Yield stress	MPa	350	290	260	340

The displacement in y direction (Fig. 4.9) of gauge point no.3, which is located on the top of the impacting body when the waveguide is made of Steel 1006 and the initial velocity of the impacting body is 22 m/s is presented in Fig. 4.10.

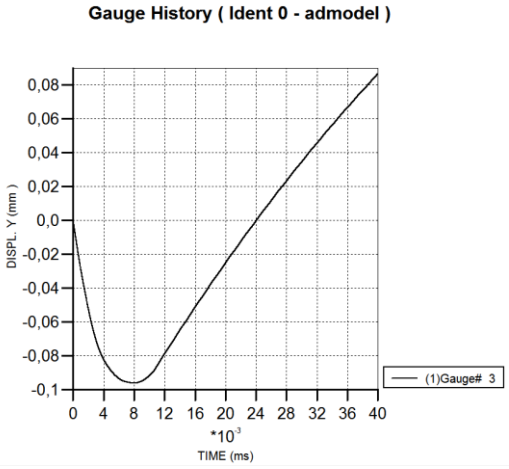

Fig. 4.10 Gauge point no. 3 displacement in y direction when the waveguide is made of Steel 1006 and the initial velocity of the impacting body is 22 m/s

The results show (Fig. 4.10) that at first, the displacement of gauge point no. 3 goes to negative side and reaches the maximum value of approximately 0.98 mm before returning to positive value. After 24 μs, the displacement becomes 0 mm and then goes forward in positive direction. This curve coincides with the movement of the impacting body. According to the Newton law, it could be considered that it corresponds with the velocity rate and duration of the generated impact. Therefore, it could be concluded that impact with the initial velocity of 22 m/s when the impacting body is made of aluminium AL6061-T6 and the impacting surface (waveguide) is made of Steel 1006 generates 24 μs long impact which corresponds with the frequency of approximately 41.7 kHz. This generated impulse duration is rather close to the desired one (23.5 μs), but to generate an impulse with a duration closer to the desired one, a different impact parameter should be chosen. For this purpose, the modelling results of the displacement duration gauge point no. 3 in y direction, thus the duration of generated impact, when the horn-type waveguide is made from various materials (see Table 12) and the initial velocity is between 2 and 50 m/s are presented in Fig. 4.11.

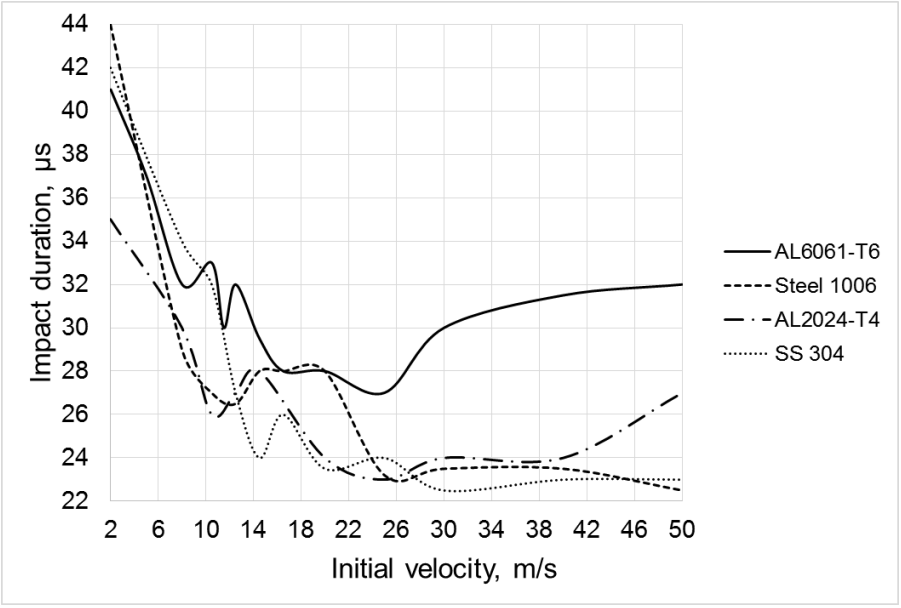

Fig. 4.11 The duration of gauge point no. 3 displacement in y direction, when the horn-type waveguide is made from different materials and the initial velocity of the impacting body is between 2 and 50 m/s

The results (Fig. 4.11) show that the generated impact duration of approximately 23.5 μs is nearly several times longer: when the horn-type waveguide is made from Steel 1006, AL2024-T4 and SS 304 and the initial velocities are 30, 23.5 and 20 m/s, respectively. The results provided in Fig. 4.11, Fig. 4.8 and Fig. 4.5 help to determine the material of the waveguide's impacting surface as well as the parameters of the upper spring depending on the desired generated impulse duration.

In our case, the desired generated impulse duration is 23.5 μs (according to USM-50-3 operating frequency of 42.6 kHz). Therefore, based on the experimental results, Al2024-T4 is chosen for the waveguide. Since the initial velocity of the impact body should be 23.5 m/s (when the waveguide is made from Al2024-T4), that the stiffness of the upper spring should be 4 N/mm. Finally, based on results presented in Fig. 4.5, it is clear that such stiffness of the spring is appears in three instances: when the wire diameter is 0.45 mm and the mean coil diameter is 2.45 mm, when the wire diameter is 0.5 mm and the mean coil diameter is 2.85 mm, or when the wire diameter is 0.55 mm and mean coil diameter is 3.2 mm. This research uses a spring of 2.85 mm mean coil diameter and 0.5 mm wire diameter, thus the inner spring diameter is 2.35 mm and the outer diameter is 3.35 mm.

Using this methodology, it is possible to determine how the desired upper spring depends on the parameters of the required impact, thus required to drive the USM.

In order to create an ergonomic solution for a person to control the USM motor, a plastic frame was designed for the piezoelectric impact energy harvester. A 3D model of the piezoelectric impact energy harvester for burst-type signal generation with the ergonomic frame and a drawing with its dimensions are presented in Fig. 4.12. The piezoelectric impact energy harvester for burst-type signal generation 4 with a shock exciter 1 on the smaller cross-sectional surface is fitted into the plastic frame 2. The harvester is softly fixed at the centre of its gravity with a rubber bushing 3 and at the bottom with a rubber pad 5. The whole system is covered with a plastic cap 6 at the bottom and tightened with screws 7.

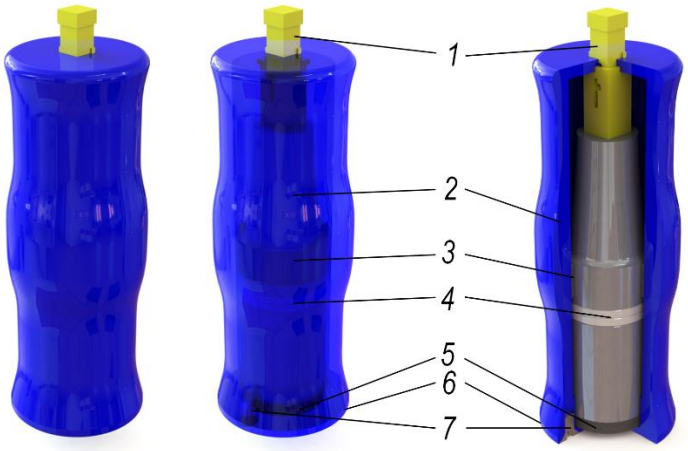

a)

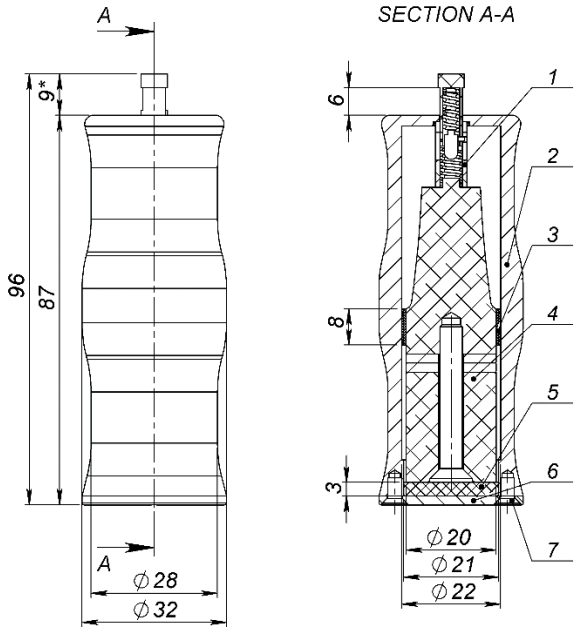

b)

Fig. 4.12 A piezoelectric impact energy harvester for burst-type signal generation: a) 3D model b) drawing: 1 – shock exciter, 2 – plastic frame, 3 – rubber bushing, 4 – piezoelectric impact energy harvester, 5 – rubber pad, 6 – plastic cap, 7 – screws for tightening

The dimensions of the harvester presented above make it easily fit into a hand and comfortably operate. This harvester allows driving the USM whenever it is needed, completely independently from any source of energy.

4.2. Experimental investigation of the piezoelectric impact energy harvester for burst-type signal generation

In order to verify the results of theoretical investigation, the piezoelectric impact energy harvester for USM-50-3 control was analysed experimentally. A prototype of the piezoelectric impact energy harvester for burst-type signal generation was fabricated and investigated with regards to the dimensions obtained during theoretical investigation.

First of all, impedance of the fabricated harvester with stepped-close exponential horn-type waveguide made of AL2024-T4 and a Langevin-type piezoelectric transducer which consists of 2 piezoelectric rings made of “soft” PZT-5A piezoelectric material, with the total capacity of 3.5 nF and the dimensions of 20x5.5x2, was measured with the Wayne Kerr 6500B impedance meter. The impedance is presented in Fig. 4.13.

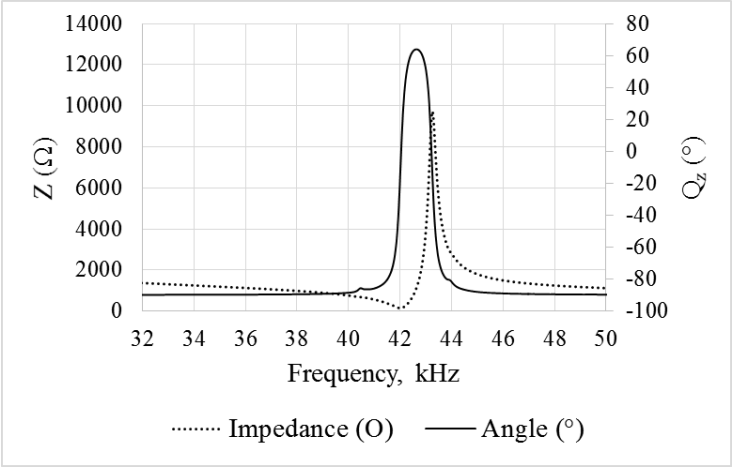

Fig. 4.13 Impedance and phase angle of the fabricated piezoelectric impact energy harvester

The resonant frequency of the longitudinal mode of the piezoelectric impact energy harvester for burst-type signal generation is approximately 42.6 kHz. The lower frequency range is not presented due to the fact that the developed piezoelectric impact energy harvester is intended for generating a burst-type signal in the ultrasonic frequency range. This verifies the theoretical calculations and proves the ability to control USM-50-3 using this type of harvester.

The voltage generated by the piezoelectric impact energy harvester was experimentally researched to investigate the parameters of the excitation signal. The layout of the experiment is presented in Fig. 4.14.

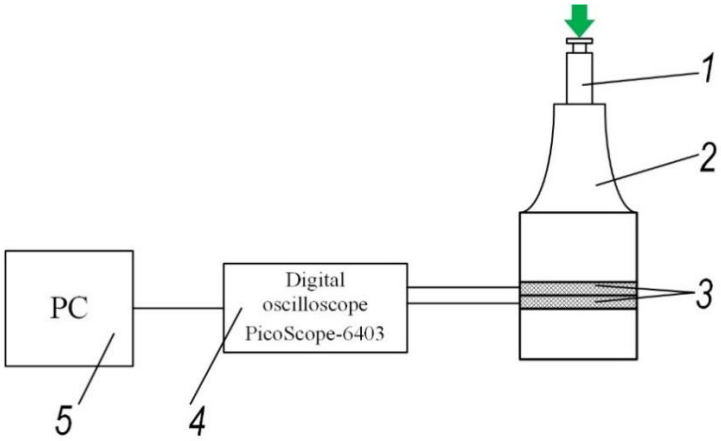

Fig. 4.14 The experimental setup for analysing the voltage generated by the piezoelectric impact energy harvester: 1 – mechanical shock exciter, 2 – stepped-close exponential horn-type waveguide, 3 – Langevin-type transducer, 4 – digital oscilloscope, 5 – PC

During the experiment, shock was generated using a mechanical shock exciter 1 by human's finger force and the transmitted generated energy to the Langevin-type piezoelectric transducer 3 made of two piezoelectric rings with total capacity of 3.5 nF. The signal generated by two piezoelectric rings 3 was measured with a digital oscilloscope 4 (PicoScope-6403). Data was acquired and analysed with a PC 5.

The signal generated by the harvester from one push of the mechanical shock exciter is presented in Fig. 4.15.

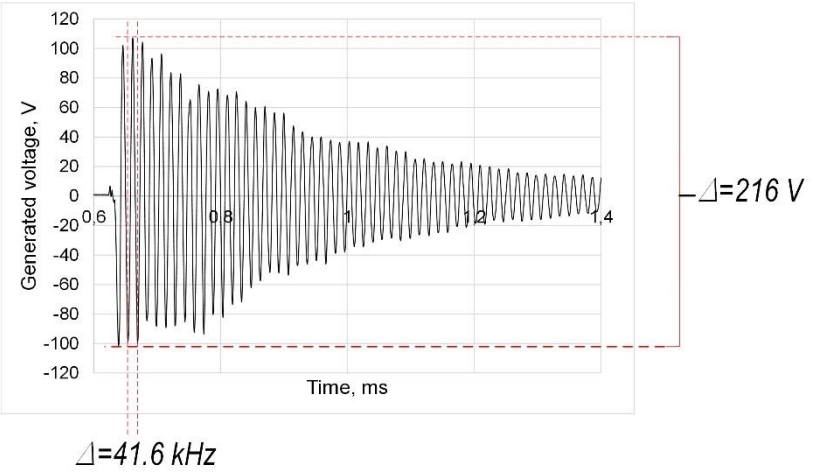

Fig. 4.15 The signal generated by the piezoelectric impact energy harvester from one push of the mechanical shock exciter

As it is seen from Fig. 4.15, the fabricated prototype of a piezoelectric impact energy harvester generates a signal with the peak-to-peak voltage of approximately 216 V and the frequency of approximately 41.6 kHz. These parameters closely resemble the operating frequency of the USM-50-3; thus this prototype is suitable for driving the USM-50-3.

Additionally, the dissertation analyses the size of USM step generated with the designed piezoelectric impact energy harvester for burst-type signal generation. The principal layout and stand view are presented in Fig. 4.16.

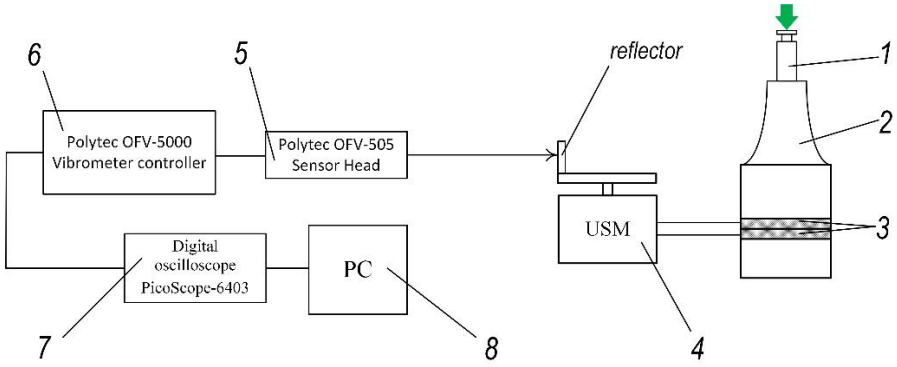

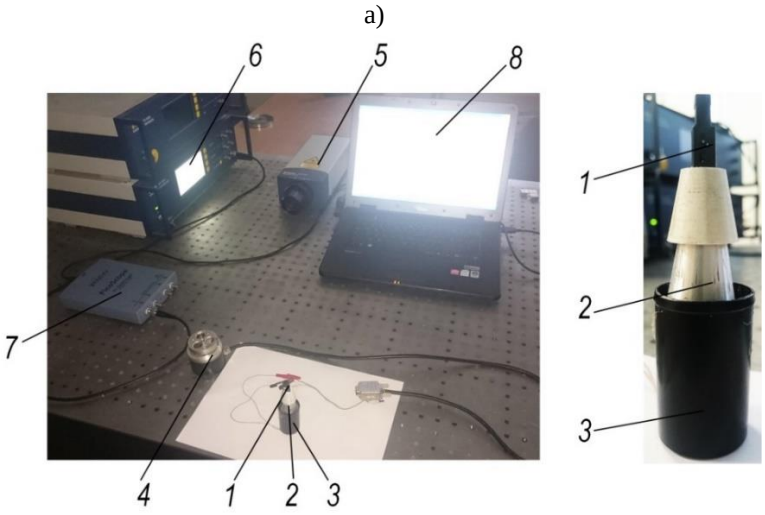

Fig. 4.16 The experimental setup of USM step generation using the designed piezoelectric impact energy harvester for burst-type signal generation: a) layout b) stand view c) prototype of the piezoelectric impact energy harvester: 1 – mechanical shock exciter, 2 – stepped-close exponential horn-type waveguide, 3 – Langevin-type transducer, 4 – USM, 5, 6 – laser vibrometer, 7 – digital oscilloscope, 8 – PC

The mechanical impact was generated using the designed mechanical shock exciter 1. The electric signal generated by the Langevin-type piezoelectric transducer 3 (with total capacity of 3.5 nF) was directly transmitted to the USM 4 (USM-50-3). The rotational steps were obtained with a laser Doppler vibrometer 5, 6 (Polytec OFV-5000/505); data were acquired a digital oscilloscope 7 (PicoScope-6403) and a PC 8.The rotational steps of the motor (USM-50-3) are presented in Fig. 4.17.

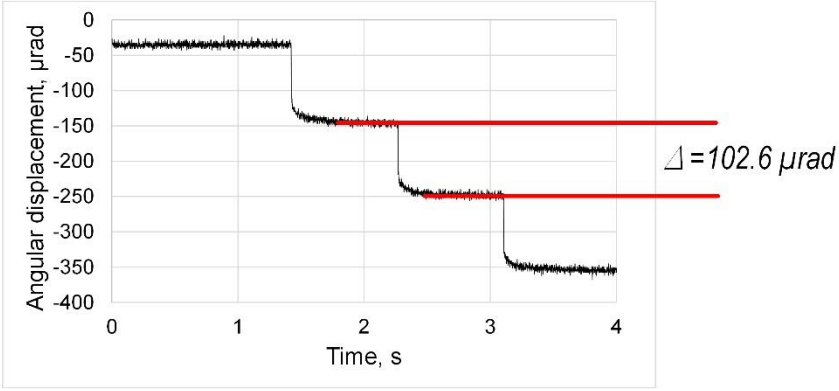

Fig. 4.17 Rotational steps of the ultrasonic motor generated using a prototype of the piezoelectric impact energy harvester for burst-type signal generation

These results (Fig. 4.17) show that the designed piezoelectric impact energy harvester for burst-type signal generation works correctly and generates 102.6 μrad step of USM-50-3 from one push of the mechanical shock exciter.

In order to obtain a smaller step of the USM, a potentiometer wired as a voltage divider [83] or an additional capacitor series wired [84] could be used in the power circuit between the Langevin-type piezoelectric transducer and the controllable USM.

4.3. Noise measurement of piezoelectric impact energy harvester for burst-type signal generation

The research has also evaluated how loudly the piezoelectric impact energy harvester for burst-type signal generation operates. The experimental layout and stand view of noise evaluation are presented in Fig. 4.18.

As in previous experiments, shock was generated using the mechanical shock exciter 1 mounted on the piezoelectric impact energy harvester 2. The sound level was measured using a sound level meter 3 (Investigator 2260, Bruel and Kjaer A/S).

Measurements were taken in one third octave bandwidth, in agreement with the LST EN ISO 1102:2010-09 standard "Acoustics – Noise emitted by machinery and equipment – Measurement of emission sound pressure levels at a work station and at other specified positions – Method requiring environmental corrections (ISO 11202:2010)" [85].

Firstly, the environmental conditions were established using a climate measurement instrument TESTO 445. In order to measure the sound level precisely and accurately, the sound level meter was calibrated using the portable acoustic calibrator no. 4231 by placing it directly over the microphone.

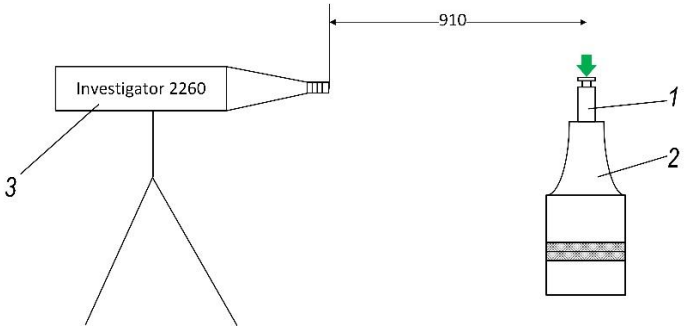

a)

b)

Fig. 4.18 Experimental research of the noise generated by the piezoelectric impact energy harvester: a) layout b) stand view: 1 – mechanical shock exciter, 2 – piezoelectric impact energy harvester, 3 – sound level meter

The distance between the microphone and piezoelectric impact energy harvester for burst-type signal generation was 0.91±0.05 m during the measurement. This distance, according to the measurement standard [85], corresponds to the distance from the seat plane to the top of the operator's head, when s/he is in a position in which s/he can reach all controls comfortably.

One factor that may influence the accuracy of measurements is the level of background noise compared to the level of sound being measured. Obviously, the background noise must not "drown out" the sound of interest. In practice this means that corrections of the sound measurement are unnecessary if the level of sound is least 3 dB higher than the background noise [86]. Therefore, background noise was determined before the measurements. Time-averaged A-weighted background noise pressure level L_{BAeq} in a 10 s interval is presented in Fig. 4.19.

The "A" weighting network was chosen because it measures a signal in a manner which approximates an inverted equal loudness contour at low sound pressure levels, whose sensitivity varies with frequency in the same way as the human ear, and is the most widely used nowadays [86].

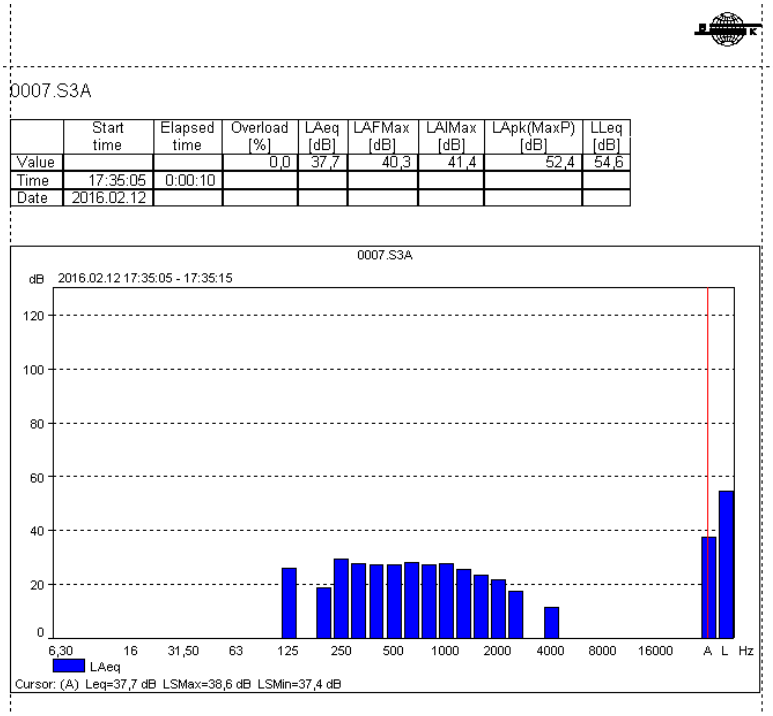

Fig. 4.19 Time-averaged A-weighted background noise pressure level L_{BAeq}

The maximum peak background noise pressure level in the measurement environment is approximately 52.4 dB and the average time-averaged A-weighted background noise pressure level is 37.7 dB.

The researched piezoelectric impact energy harvester generates the same sound level regardless of the number of clicks, thus the time interval was set to 10 s for sound measurement as well. During this interval, the mechanical shock exciter was clicked 10 times and the sound pressure level was measured. The time-averaged A-weighted sound pressure level L_{Aeq} in a 10 s interval, during which the piezoelectric impact energy harvester generated 10 steps, is presented in Fig. 4.20.

This result (Fig. 4.20) show that the maximum peak sound pressure level L_{Apk} is 100.2 dB and the average time-averaged A-weighted sound pressure level L_{Aeq} is 63.8 dB. Comparing the results to the background noise (Fig. 4.19), it is seen that the average sound pressure level during piezoelectric impact energy harvester operation is more than 3dB higher than the average background noise pressure level. Therefore, corrections of the sound measurement are unnecessary according to measurement standard [85].

0008.S3A

	Start time	Elapsed time	Overload [%]	LAeq [dB]	LAFMax [dB]	LAIMax [dB]	LApk(MaxP) [dB]
Value			0,0	63,8	70,2	75,4	100,2
Time	17:35:50	0:00:10					
Date	2016.02.12						

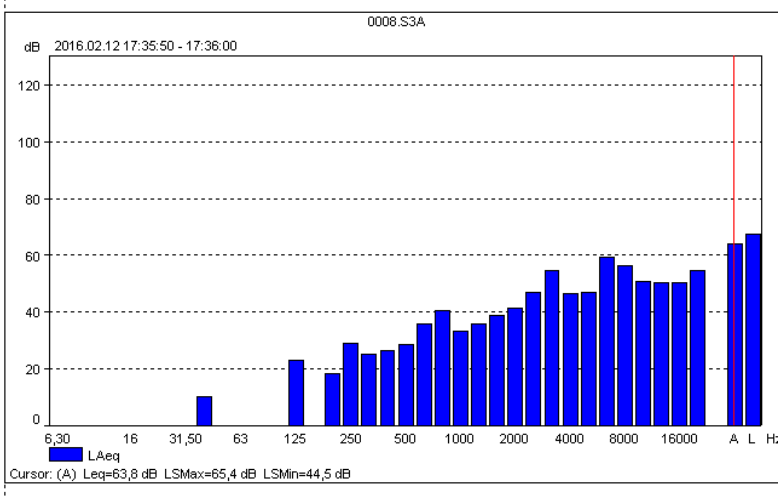

Fig. 4.20 Time-averaged A-weighted sound pressure level L_{Aeq}

The information in Fig. 4.20 also allows the conclusion that the piezoelectric impact energy harvester for burst-type signal generation with mechanical shock exciter is suitable for use in various industrial areas, because the average time-averaged A-weighted sound pressure level does not exceed the maximum allowed time-averaged A-weighted sound pressure level, which, for example in laboratories with noise generating devices L_{Aeq} is 75 dB according to the standard [85]. Moreover, the maximum peak sound pressure level value also does not exceed the maximum allowed peak sound pressure level L_{Apk} of 110 dB.

4.4 Conclusions of the section

This section presented the methodology for designing the piezoelectric impact energy harvester for burst-type signal generation. A new piezoelectric impact energy harvester with mechanical impact exciter, ergonomic handle and a resonant frequency of 42,6 kHz which corresponds with the operating frequency of the USM-50-3 was designed and investigated.

The following conclusions are formulated:

- The new piezoelectric impact energy harvester has been investigated experimentally and the results show the burst-type signal generated by this type of harvester drives the USM-50-3 with a maximum rotational step of 102.6 μrad.

- The noise generated by the piezoelectric impact energy harvester has been evaluated according to the LST EN ISO 1102:2010-09 standard with the Bruel and Kjaer sound lever meter. The maximum peak sound pressure level L_{Apk} is100.2 dB and the average time-averaged A-weighted sound pressure level L_{Aeq} is 63.8 dB. The results of the measurement show that both parameters L_{Apk} and L_{Aeq} do not exceed the maximum permitted values according to the standard.
- The novel piezoelectric impact energy harvester for burst-type signal generation can be used both for linear and rotary ultrasonic motors. This reveals the possibility to use such a harvester in a wide variety of precise positioning applications such as laboratory microscope table, laser beam and laser mirror positioning devices, piezoelectric micro dispensing technologies, space technology positioning systems, etc.

CONCLUSIONS

1. A literature review of the conventional energy harvesters has revealed the possibility to improve the effectiveness of the impact-based harvesting technique for generating ultrasonic-range frequency burst-type electric signal.
2. A novel piezoelectric impact energy harvester for burst-type signal generation has been designed; it consists of a mechanical shock exciter, a specially designed horn-type waveguide and a piezoelectric transducer. The results of a modelling using the ANSYS 17.1 software package, has revealed that the close-exponential waveguide generates 3.8 times higher vibration amplitude of the greater cross-sectional surface. The stepped waveguide produces the lowest discrepancy as compared to the cylindrical one, when both waveguides are excited with the same impact applied on the smaller cross-sectional surface. The simulation of horn-type waveguides with impulse-type excitation has revealed that the highest vibration amplitude of the greater cross-sectional surface is achieved when the duration of the excitation impulse corresponds to half of the resonant frequency period of the horn-type waveguide.
3. The results of theoretical research have been verified by experimentally researching the cylindrical and other shapes horn-type waveguides. A holographic technique and a 3D laser Doppler scanner were used to determine the modes and amplitude of vibrations of the researched waveguides. It has been determined that the conical waveguide produces an amplitude of vibrations of the greater cross-sectional surface which is from 1.27 to 1.87 times higher than that of a cylindrical waveguide. Experimental results show that the voltage generated by the piezoelectric impact energy harvester can be increased by up to 1.4 times by using the "soft" (PZT-5A) piezoelectric material. A piezoelectric impact energy harvester for burst-type signal generation with a resonant frequency of 21.1 kHz and a stepped-close exponential horn-type waveguide has been developed and fabricated. Experimental results show that the subharmonic burst-type signal generated by this device drives the USM-50-3 with rotational steps from 1.55 μrad to 10.4μrad.
4. A new piezoelectric impact energy harvester with a mechanical impact exciter and a resonant frequency of 42.6 kHz, which corresponds to the operating frequency of the USM-50-3 has been designed and investigated using the developed methodology. The results of investigation show that the burst-type signal generated with such a harvester drives the USM-50-3 with the maximum rotational step of 102.6 μrad. The Bruel and Kjaer sound lever meter was used to measure the noise level according to the LST EN ISO 1102:2010-09 standard. The level of noise generated by the developed impact energy harvester does not exceed the maximum permitted values according to the standard.

REFERENCES

1. Qi Q, Li R, Luo J, Zheng B, Huang KW, Wang P, Wu J. Push–pull type porphyrin based sensitizers: The effect of donor structure on the light-harvesting ability and photovoltaic performance. Dyes and Pigments. 2015 Nov 30;122:199-205.
2. Yildiz F. Potential ambient energy-harvesting sources and techniques.
3. Yang HD, Tufa LT, Bae KM, Kang TJ. A tubing shaped, flexible thermal energy harvester based on a carbon nanotube sheet electrode. Carbon. 2015 May 31;86:118-23.
4. Sun W, Jung J, Seok J. Frequency-tunable electromagnetic energy harvester using magneto-rheological elastomer. Journal of Intelligent Material Systems and Structures. 2015 Jun 10:1045389X15590274.
5. Wang F, Hansen O. Electrostatic energy harvesting device with out-of-the-plane gap closing scheme. Sensors and Actuators A: Physical. 2014 May 1;211:131-7.
6. Dow AB, Schmid U, Kherani NP. Unimorph and bimorph piezoelectric energy harvester stimulated by β-emitting radioisotopes: a modeling study. Microsystem technologies. 2014 Apr 1;20(4-5):933-44.
7. Lumentut MF, Howard IM. Parametric design-based modal damped vibrational piezoelectric energy harvesters with arbitrary proof mass offset: Numerical and analytical validations. Mechanical Systems and Signal Processing. 2016 Feb 29;68:562-86.
8. Gatti G, Brennan MJ, Tehrani MG, Thompson DJ. Harvesting energy from the vibration of a passing train using a single-degree-of-freedom oscillator. Mechanical Systems and Signal Processing. 2016 Jan 31;66:785-92.
9. Williams CB, Yates RB. Analysis of a micro-electric generator for microsystems. sensors and actuators A: Physical. 1996 Apr 30;52(1):8-11.
10. Hehn T, Manoli Y. CMOS circuits for piezoelectric energy harvesters. Springer Series in Advanced Microelectronics. 2015;38:21-40.
11. Renaud M, Fiorini P, van Schaijk R, Van Hoof C. Corrigendum: Harvesting energy from the motion of human limbs: the design and analysis of an impact-based piezoelectric generator. Smart Materials and Structures. 2012 Apr 1;21(4):049501.
12. Moheimani SR, Fleming AJ. Fundamentals of Piezoelectricity. Piezoelectric Transducers for Vibration Control and Damping. 2006:9-35.
13. Townley A. Vibrational energy harvesting using MEMS piezoelectric generators.
14. Beeby SP, Tudor MJ, White NM. Energy harvesting vibration sources for microsystems applications. Measurement science and technology. 2006 Oct 26;17(12):R175.
15. Renaud M, Fiorini P, Van Hoof C. Optimization of a piezoelectric unimorph for shock and impact energy harvesting. Smart Materials and Structures. 2007 Jun 25;16(4):1125.
16. Roundy S, Leland ES, Baker J, Carleton E, Reilly E, Lai E, Otis B, Rabaey JM, Wright PK, Sundararajan V. Improving power output for vibration-based energy scavengers. Pervasive Computing, IEEE. 2005 Jan;4(1):28-36.
17. Blystad LC, Halvorsen E. An energy harvester driven by colored noise. Smart Materials and Structures. 2011 Jan 14;20(2):025011.
18. Al Ahmad M. Piezoelectric Water Drop Energy Harvesting. Journal of electronic materials. 2014 Feb 1;43(2):452-8.

19. Umeda M, Nakamura K, Ueha S. Analysis of the transformation of mechanical impact energy to electric energy using piezoelectric vibrator. Japanese Journal of Applied Physics. 1996 May;35(5S):3267.
20. Van Minh L, Hara M, Oguchi H, Kuwano H. Lead-free (K, Na) NbO 3 based impact type energy harvesters integrated with a cylindrical cavity for metal ball. InMicro Electro Mechanical Systems (MEMS), 2013 IEEE 26th International Conference on 2013 Jan 20 (pp. 833-836). IEEE.
21. He XF, Gao J. Wind energy harvesting based on flow-induced-vibration and impact. Microelectronic Engineering. 2013 Nov 30;111:82-6.
22. Milasauskaite I, Dauksevicius R, Ostasevicius V, Gaidys R, Janusas G. Influence of contact point location on dynamical and electrical responses of impact-type vibration energy harvester based on piezoelectric transduction. ZAMM-Journal of Applied Mathematics and Mechanics/Zeitschrift für Angewandte Mathematik und Mechanik. 2014 Nov 17;94(11):898-903.
23. Ostasevicius V, Janusas G, Milasauskaite I, Zilys M, Kizauskiene L. Peculiarities of the Third Natural Frequency Vibrations of a Cantilever for the Improvement of Energy Harvesting. Sensors. 2015 May 28;15(6):12594-612.
24. Wei S, Hu H, He S. Modeling and experimental investigation of an impact-driven piezoelectric energy harvester from human motion. Smart Materials and Structures. 2013 Sep 5;22(10):105020.
25. Pillatsch P, Yeatman EM, Holmes AS. A scalable piezoelectric impulse-excited energy harvester for human body excitation. Smart Materials and Structures. 2012 Oct 4;21(11):115018.
26. Alghisi D, Dalola S, Ferrari M, Ferrari V. Triaxial ball-impact piezoelectric converter for autonomous sensors exploiting energy harvesting from vibrations and human motion. Sensors and Actuators A: Physical. 2015 Sep 1;233:569-81.
27. Yang Y, Shen Q, Jin J, Wang Y, Qian W, Yuan D. Rotational piezoelectric wind energy harvesting using impact-induced resonance. Applied Physics Letters. 2014 Aug 4;105(5):053901.
28. Ostasevicius V, Markevicius V, Jurenas V, Zilys M, Cepenas M, Kizauskiene L, Gyliene V. Cutting tool vibration energy harvesting for wireless sensors applications. Sensors and Actuators A: Physical. 2015 Sep 1;233:310-8.
29. Polukoshko S, Viba J, Kononova O, Sokolova S. Rigid body impact models partially considering deformation. Proc. Estonian Acad. Sci. Eng. 2007;13(2):140-55.
30. Tong JH, Wu TT, Lee CK. Fabrication of a piezoelectric impact hammer and its application to the in-situ nondestructive evaluation of concrete, the Japan Society of Applied Physics. Part. 2002;1(41):6595-00.
31. Zhou L, He Z, Sun H. Lamb wave mode conversion-based crack detection for plate-like structures without baseline information. Journal of Vibroengineering. 2013 Jun 1;15(2).
32. Piezomechanik, *High power piezoelectric axial shockwave generation*, brochure, [interactive] [last accessed 24 April 2016], available at http://www.scilab.co.jp/product/mems/download/piezo_catalog_120930_7.pdf
33. Liu YT, Jiang CC. Pneumatic actuating device with nanopositioning ability utilizing piezoelectric impact force. InProceedings of the first international conference on positioning technology 2004 (pp. 247-52).
34. Gilardi G, Sharf I. Literature survey of contact dynamics modelling. Mechanism and machine theory. 2002 Oct 31;37(10):1213-39.

35. Nicklich H, Brucke M, Mende M. The need for controlled shocks-A new type of shock exciter allows to apply well defined mechanical shocks. InXIX IMEKO World Congress Fundamental and Applied Metrology 2009. Red Hook, NY: Curran Associates, Inc.
36. Product Data of Impact Hammer — Type 8202. Brüel & Kjær corporation catalogue.
37. Piezomechanik, *Piezo impactors/accelerators (PIA) for shock and impact generation*, brochure, [interactive] [last accessed 14 April 2016], available at http://www.atr-tr.co.jp/product/download/piezo_impactors_accelerators_pia.pdf.
38. Altgilbers LL, Stults AH, Kristiansen M, Neuber A, Dickens J, Young A, Holt T, Elsayed M, Curry R, O'Connor K, Baird J. Recent advances in explosive pulsed power. Journal of Directed Energy. 2009;3(2):149-91.
39. Shkuratov SI, Talantsev EF, Baird J. Application of piezoelectric ceramics in pulsed power technology and engineering.
40. Li T, Low AF, Ma J. Horn-Type Piezoelectric Ultrasonic Transducer: Modelling and Applications. INTECH Open Access Publisher; 2011.
41. Zhang Q, Shi S, Chen W. An electromechanical coupling model of a bending vibration type piezoelectric ultrasonic transducer. Ultrasonics. 2016 Mar 31;66:18-26.
42. Choi YJ, Park KH, Hong YH, Kim KT, Lee SW, Choi HZ. Effect of ultrasonic vibration in grinding; horn design and experiment. International Journal of Precision Engineering and Manufacturing. 2013 Nov 1;14(11):1873-9.
43. Al-Sarraf Z, Lucas M, Harkness P. A numerical and experimental study of ultrasonic metal welding. InIOP Conference Series: Materials Science and Engineering 2012 (Vol. 42, No. 1, p. 012015). IOP Publishing.
44. Kim H, Lee Y, Lim E. Dual-Frequency Megasonic Waveguide for Nano-Pattern Cleaning. Semiconductor Manufacturing, IEEE Transactions on. 2015 Nov;28(4):521-7.
45. Huang YC, Ding GZ, Chen BH, Huang YJ. Simulation and experiment of langevin-type piezoelectric ultrasonic horn for micro tool motion. InIntelligent Technologies and Engineering Systems 2013 (pp. 967-974). Springer New York.
46. Wang DA, Chuang WY, Hsu K, Pham HT. Design of a Bézier-profile horn for high displacement amplification. Ultrasonics. 2011 Feb 28;51(2):148-56.
47. Rani MR, Rudramoorthy R. Computational modeling and experimental studies of the dynamic performance of ultrasonic horn profiles used in plastic welding. Ultrasonics. 2013 Mar 31;53(3):763-72.
48. Naď M. Ultrasonic horn design for ultrasonic machining technologies. Applied and Computational Mechanics. 2010 Mar 12;4(1).
49. Song YL, Chou YF, Lee CT. Design and Simulation of Silicon-Based Ultrasonic Nozzles for Production of Monodispersed Droplets.
50. Shu KM, Hsieh WH, Yen HS. On the design and analysis of acoustic horns for ultrasonic welding. Transactions of the Canadian Society for Mechanical Engineering. 2013 Jan 1;37(3):905-16.
51. Ngo TT, Huang JH, Wang CC. The BFGS method for estimating the interface temperature and convection coefficient in ultrasonic welding. International Communications in Heat and Mass Transfer. 2015 Dec 31;69:66-75.
52. Choi YJ, Park KH, Hong YH, Kim KT, Lee SW, Choi HZ. Effect of ultrasonic vibration in grinding; horn design and experiment. International Journal of Precision Engineering and Manufacturing. 2013 Nov 1;14(11):1873-9.

53. Azarhoushang B, Akbari J. Ultrasonic-assisted drilling of Inconel 738-LC. International Journal of Machine Tools and Manufacture. 2007 Jun 30;47(7):1027-33.
54. Wang DA, Nguyen HD. A planar Bézier profiled horn for reducing penetration force in ultrasonic cutting. Ultrasonics. 2014 Jan 31;54(1):375-84.
55. Bae H, Park K. Design and analysis of ultrasonic horn for polymer sheet forming. International Journal of Precision Engineering and Manufacturing-Green Technology. 2016 Jan 1;3(1):49-54.
56. Samani BH, Khoshtaghaza MH, Minaei S, Zareifourosh H, Eshtiaghi MN, Rostami S. Design, development and evaluation of an automatic fruit-juice pasteurization system using microwave–ultrasonic waves. Journal of food science and technology. 2016 Jan 1;53(1):88-103.
57. Sadiq M, Kuang Y, Cochran S, Huang Z. High-performance planar ultrasonic tool based on d 31-mode piezocrystal. Ultrasonics, Ferroelectrics, and Frequency Control, IEEE Transactions on. 2015 Mar;62(3):428-38.
58. Lockhart R, Friedrich F, Briand D, Margairaz P, Sandoz JP, Brossard J, Keppner H, Olson W, Dietz T, Tardy Y, Meyer H. Silicon micromachined ultrasonic scalpel for the dissection and coagulation of tissue. Biomedical microdevices. 2015 Aug 1;17(4):1-2.
59. Peng T, Wu X, Liang X, Shi H, Luo F. Investigation of a rotary ultrasonic motor using a longitudinal vibrator and spiral fin rotor. Ultrasonics. 2015 Aug 31;61:157-61.
60. Asami T, Miura H. Ultrasonic welding of dissimilar metals by vibration with planar locus. Acoustical Science and Technology. 2015;36(3):232-9.
61. Ragulskis K, Bansevicius R, Barauskas R, Kulvietis G. Vibromotors for Precision Microrobots, Hemisphere Publ. Co., New York. 1988.
62. Liu Y, Xu D, Yu Z, Yan J, Yang X, Chen W. A Novel Rotary Piezoelectric Motor Using First Bending Hybrid Transducers. Applied Sciences. 2015 Aug 27;5(3):472-84.
63. Xu L, Xing J. Forced response of the inertial piezoelectric rotary motor to electric excitation. Journal of Mechanical Science and Technology. 2015 Nov 1;29(11):4601-10.
64. Bansevicius R, Blechertas V. Multi-degree-of-freedom ultrasonic motors for mass-consumer devices. Journal of Electroceramics. 2008 Aug 1;20(3-4):221-4.
65. Liu Y, Yang X, Chen W, Liu J. A rotary piezoelectric actuator using longitudinal and bending hybrid transducer. AIP Advances. 2012 Dec 1;2(4):042136.
66. Grybas I, Bubulis A, Bansevičius R, Jūrėnas V. Research of rotary piezotable driven by two harmonic signals. Mechanics. 2015 Aug 1;20(6):573-6.
67. Ho ST, Jan SJ. A piezoelectric motor for precision positioning applications. Precision Engineering. 2016 Jan 31;43:285-93.
68. Ho ST, Chiu WH. A piezoelectric screw-driven motor operating in shear vibration modes. Journal of Intelligent Material Systems and Structures. 2016;27(1):134-45.
69. Wang YJ, Chen YC, Shen SC. Design and analysis of a standing-wave trapezoidal ultrasonic linear motor. Journal of Intelligent Material Systems and Structures. 2014 Oct 16:1045389X14554130.
70. Mazeika D, Bansevicius R, Kulvietis G. Investigation of contact point trajectories of the beam type piezoelectric actuator with two preloaded masses. Journal of Vibroengineering. 2009 Dec 1;11(4).

71. Morita T. Miniature piezoelectric motors. Sensors and Actuators A: Physical. 2003 Feb 15;103(3):291-300.
72. Wang S, Zhang Z, Ren L, Zhao H, Liang Y, Zhu B. Design and driving characteristic researches of a novel bionic stepping piezoelectric actuator with large load capacity based on clamping blocks. Microsystem Technologies. 2015 Aug 1;21(8):1757-65.
73. Glazounov AE, Zhang QM, Kim C. Torsional actuator and stepper motor based on piezoelectric d15 shear response. Journal of intelligent material systems and structures. 2000 Jun 1;11(6):456-68.
74. Qiao P, Yang M, Bobaru F. Impact mechanics and high-energy absorbing materials: review. Journal of Aerospace Engineering. 2008 Oct;21(4):235-48.
75. Johnson KL, Johnson KL. Contact mechanics. Cambridge university press; 1987 Aug 28.
76. Goldsmith W. Impact, Arnold, London. I960. 1960.
77. Nguyen MQ, Jacombs SS, Thomson RS, Hachenberg D, Scott ML. Simulation of impact on sandwich structures. Composite Structures. 2005 Feb 28;67(2):217-27.
78. Kozicki J, Donzé FV. A new open-source software developed for numerical simulations using discrete modeling methods. Computer Methods in Applied Mechanics and Engineering. 2008 Sep 15;197(49):4429-43.
79. Timmel M, Kolling S, Osterrieder P, Du Bois PA. A finite element model for impact simulation with laminated glass. International Journal of Impact Engineering. 2007 Aug 31;34(8):1465-78.
80. Nanu AS, Marinescu NI, Ghiculescu D. Study on ultrasonic stepped horn geometry design and FEM simulation. Revista de Tehnologii Neconventionale. 2011 Dec 1;15(4):25.
81. Rosca IC, Pop MI, Cretu N. Experimental and numerical study on an ultrasonic horn with shape designed with an optimization algorithm. Applied Acoustics. 2015 Aug 31;95:60-9.
82. *Engineers edge spring calculator*, [interactive] [last accessed 25 May 2016], available at http://www.engineersedge.com/spring_comp_calc_k.htm
83. *Measuring Sound/Pressure in a Combustion Spud Gun Using a Piezo Transducer*, [interactive] [last accessed 25 July 2016], available at http://www.inpharmix.com/jps/Piezo_Spud.html
84. Pulsar Development Ltd., *Piezo Tweeter Application Note*, [interactive] [last accessed 26 July 2016], available at http://www.pulsardevelopments.com/products/detail/piezoan.html
85. Standard LST EN ISO 1102:2010-09, *Acoustics – Noise emitted by machinery and equipment – Measurement of emission sound pressure levels at a work station and at other specified positions – Method requiring environmental corrections (ISO 11202:2010),* [interactive] [last accessed 21 June 2016], available at http://www.lsd.lt/standards/catalog.php?ics=0&pid=632589
86. Brüel & Kjær, *Measuring sound*, brochure, [interactive] [last accessed 14 May 2016], available at http://www.bksv.com/doc/br0047.pdf

List of publications

Indexed in the Web of Science with Impact Factor

1. **Eidukynas, Darius**; Jūrėnas, Vytautas; Dragašius, Egidijus; Mystkowski, Arkadiusz. A burst type signal generator for ultrasonic motor control // Eksploatacja i niezawodnosc = Maintenance and reliability. Lublin: Polskie Naukowo-Techniczne Towarzystwo Eksploatacyjne. ISSN 1507-2711. 2016, vol. 18, no. 4, p. 488-491. [Science Citation Index Expanded (Web of Science)]. [IF: 1,248; AIF: 1,505; IF/AIF: 0,829; ; 2015 Journal Citation Reports® Science Edition (Thomson Reuters, 2016)]. [Contribution: 0,250]
2. **Eidukynas, Darius**; Jūrėnas, Vytautas; Mažeika, Darius. Analysis of horn type waveguide with impulse excitation // Journal of vibroengineering. Kaunas: JVE International. ISSN 1392-8716. 2016, vol. 18, iss. 3, p. 1585-1590. [Science Citation Index Expanded (Web of Science); Inspec; Academic Search Complete; Central & Eastern European Academic Source (Ebsco); Computers & Applied Sciences Complete; Current Abstracts; TOC Premier]. [IF: 0,384; AIF: 2,315; IF/AIF: 0,166; Q4; 2015 Journal Citation Reports® Science Edition (Thomson Reuters, 2016)]. [Contribution: 0,333]
3. Dragašius, Egidijus; **Eidukynas, Darius**; Mažeika, Darius; Mystkowski, A.; Ažubalis, Mindaugas. The strength investigation of the composite material with implanted sensors // Mechanika / Kauno technologijos universitetas, Lietuvos mokslų akademija, Vilniaus Gedimino technikos universitetas. Kaunas: KTU. ISSN 1392-1207. 2015, Vol. 21, No. 1, p. 23-27. [Science Citation Index Expanded (Web of Science); Academic Search Complete; Inspec; Compendex; FLUIDEX; Scopus]. [IF: 0,277; AIF: 2,041; IF/AIF: 0,136; Q4; 2015 Journal Citation Reports® Science Edition (Thomson Reuters, 2016)]. [Contribution: 0,200]

Indexed in other international databases

1. **Eidukynas, Darius**; Jūrėnas, Vytautas; Mažeika, Darius. R and D of system for mechanical impact generation // Vibroengineering procedia : international conference Vibroengineering - 2014, Katowice, Poland, 13-15 October, 2014. Kaunas: JVE International. ISSN 2345-0533. 2014, vol. 3, p. 128-132. [Compendex; Academic OneFile]. [Contribution: 0,333]

In peer-reviewed conference proceedings

1. **Eidukynas, Darius**; Jūrėnas, Vytautas. Peculiarities of harmonic vibrations excitation with horn type waveguides // Mechanika 2016 : proceedings of the 21st international scientific conference, 12, 13 May 2016, Kaunas University of Technology, Lithuania / Kaunas University of Technology, Lithuanian Academy of Science, IFTOMM National Committee of Lithuania, Baltic Association of Mechanical Engineering. Kaunas: Kauno technologijos universitetas. ISSN 1822-2951. 2016, p. 77-81. [Contribution: 0,500]
2. Mažeika, Darius; **Eidukynas, Darius**; Dragašius, Egidijus. Coefficient of restitution control using piezoelectric material // Mechatronic systems and materials : abstracts of the 11th international conference, MSM 2015, 7-9 July 2015, Kaunas, Lithuania / Editors: I. Skiedraitė, R. Rimašauskienė, L. Zubrickaitė, E. Drafašius. Kaunas: Kauno technologijos universitetas. ISSN 1822-8283. 2015, p. 44-45. [Contribution: 0,333]

Scientific LR invention patent application

“Gęstančių virpesių elektrinio signalo generatorius” (application no. 2016-108)

SL344. 2017-03-20, 14,75 leidyb. apsk. l. Tiražas 10 egz. Užsakymas 17-0103.
Išleido Kauno technologijos universitetas, K. Donelaičio g. 73, 44249 Kaunas
Spausdino leidyklos „Technologija“ spaustuvė, Studentų g. 54, 51424 Kaunas

APPENDIXES

Appendix No. 1. Scientific LR invention patent application

IP - 1/2011 forma

LIETUVOS RESPUBLIKOS
VALSTYBINIAM PATENTŲ BIURUI
Kalvarijų g. 3, LT-09310 Vilnius

PRAŠYMAS
IŠDUOTI PATENTĄ

22	Paraiškos padavimo data	*
	2016-10-31	
21	Paraiškos numeris	*
	2016- 108	
11	Patento numeris	*

* *Užpildo Valstybinis patentų biuras*

Pareiškėjo/atstovo žyma
G-2-6/JA

** *Čia gali būti nurodytas šiam prašymui suteiktas numeris*

71	74
Pareiškėjas: pavadinimas arba vardas ir pavardė, adresas (buveinė), valstybės kodas; jeigu pareiškėjas yra Lietuvos Respublikos pilietis ar Lietuvos Respublikoje registruotas juridinis asmuo – fizinio ar juridinio asmens kodas; telefonas, faksas, el. paštas	Atstovas: vardas ir pavardė, asmens kodas arba patentinio patikėtinio Nr./juridinio asmens pavadinimas, registracijos kodas; adresas (buveinė), valstybės kodas, telefonas, faksas, el. paštas
KAUNO TECHNOLOGIJOS UNIVERSITETAS, kodas 111950581, K. Donelaičio g.73, LT-44249 Kaunas, LT	Reda Žabolienė, a.k. 46107260227, Advokatų profesinė bendrija "Žabolienė ir partneriai METIDA", Verslo centras VERTAS, Gynėjų g. 16, LT- 01109 Vilnius, LT tel. 2490830, faks. 2490833, patent@metida.lt

Susirašinėjimo Lietuvos Respublikoje adresas, telefonas, faksas, el. paštas (kai pareiškėjo ir (arba) atstovo adresas (buveinė) nėra Lietuvos Respublikos teritorijoje)

54 Išradimo pavadinimas

GĘSTANČIŲ VIRPESIŲ ELEKTRINIO SIGNALO GENERATORIUS

31	32	33	86	Anksčiau paduotos paraiškos numeris, data, valstybės kodas	51 Tarptautinės patentų klasifikacijos indeksai

72 Išradėjo vardas, pavardė, adresas, valstybės kodas, jeigu išradėjas yra Lietuvos Respublikos pilietis – asmens kodas

1. Ramutis Bansevičius a.k. 33902230068
   Eivenių g. 31-40, Kaunas, LT-51067
2. Darius Eidukynas a.k. 38712270082
   Erškėčių g. 12, Kaunas, LT-47483
3. Vytautas Jūrėnas a.k. 35608240110
   P. Višinskio g. 17-2, Kaunas, LT-44151

☐ kiti išradėjai nurodyti ant atskiro lapo

1. Prašymas paduodamas 3 egzemplioriai.
2. Šis dokumentas su Valstybinio patentų biuro užpildytais rekvizitais yra paraiškos priėmimo pažyma.

Paraiškų priėmimo ir dokumentų valdymo skyrius — PARAIŠKŲ PRIĖMIMO IR DOKUMENTŲ VALDYMO SKYRIUS — (pareigos) ..... (parašas) Vida Viliuvienė (vardas, pavardė) Data 2016 ..

GĘSTANČIŲ VIRPESIŲ ELEKTRINIO SIGNALO GENERATORIUS

Išradimo sritis

Išradimas priskiriamas energijos surinkimo įrenginių (angl. „harvester“) sričiai, konkrečiai gęstančių virpesių elektriniam signalui generuoti ir tiesiogiai valdyti ultragarsinį variklį, taip išvengiant tradicinių maitinimo šaltinių, tokių kaip elektros tinklas, akumuliatorius, baterija ir pan.

Technikos lygis

Yra žinomas pjezoelektrinis gęstančių virpesių elektrinio signalo generatorius, sudarytas iš bronzinio disko ir disko formos pjezoelektrinės keramikos, pritvirtintos ant bronzinio disko. Bronzinio disko kraštai standžiai įtvirtinti rėme. Gęstančių virpesių elektrinis signalas generuojamas iš disko (tuo pačiu ir pjezoelektrinės keramikos) vibracijų, sukeltų plieninės sferos, krentančios iš tam tikro nustatyto aukščio.

Nurodytame įrenginyje generuojamo gęstančių virpesių elektrinio signalo maksimalus dažnis yra 4 kHz. Be to, plieninė sfera tiesiogiai smūgiuoja į pjezoelektrinę keramiką, kuri yra labai trapi ir gali būti lengvai pažeista smūginių jėgų. Kitas tokio generatoriaus trūkumas – nevienodos amplitudės smūgis priklausomai nuo žadinimo sąlygų, ko pasekoje negaunamas vienodas sugeneruotas gęstančių virpesių elektrinis signalas.

Taip pat yra žinomas smūginis energijos surinkimo (angl. „harvester“) prietaisas, skirtas gęstančių virpesių elektriniam signalui generuoti, sudarytas iš trijų sluoksnių rėmo su viduryje suformuota cilindrine ertme ir joje esančia plienine sfera bei pjezoelektrinės gembės, pritvirtintos prie viršutinio rėmo sluoksnio. Gęstančių virpesių elektrinis signalas generuojamas tuomet, kuomet dėl aplinkos poveikio cilindrinėje ertmėje esanti sfera smūgiuoja į pjezoelektrinę gembę taip sužadindama savuosius pjezoelektrinės gembės virpesius.

Nurodytas prietaisas tinkamas darbui žemuose, 20-190 Hz diapazono, dažniuose. Be to, čia irgi plieninė sfera tiesiogiai smūgiuoja į pjezoelektrinę gembę, todėl galimas trapios pjezoelektrinės medžiagos pažeidimas ar visiškas jos suskaldymas. Kitas tokio prietaiso trūkumas – nevienodos amplitudės smūgis priklausomai nuo žadinimo sąlygų, ko pasekoje negaunamas vienodas sugeneruotas gęstančių virpesių elektrinis signalas.

Dar yra žinomas pjezoelektrinis gęstančių virpesių elektrinio signalo generatorius, sudarytas iš cilindrinio tuščiavidurio korpuso, dviejų apsaugine plokštele dengtų disko formos pjezoelektrinių elementų, priklijuotų jo galuose statmenai cilindro išilginei ašiai bei plieninės sferos, esančios kreipiančiajame vamzdyje cilindrinio korpuso viduje. Gęstančių virpesių elektrinis signalas generuojamas tuomet, kuomet plieninė sfera dėl viso cilindrinio korpuso virpesių smūgiuoja į pjezoelektrinius elementus, todėl sužadinami pjezoelektrinių elementų rezonansiniai virpesiai (žr. JAV patento paraiška Nr. US20040041498 A1, paskelbta 2004.03.04)

Tačiau nurodytame įrenginyje gaunamas nevienodos amplitudės smūgis priklausomai nuo žadinimo sąlygų, ko pasėkoje negaunamas vienodas sugeneruotas gęstančių virpesių elektrinis signalas.

Išradimo esmė

Išradimo tikslas – generuojamo gęstančių virpesių elektrinio signalo dažnio padidinimas, pjezoelektrinės medžiagos apsaugojimas nuo tiesioginio smūgio jėgų bei smūgio, turinčio vienodą amplitudę, sukūrimas.

Išradimo tikslas pasiekiamas tuo, kad generatoriaus konstrukcija turį mechaninį smūgiuotuvą, kuriantį vienodos amplitudės mechaninį smūgį į rezonatorių – specialios formos koncentratorių, turintį ultragarsinį dažnį, kas leidžia generuoti gęstančių virpesių elektrinį signalą ultragarsiniame dažnių diapazone, bei visu paviršiaus plotu kontaktuojantį su pjezoelektrine medžiaga, taip apsaugant pjezoelektrinę medžiaga nuo smūgio efekto.

Išradimo esmė paaiškinama pateiktu paveikslu

1 paveiksle pateiktas gęstančių virpesių elektrinio signalo generatoriaus brėžinys (pjūvis).

Išradimo įgyvendinimo variantai (detalus aprašymas)

Gęstančių virpesių elektrinio signalo generatorių sudaro mechaninis smūgiuotuvas 1, siaurėjančio profilio formos aliuminio lydinio koncentratorius 2, plastikinis korpusas 3, guminė įvorė 4, pjezoelektriniai žiedai 5, atsvaras 6, įveržimo sraigtas 7, atraminė guma 8, dangtelio įveržimo sraigtai 9, plastikinis dangtelis 10.

Gęstančių virpesių elektrinis signalas generuojamas taip:

Mechaninis smūgis generuojamas mechaniniu smūgiuotuvu 1 nuspaudžiant jo judamą dalį kryptimi, pažymėta figūroje strėlyte (į apačią). Smūgio energija perduodama siaurėjančio profilio formos koncentratoriaus 2 paviršiui su mažesniu skerspjūvio plotu. Iš čia smūgio energija sklandžiai paskleidžiama ir perduodama visu koncentratoriaus 2 paviršiumi su didesniu skerspjūvio plotu pjezoelektriniams žiedams 5. Pjezoelektriniai žiedai 5 dėl smūgio energijos poveikio bei atsvaro 6 deformuojami ir taip sugeneruojamas gęstančių virpesių elektrinis signalas, kuris tiesiogiai perduodamas į norimą valdyti pavarą. Siekiant gauti aukštą generuojamo signalo dažnį, siaurėjančio profilio formos koncentratorius 2, pjezoelektriniai žiedai 5 bei atsveriamoji masė 6 sujungiami su įvarža įveržimo sraigto 7 pagalba, taip sudarant vientisą pjezoelektrinio keitiklio sistemą. Patogiam gęstančių virpesių elektrinio signalo generatoriaus naudojimui, ši sistema (kuri sudaryta iš: koncentratoriaus 2, pjezoelektrinių žiedų 5, atsveriamosios masės 6 bei įveržimo sraigto 7) per guminę įvorę 4 iš šonų tvirtinama plastikiniame korpuse 3. Sistema iš galo tvirtinama per atraminę gumą 8 plastikiniu dangteliu 10 įveržiant į korpuso 3 viršų panaudojant įveržimo sraigtus 9.

Palyginus su prototipu, nauja konstrukcinių elementų visuma dėl to, kad turi mechaninį smūgiuotuvą 1, kuriantį vienodos amplitudės smūgį į ultragarsinio rezonansinio dažnio rezonatorių – koncentratorių 2, kuris perduoda smūgio energiją į pjezoelektrinius žiedus 5 taip apsaugant medžiagą nuo tiesioginio smūgio efekto, gali generuoti vienodų parametrų ultragarsinio dažnio gęstančių virpesių elektrinį signalą, skirtą ultragarsinės pavaros valdymui. Tokia sistema turi apsaugotą pjezoelektrinę medžiagą, taip padidinant gęstančių virpesių elektrinio signalo generatoriaus veikimo laiką bei patikimumą.

Išradimo apibrėžtis

1. Gęstančių virpesių elektrinio signalo generatorius, turintis mechaninį smūgį generuojantį elementą, pjezoelektrinę medžiagą, **besiskiriantis tuo, kad** turi mechaninį smūgiuotuvą 1, kuris generuoja

vienodų parametrų mechaninį smūgį, perduodamą siaurėjančio profilio formos koncentratoriaus 2, tuo pačiu generuodamas vienodų parametrų gęstančių virpesių ultragarsinio dažnio elektrinį signalą.

2. Gęstančių virpesių elektrinio signalo generatorius pagal 1 punktą, **besiskiriantis tuo, kad** turi ultragarsinio dažnio rezonatorių – koncentratorių 2, apsaugantį pjezoelektrinę medžiagą nuo tiesioginio smūgio efekto.

REFERATAS

GĘSTANČIŲ VIRPESIŲ ELEKTRINIO SIGNALO GENERATORIUS

Šio išradimo tikslas – generuojamo gęstančių virpesių elektrinio signalo dažnio padidinimas, pjezoelektrinės medžiagos apsaugojimas nuo tiesioginio smūgio jėgų bei smūgio, turinčio vienodą amplitudę, sukūrimas. **Išradimo tikslas pasiekiamas tuo, kad** generatoriaus konstrukcija turi mechaninį smūgiuotuvą, kuriantį vienodos amplitudės mechaninį smūgį į rezonatorių – specialios formos koncentratorių, turintį ultragarsinį dažnį, kas leidžia generuoti gęstančių virpesių elektrinį signalą ultragarsiniame dažnių diapazone, bei visu paviršiaus plotu kontaktuojantį su pjezoelektrine medžiaga, taip apsaugant ją nuo smūgio efekto.

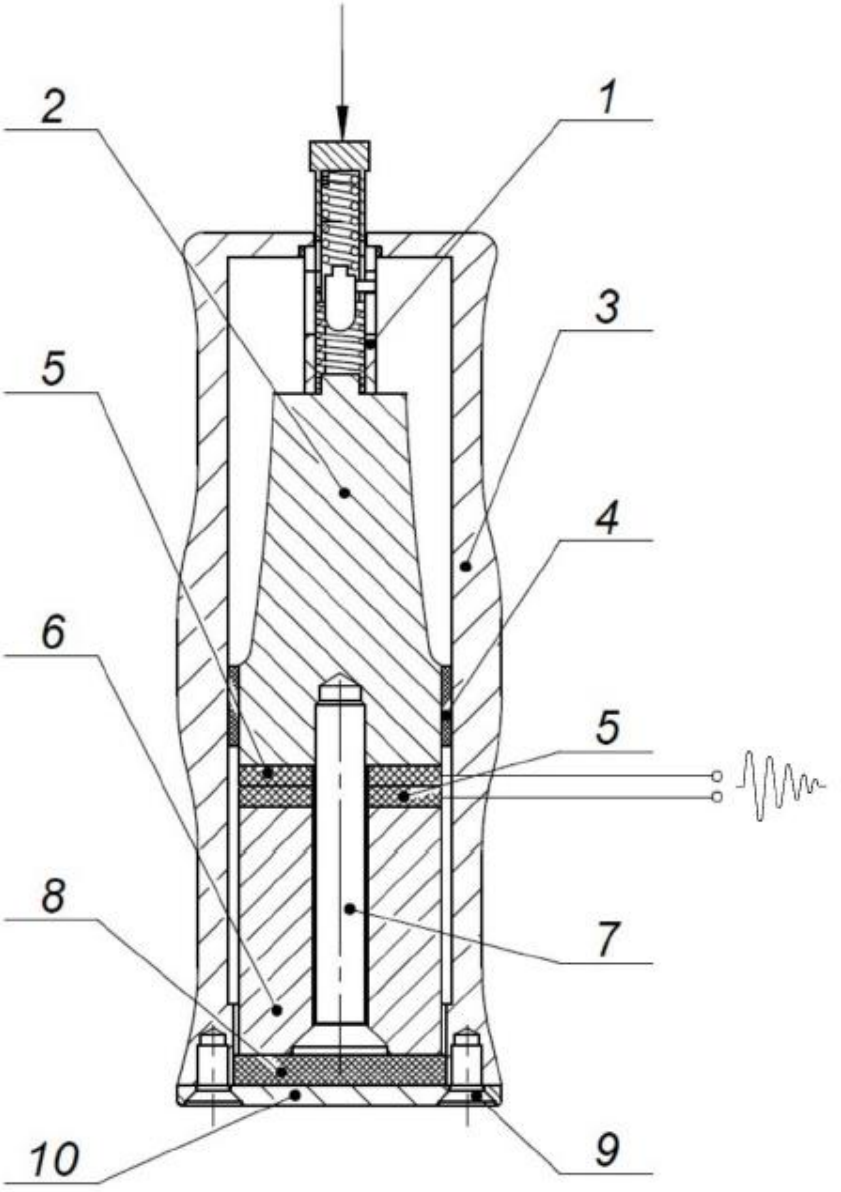

Pav. 1